A Dissertation for The Degree of Doctor of Philosophy

Highly Resilient Hydrogel Adhesives Based on Dopamine-Modified Crosslinking Agents

도파민개질 가교제 기반 고탄력 하이드로겔 접착소재

By

Gi-Yeon Han

Environmental Materials Science Major

Department of Agriculture, Forestry and Bioresource

Graduate School, Seoul National University

August, 2024

SEOUL NATIONAL UNIVERSITY

GRADUATE SCHOOL

PROGRAM IN ENVIRONMENTAL MATERIALS SCIENCE

WE HEREBY RECOMMEND THE THESIS BY
Gi-Yeon Han

ENTITLED

Highly Resilient Hydrogel Adhesives Based on Dopamine-Modified Crosslinking Agents

BE ACCEPTED IN FULFILLMENT OF THE REQUIREMENTS FOR THE DEGREE OF DOCTOR OF PHILOSOPHY

AUGUST, 2024

COMMITTEE ON FINAL EXAMINATION

Chairman _____
Prof. Cheol-Hee Ahn

Co-Chairman _____
Prof. Hyun-Joong Kim

Member _____
Prof. Chong-Su Cho

Member _____
Ph.D. Ick-Kyung Sung

Member _____
Ph.D. Jung-Min Kim

Abstract

Highly Resilient Hydrogel Adhesives

Based on Dopamine-Modified Crosslinking Agents

Gi-Yeon Han
Program in Environmental Materials Science
Graduate School
Seoul National University

Every year, more than a million people in the world experience various wounds due to traumatic incidents, surgical incisions, and diabetic ulcers. Traditionally, invasive techniques such as sutures, staples, clips, and skin closure strips are the gold standard for wound closure and restoring tissue structure and function. Among them, sutures are preferred for deeper wounds due to their flexibility and ease of use, and they do not require removal after the wound has healed. However, sutures have several limitations, including the risk of infection, granuloma formation, the inherent length of the suturing process, anesthesia requirements, and skilled by trained personnel requirements. Therefore, the use of tissue adhesives has attracted the attention of scientists and industries because of several advantages, such as blood leakage prevention, less pain, less surgery time, infection mitigation, non-requirement for removal procedures, and minimally invasive surgery.

Recently, hydrogel-based tissue adhesives have gained the attention of scientists and industries as alternatives to sutures for sealing and closing wounds or incisions because of their similarity to biological tissues, ease of use, and short application

time. Various functionalities of hydrogel adhesives, such as hemostasis, cell adhesion, anti-microbial, and anti-inflammatory properties, make them promising materials for applications in wound dressing and tissue engineering. However, poor mechanical properties and weak adhesion limit the application of hydrogel adhesives. Poor interface adhesion between a hydrogel and wound increases the risk of infections and delays tissue regeneration, and the low mechanical resilience of hydrogels limits wound dressing in movable parts where a large range of motion occurs.

In this study, the dopamine-modified oligomers were designed and applied as crosslinking agents to fabricate hydrogel adhesives. To manufacture a hydrogel with high mechanical resilience, robust tissue adhesion, and biocompatibility, dopamine-modified crosslinking agents were designed to have the following structural characteristics: 1) The end group of oligomers was functionalized with acrylate, 2) incorporating multiple dopamine molecules with short intervals, 3) hydrolyzable ester bonds. Both ends of the oligomer were functionalized with acrylate, which acts as a crosslinking agent. The short intervals between dopamine molecules enable crosslinking agents to be associated in the hydrogel network through reversible physical interactions of dopamine, such as hydrogen bonds and hydrophobic interactions. Therefore, this structure enables hydrogel to dissipate energy and exhibits mechanical resilience. The high dopamine content due to the crosslinking agent enables hydrogel to form robust tissue adhesion through physical and chemical intermolecular interactions, such as hydrogel bonds, Schiff-base reaction, and the Michael addition reaction of dopamine. Finally, the ester bond in a dopamine-modified crosslinking agent makes fabricated hydrogel using a dopamine-modified crosslinking agent hydrolyzable under physiological conditions.

Moreover, after optimizing the hydrogel system using a dopamine-modified crosslinking agent, the toughness of hydrogel was enhanced through the modification of the structures of the dopamine-modified crosslinking agent and hydrogel network. By modifying the backbone of the dopamine-modified crosslinking agent to a bulkier backbone, the stretchability of the hydrogel adhesive was dramatically enhanced. By modifying the network structure of hydrogel from a single network to a double network, the toughness of the hydrogel adhesive was enhanced.

In this study, we successfully developed a stretchable and highly resilient hydrogel adhesive with robust adhesion. By introducing a dopamine-modified crosslinking agent and a double network structure, a hydrogel adhesive with a well-balanced combination of tissue adhesion, toughness, and mechanical resilience, which are typically negatively correlated, was fabricated. Furthermore, hydrolyzable ester bonds in the crosslinking agent enable the hydrogel adhesive to degrade under physiological conditions. Through these characteristics, the resultant hydrogel adhesives exhibit the potential to be used as wound-sealing patches in movable parts. This study provides a straightforward method to develop functional hydrogels using only a crosslinking agent, which can be potentially applied to electronic skins, sensors, and tissue scaffolds beyond the wound dressing materials.

Keywords: Hydrogel Adhesives, Crosslinking Agents, Dopamine, Mechanical Resilience, Wound Sealing Patches

Student Number: 2019–24629

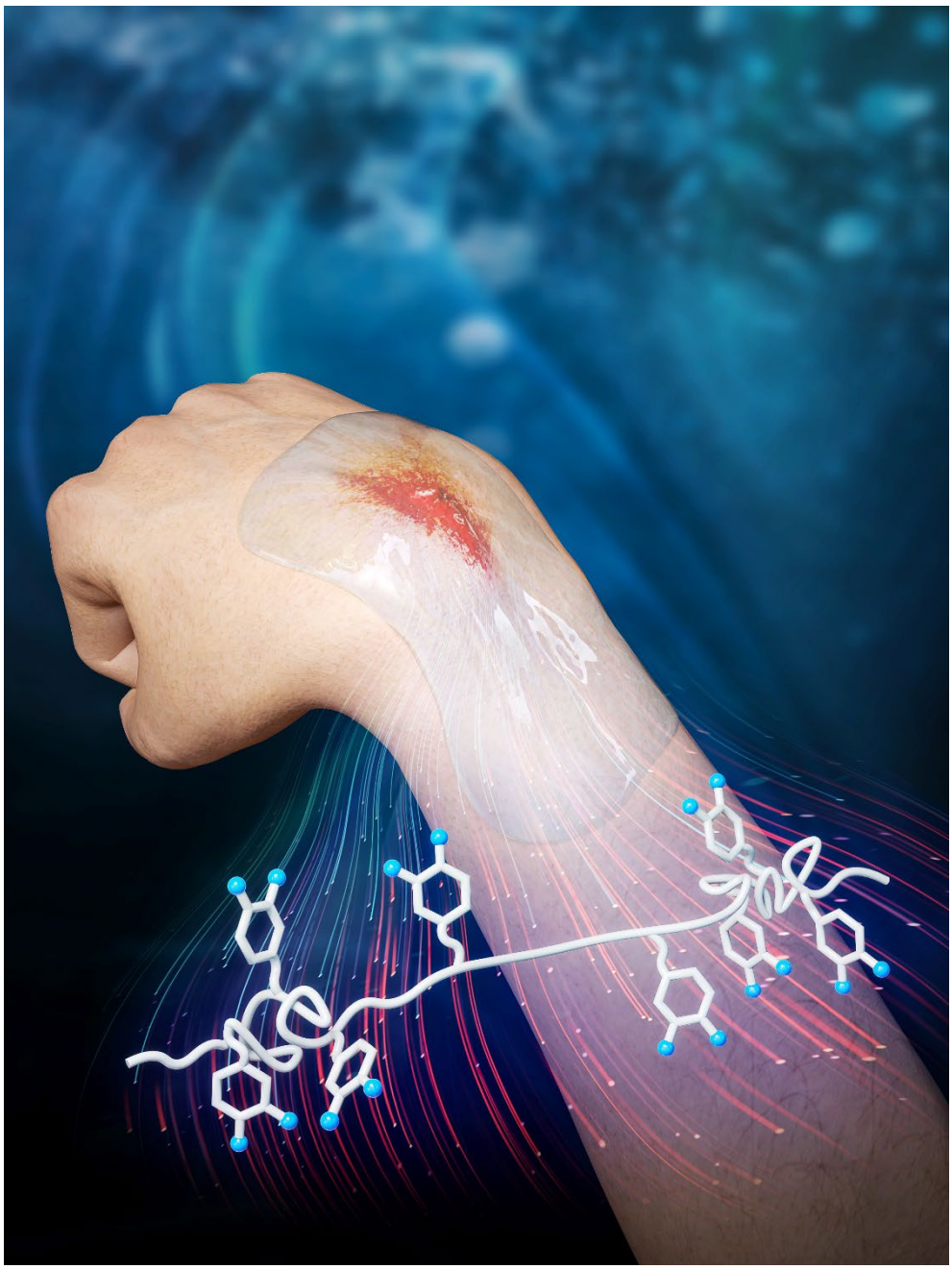

Table of Contents

Highly Resilient Hydrogel Adhesives

Toughness Enhanced Hydrogel Adhesives

List of Tables

List of Figures

Introduction

1. Research Background

1.1. Hydrogels

1.1.1. Characteristics of Hydrogels

Hydrogel is a three–dimensional crosslinked hydrophilic polymeric network infiltrated with a large amount of water (50~90%). The crosslinked network structure of hydrogels results in a transformable and interconnected network structure with various mechanical properties and length scales from nano - to macroscopic dimensions (Zhao*, et al.*, 2021). These characteristics of the hydrogels allow them to be applied in various fields, such as agriculture and food chemistry, environmental engineering, medicine, and tissue engineering (Dai*, et al.*, 2015, Liu*, et al.*, 2020, Wang*, et al.*, 2022, Yahia, 2015). In particular, in biomedical fields, hydrogels have received significant attention due to their high similarity to biological tissue; therefore, hydrogels are used as biomaterials, such as contact lenses, drug delivery carriers, and wound dressing materials (Cheng*, et al.*, 2022, Ma*, et al.*, 2014, Pinnaratip*, et al.*, 2019).

The hydrogel can be divided into three generations based on a historical classification (Cascone*, et al.*, 2020, El-Sherbiny*, et al.*, 2018). First–generation hydrogel is covalently crosslinked hydrogel with high water content. The first–generation hydrogels were simply made by free radical polymerization of vinyl or acrylate monomers [such as poly(ethylene glycol), poly(hydroxyethyl methacrylate), and poly(vinyl alcohol)] **(Figure 1a)**. The second–generation hydrogel is an energy

transfer hydrogel that can change chemical energy into mechanical work. These stimuli–responsive hydrogels respond to pH, temperature, light, and magnetic fields, and by these external stimuli, the hydrogel can trigger specific events such as gel formation, drug release, and polymer erosion (Ahmed, 2015). Representatives include, temperature–responsive poly(*N*–isopropyl acrylamide), poly(*N*–2–hydroxypropyl acrylamide) hydrogels, pH–sensitive poly(acrylic acid) and poly(acryl amide) hydrogels. Furthermore, glucose–sensitive biomolecules and protein hydrogels have been used as drug delivery carriers **(Figure 1b)**. Third–generation hydrogels are stereo–complex hydrogels that include complex formation, metal–ligand coordination, and peptide interactions. The physical properties of the hydrogels are modified through stereoselective interactions between polymers and reactive functional moieties. Representative examples include thermo–responsive Poloxamer [poly(ethylene glycol)– poly(propylene glycol)– poly(ethylene glycol) block copolymer], catechol, which can undergo complex formation with metal, and cyclodextrins, which contain a hydrophobic cavity that can host diverse molecules **(Figure 1c)**.

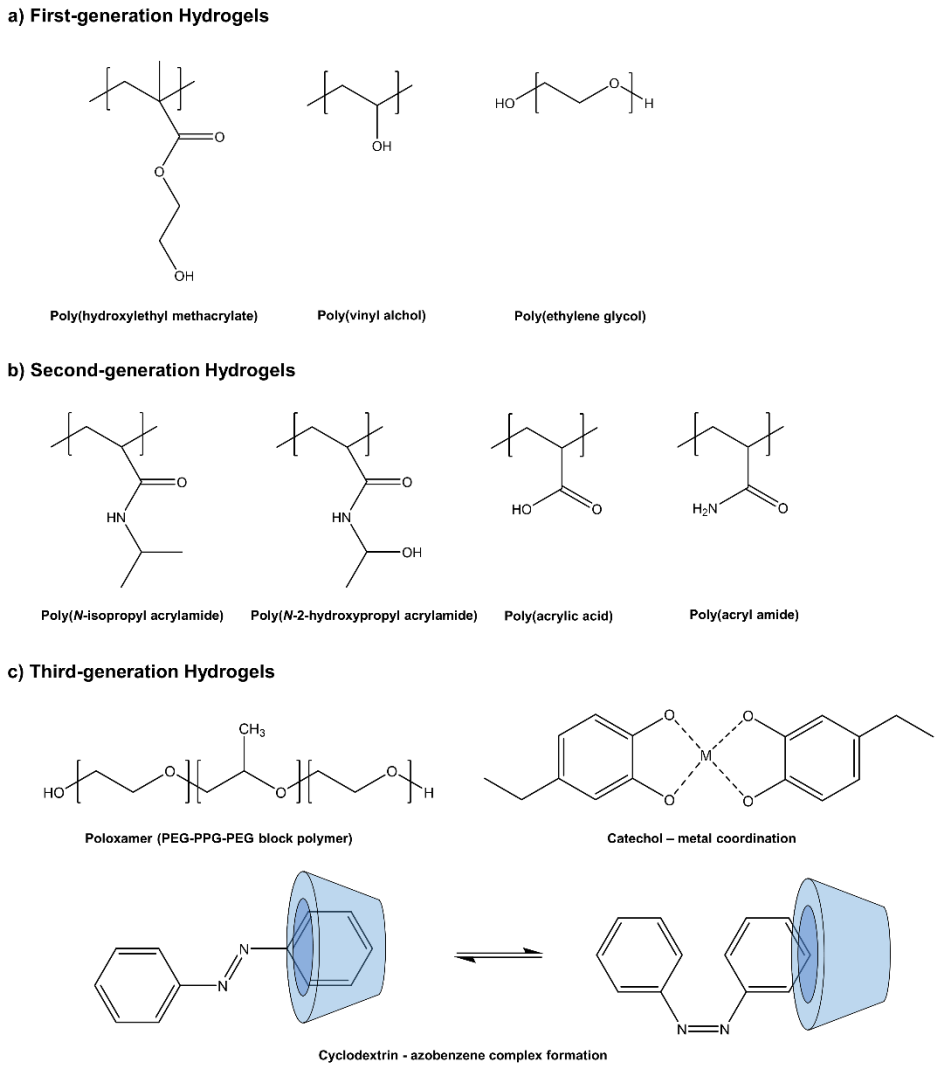

Figure 1. Classification of polymers and reactive moieties used for hydrogels in the a) first, b) second, and c) third generations.

Recently, by introducing diverse synthetic techniques and reactive functional groups in hydrogels, the mechanical properties and functionalities of the hydrogel have been dramatically enhanced. Examples include the following: 1) highly stretchable, tough hydrogels using multiple network structures **(Figure 2a)** (Chen*, et al.*, 2021). 2) Self–healable hydrogels using reversible bonds and intermolecular interactions **(Figure 2b)** (Ren*, et al.*, 2019). 3) Conductive hydrogels using conductive nanofibrils **(Figure 2c)** (Han*, et al.*, 2018). 4) Crack propagation resistance tough hydrogels using microspheres **(Figure 2d)** (Li*, et al.*, 2022).

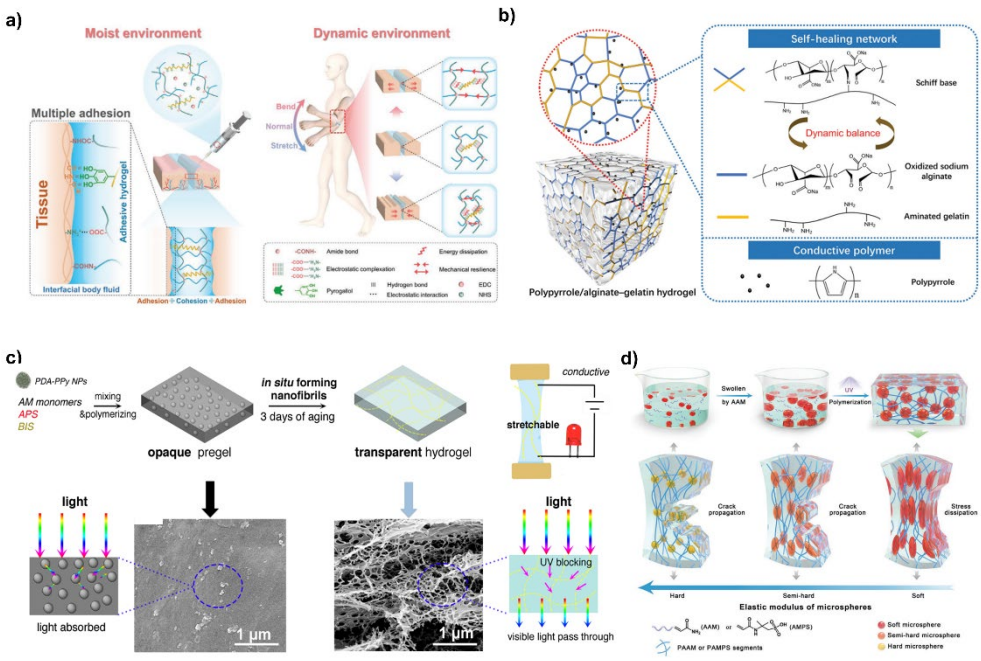

Figure 2. Reported multifunctional hydrogels with high mechanical properties. a) Highly stretchable adhesive, b) self–healable, c) conductive, and d) tough hydrogels.

(Adapted from Chen, et al., 2021, Ren, et al., 2019, Han, et al., 2018, Li, et al., 2018, with permission from John Wiley and Sons, Royal Society of Chemistry, American Chemical Society)

1.1.2. Network Structure of Hydrogels

Hydrogels are covalently or physically crosslinked soft materials. By controlling the crosslinking density of the hydrogel, the mechanical properties of the hydrogel can be controlled. However, conventional hydrogels, composed of a single network structure, have limitations in control of mechanical properties. Usually, the single network structure hydrogels fail less than 100% elongation and sub–MPa (Gong, 2010). Single network hydrogels exhibit low mechanical properties compared to load–bearing soft tissues such as cartilage and muscle, which exhibit flexibility, high toughness, and low sliding friction despite comprising 30~80% water.

Multiple–network/crosslinked/architecture hydrogels are developed to overcome these limitations inspired by the load–bearing soft tissues. These hydrogels contain a combination of 1) covalent, non–covalent, and reversible dynamic bonds, 2) crystalline and amorphous network structures, and 3) natural and synthetic polymer networks. The multiple–network/crosslinked/architecture hydrogels comprise a structure maintaining rigid/hard moieties and energy dissipating flexible/soft moieties. When the mechanical load is applied to the materials, flexible soft moieties dissipate energy by being destroyed first, and the rigid/hard moieties impart the elasticity of hydrogel (Sun*, et al.*, 2013). Then, when a higher load is applied to the extent that the rigid/hard moieties are destroyed, these destroyed moieties can act as a crosslinking point of the flexible/soft moieties **(Figure 3a)** (Gong, 2010). Therefore, complex structure hydrogels exhibit dramatically increased tensile strength, toughness (over 1,000% strain and several MPa), and other mechanical properties such as crack propagation resistance **(Figure 3b)** (Chen*, et al.*, 2015).

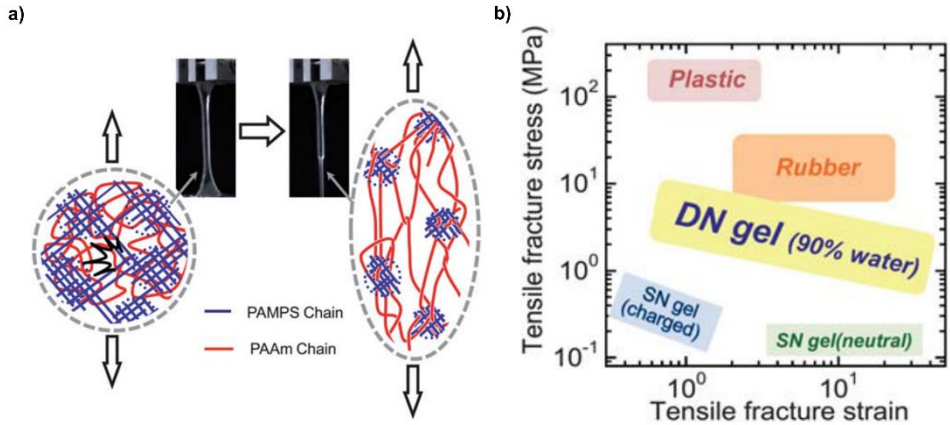

Figure 3. a) Change in the network structure of the multiple network hydrogel when a load is applied. b) Comparison of the mechanical strength of diverse polymeric materials.

(Adapted from J. P. Gong, 2010, with permission from Royal Society of Chemistry)

Sun *et al*. reported a physically crosslinked hydrogel composed of polyampholytes. They designed a hydrogel with weak and strong ionic bondable moieties in the polymer. These ionic combinations make hydrogel exhibit high toughness with elasticity (Sun, *et al.*, 2013). Fang et al. reported that the hydrophobic domain contained hydrogel. They fabricated a hydrogel using 4–carboxybenzaldehyde, which can form reversible bonds through hydrogen bonds and hydrophobic interaction. Through this moiety, the resultant hydrogel exhibits high elasticity and self–healability (Liu, *et al.*, 2022). Liu et al. reported a topoarchitectured polymer network. They embedded hard blocks in the soft matrix by sequential polymerization and photolithography (Fang, *et al.*, 2020). Chen *et al*. reported a poly(ethylene glycol)–based double network hydrogel. They added a diffusive long linear poly(ethylene glycol) chain. These long chains were entangled in a hydrogel network and could diffuse in the substrate. Therefore, the resultant hydrogel exhibits high stretchability and adhesion properties (Chen, *et al.*, 2019).

1.1.3. Hydrogel Adhesives for Biomedical Applications

The use of hydrogel adhesives (or tissue adhesives) as a replacement for sutures and staples to close and seal incisions or wounds has received significant attention. Compared to traditional suturing and stapling, hydrogel wound dressing requires less surgery time and prevents secondary tissue damage (Bertsch*, et al.*, 2022, Freedman*, et al.*, 2021). Moreover, hydrogel adhesives should meet the following properties to serve as a substitute for sutures and staples (Nam*, et al.*, 2021, Scognamiglio*, et al.*, 2016, Yilmaz*, et al.*, 2011).

1) Biocompatibility with non–local irritation, anti–inflammatory activity, non–toxicity, and non–antigenicity
2) Straightforward applicability on the target tissue surface
3) Biodegradability after exerting their functions
4) Occurrence of the reticulation process in the presence of body fluids in a short timespan, based on the operation requirements
5) Flexibility similar to the target tissue to follow expansion/contraction based on the physiological conditions of the target tissue
6) A strong binding efficacy to ensure adequate mechanical properties
7) Maintenance of bonding in a wet physiological environment.

Diverse synthetic and natural polymer–based hydrogel adhesives have been reported, but each adhesive has pros and cons. Synthetic adhesives such as poly(cyanoacrylate), polyurethane, and poly(ethylene glycol) exhibit strong mechanical and adhesion strength but exhibit low biocompatibility **(Figure 4a)**. In the case of natural polymer–based adhesives such as fibrin and albumin exhibit high biocompatibility, but exhibit low mechanical and adhesion strength **(Figure 4b)**. Recently, synthetic/natural polymer complex network structures and reactive functional groups have been introduced to the hydrogels to fabricate hydrogel adhesives with high mechanical strength and biocompatibility.

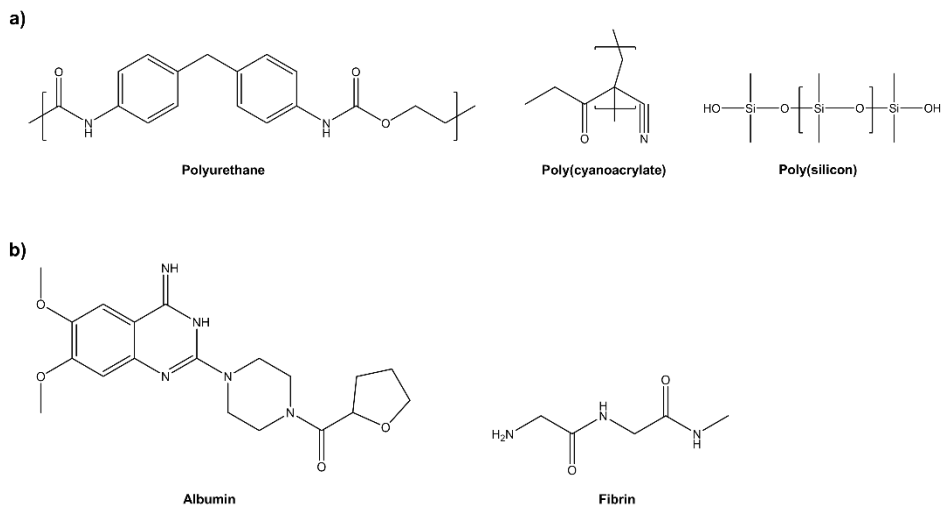

Figure 4. Classification of hydrogel adhesives. a) Synthetic polymer– and b) natural polymer–based hydrogel adhesives.

1.2. Underwater Adhesion

1.2.1. Underwater Adhesion Strategies

Adhesion occurs through interactions between adhesives and the adherend. Various chemical and physical interactions such as Van der Waals interaction, hydrogen bonding, mechanical interlocking, and chain entanglement **(Figure 5a)** affect adhesion. For robust adhesion, adhesives are wetted well on the adherend and then interact with it enough. However, when water exists at the surface of the adhesive or adherend (underwater conditions), the water layer is formed at the interface. The water layer at the interface interferes with the wetting of the adhesive and the direct contact between the adhesive and the adherend. Moreover, there is a risk that water molecules penetrate the adhesive material and cause swelling or decomposition.

Several strategies have been introduced to remove water on the surface for favorable underwater adhesion. Hydrophobic moieties or polyampholytes are introduced into the polymer to repel water. A filler is added to absorb water at the interface. A water drainage channel is fabricated at the surface of the adhesive **(Figure 5b)** (Fan*, et al.*, 2021). Recently, the dry state of hydrophilic polymeric film has been applied to absorb water and adhere simultaneously (Yuk*, et al.*, 2019). Water–repellent silicon oil and functional groups that induce reactions through water on the surface have also been introduced (Singh*, et al.*, 2024, Yuk*, et al.*, 2021).

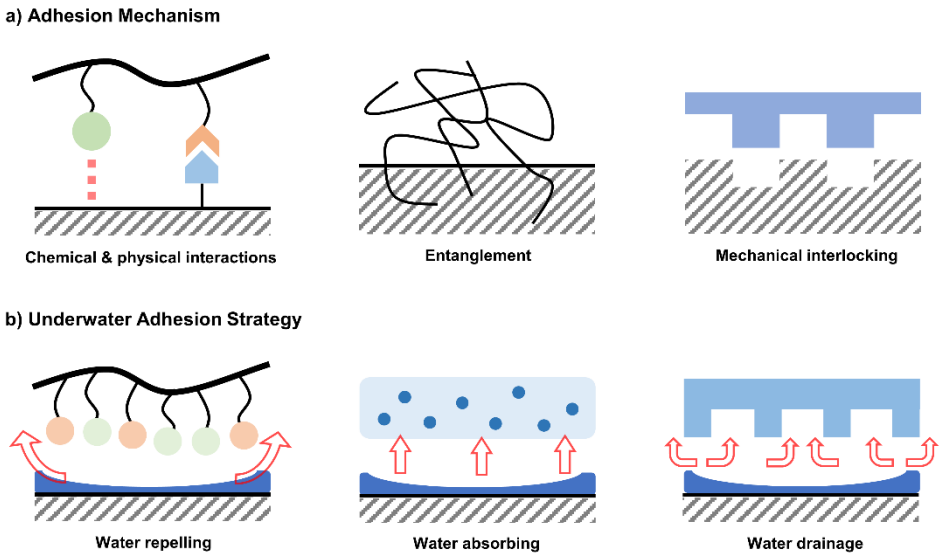

Figure 5. a) Principal adhesion mechanism and b) adhesion strategy in the underwater environments.

1.2.2. Surface Energy of Hydrogel Adhesives

The hydrogel adhesives intake a lot of water. Therefore, a hydrogel adhesive exhibits a different adhesion mechanism compared to a dry adhesive (Zhang*, et al.*, 2020). From the point of view of surface energy, the work of adhesion (ω) of dry adhesive can be expressed under equation (1).

$$\omega = \gamma_{adhesive} + \gamma_{substrate} - \gamma_{interface} \qquad (1)$$

Where γ represents the surface energy.

The surface energy of adhesives is different due to their intake of water. The work of adhesion of the hydrogel adhesive can be expressed under equations (2) and (3).

$$\omega = \gamma_{hydrogel} + \gamma_{substrate} - \gamma_{interface} \qquad (2)$$

$$\gamma_{hydrogel} = \Phi_s \gamma_{network} - (1 - \Phi_s) \gamma_{water} \qquad (3)$$

Where Φ_s represents the polymer content of the gel.

As shown in equation (3), the water content of hydrogel is affected significantly. When a significant amount of water ($\Phi_s \fallingdotseq 0$) is present in the hydrogel matrix, the surface energy of hydrogel is similar to the surface energy of water (i.e., $\gamma_{hydrogel} \fallingdotseq \gamma_{water}$). Therefore, when designing hydrogel adhesives, the type of monomer and filler, the structure of the polymer matrix, and molecular interactions between water, the matrix, and the substrate have to be considered.

1.2.3. Physical Adhesion Mechanisms

Physical intermolecular interactions are essential for initial adhesion. Hydrogen bonding, van der Waals forces, and electrostatic interactions are the fundamental interactions that affect adhesion. These interactions can simply be induced by introducing polar functional groups. Moreover, adhesion can occur in direct interactions such as mechanical interlocking and chain entanglement.

1) Hydrogen bonding and electrostatic interactions

The hydrogen bond is an interaction that occurs between a proton donor and a proton acceptor species. In the hydrogels, acrylic acid, acrylamide, and vinyl alcohol are commonly used due to their polar functional groups (carboxylic acid, amide, and hydroxyl groups, respectively), which can form hydrogen bonds with water (i.e., hydrophilic). Moreover, these polar monomers can form hydrogen bonds with substrates and exhibit highly adhesive properties. In the hydrogel adhesives, catechol and gallol groups, which have two and three hydroxyl groups at the benzene ring, respectively, are widely used as a functional group for underwater adhesion. The catechol and gallol groups containing hydrogel adhesives exhibit high adhesiveness through their multiple hydroxyl groups. Electrostatic interactions occur between oppositely charged molecules. Electrostatic interactions are most easily observed among polar molecules containing carboxylic acid and amine groups. Moreover, the polyampholyte (contains anion and cation moieties in the polymer) and zwitterionic (contains anion and cation moieties in one molecule) moieties are introduced in hydrogels for multi–functionality such as anti–cell adhesion, conductive, and shape–memory properties (Sun*, et al.*, 2013, Zhang*, et al.*, 2021). Zhao et al. fabricated

biocomponent adhesives based on lysine–rich recombinant proteins. They fabricated a lysine–rich engineered protein (LEP) adhesive through crosslinking between lysine–rich protein, glutaraldehyde, and oxidized hyaluronic acid. LEP exhibited high tissue adhesion due to the hydrogen and electrostatic bonds between amine groups in lysine and the tissue surface, and carboxylic acid groups in the oxidized hyaluronic acid **(Figure 6a)** (Zhao*, et al.*, 2023). Choi et al. constructed a densely assembled network hydrogel using green tea extracts such as epigallocatechin gallate and catechin. Through the dynamic and reversible hydrogen bonding, the hydrogel exhibited high tissue adhesion with strain tolerance (Choi*, et al.*, 2022). Wang et al. reported a tough hydrogel adhesive based on hydrogen bonding and electrostatic interactions. Carboxylic acid and imidazole groups can interact with each other and the tissue surface, thereby exhibiting excellent toughness and adhesiveness **(Figure 6b)** (Wang*, et al.*, 2022).

2) Mechanical Interlocking and Chain Entanglement

Mechanical interlocking is a method for increasing adhesion strength by expanding the adhesion surface area. This method can be achieved by wetting the adhesive into the irregularities of a rough r patterned surface. Yang et al. introduced a biphasic microneedle with a non–swellable core and swellable tip at the adhesive surface for mechanical interlocking. By introducing this needle, the adhesive could penetrate the soft tissue surface, and this caused a swellable tip interlocking with the dermis (Yang*, et al.*, 2013). The diffusion of polymer chains can lead to chain entanglement between dissimilar materials. The diffusion of the chain occurs through capillary action and electrostatic interactions. Chain diffusion is affected by molecular weight, chain length, and chain concentrations **(Figure 6c)** (Mansuri*, et al.*, 2016). The most widely used diffusive polymer in the biomedical field is chitosan. Ying et al. used

chitosan as a bridging polymer. Chitosan can be absorbed by the target surface through electrostatic interactions and then form physical entanglements. Through these bridging polymers, their hydrogels exhibit high adhesion energy at various tissue and polymeric surfaces (Ying*, et al.*, 2021).

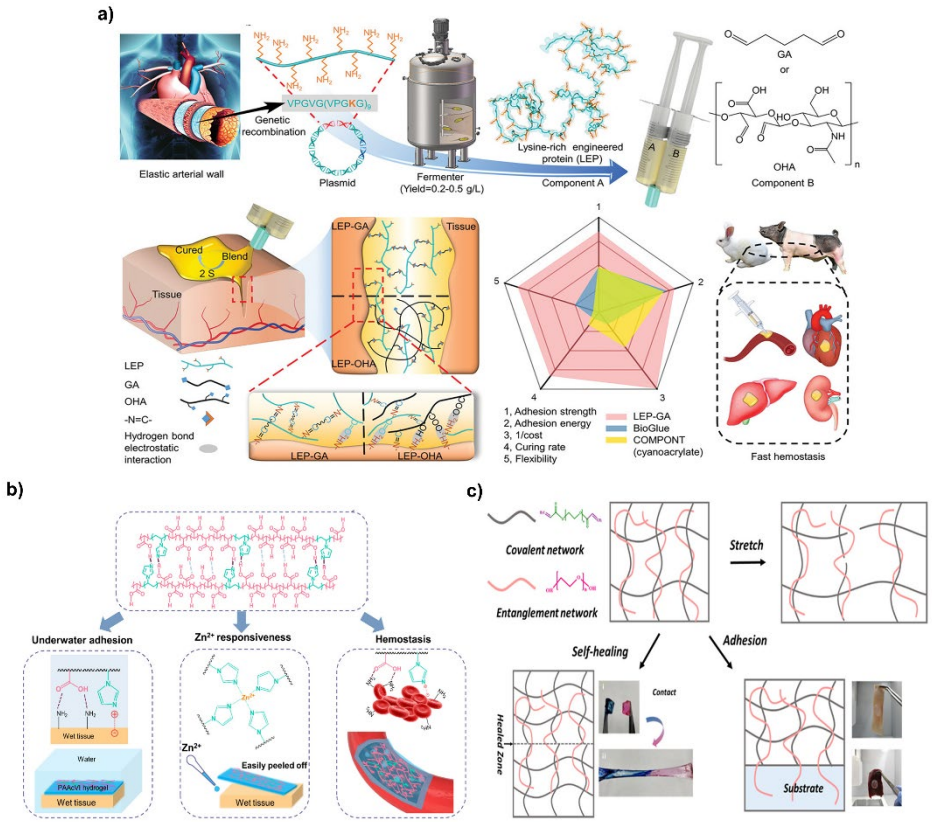

Figure 6. Physical adhesion mechanisms. a), b) Hydrogen bonds and electrostatic interactions. c) Chain entanglements

(Adapted from Zhao, *et al*., 2023, Wang, *et al*., 2022, Han, *et al*., 2018, Chen, *et al*., 2019, with permission from John Wiley and Sons, American Chemical Society)

1.2.4. Chemical Adhesion Mechanisms

Chemical crosslinking is stronger than physical interactions and can form robust adhesion between the adhesive and the substrate. Chemical crosslinking reactions are of many types. Among them, amide–based crosslinking reactions are used for tissue adhesives because biological tissue contains a large amount of amide groups. Moreover, various interactions between biomolecules during the metabolic process of organisms are possible mechanisms for tissue adhesion (Shokrani*, et al.*, 2022). Tissue adhesion can occur under mild conditions without any specific pH and temperature.

1) Carbodiimide Coupling and Imine Reactions

A carbodiimide coupling reaction occurs between carboxyl and amine groups **(Figure 7a)**, and an imine coupling reaction occurs between an aldehyde or ketone and an amine **(Figure 7b)**. The imine coupling reaction is also called the Schiff base reaction. Both types of coupling reactions have been widely used. Cintron–Cruz *et al*. achieved additional tissue adhesion strength through carbodiimide coupling reactions of chitosan. They performed the robust adhesion through a carbodiimide reaction between topologically entangled chitosan and an alginate adherend (Cintron-Cruz*, et al.*, 2022). Wu *et al*. incorporated *N*–hydroxysuccinimide (NHS) ester groups in the adhesive, and the NHS ester group formed covalent bonds through a carbodiimide reaction. Therefore, the NHS ester group containing adhesives exhibited robust and long–term stable tissue adhesiveness (Wu*, et al.*, 2021). Ma *et al*. introduced O–nitrobenzene in chitosan to fabricate photo–responsive hydrogel adhesives. Under UV irradiation, O–nitrobenzene was converted into O–

nitrobenzylaldehyde, and the aldehyde group formed crosslinks with the amine groups of chitosan and the tissue surface through an imine reaction (Ma*, et al.*, 2020).

2) Michael Addition Reaction

The Michael addition reaction occurs between a Michael donor (amine or thiol group) and a Michael acceptor (vinyl or acrylate group) **(Figure 7c)**. This reaction is commonly observed in catechol chemistry. When a dopamine molecule is oxidized to the quinone form, an amine or a thiol can form a covalent bond through the Michael coupling reaction (Salazar*, et al.*, 2016). Moreover, this reaction is used to crosslink bioadhesives. Shin et al. grafted dopamine on chitosan for use as the sealing and hemostatic agent. The grafted dopamine molecules form crosslinks with the amine groups of chitosan and the tissue. They suggested that the dopamine–grafted film exhibited a self–sealing property (Shin*, et al.*, 2017).

3) Biological Interactions

The interactions that occur in living organisms can act as adhesion mechanisms. Representatively, the disulfide bond, thrombin–fibrinogen, and avidin–biotin interactions exist. 1) The disulfide bonds are frequently observed in protein interactions. The formation of disulfide bonds during protein–protein interactions is critical in the initial folding, refolding, regulation of biological function, and stabilization of proteins (Adams, 2023). 2) The thrombin–fibrinogen interactions are observed during the blood coagulation stage. Thrombin induces the conversion of fibrinogen to fibrin, which forms a firm clot in the presence of the coagulation factor

FXIII (Wang*, et al.*, 2022). Therefore, the thrombin–fibrinogen interaction has been used as the main interaction of the hemostasis agent. 3) The avidin–botin interaction is strong and specific. Therefore, the avidin–biotin interaction has been applied in immunoassays, diagnostics, chromatography, drug delivery, cell culture, and tissue engineering (Tsai*, et al.*, 2005).

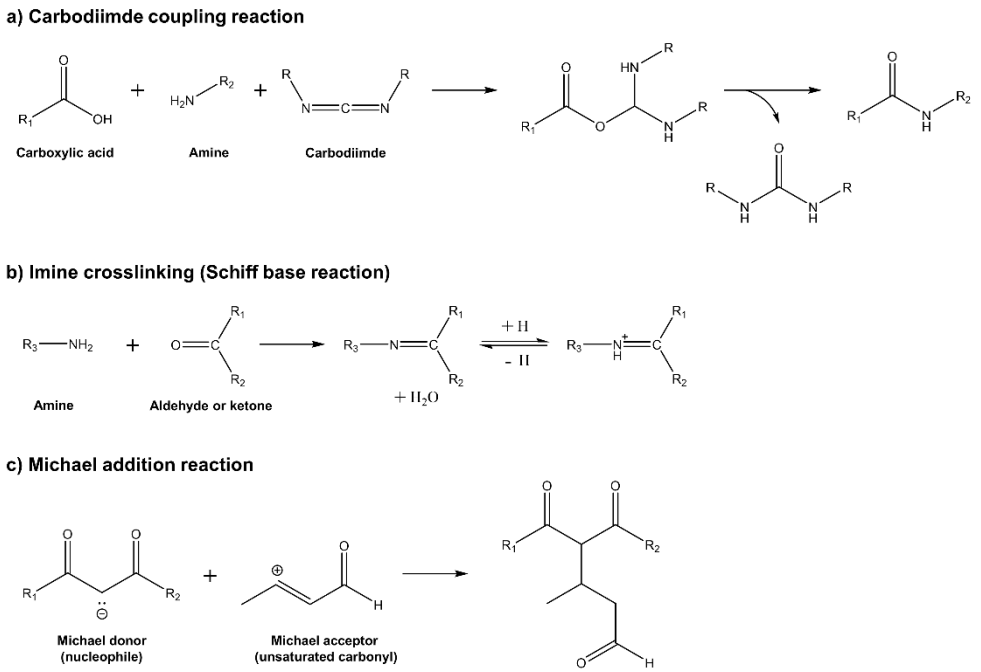

Figure 7. Chemical adhesion interactions. a) Carbodiimide interactions, b) imine crosslinking, and c) Michael addition reaction.

1.3. Catechol Chemistry

1.3.1. Catechol Chemistry

Inspired by marine organisms such as mytilus mussels, barnacles, and sandcastle worms, which can adhere to submerged substrates under harsh and wet conditions, researchers are looking into underwater adhesion chemistry. These marine organisms secrete several types of proteins to glue on calcareous–base rigid substrates. Researchers have observed that a catecholic amino acid (hydroxylated tyrosine), known as 3,4–dihydroxy–L–phenylalanine (L–DOPA, dopamine), can activate adhesion (Hofman*, et al.*, 2018). Dopamine is a catechol amine with a hydrophilic di–hydroxyl group and a hydrophobic benzene ring. The unique chemical structure of dopamine can participate in various interactions, including physical interactions such as hydrophobic interaction, π– π stacking, π–cation interaction, metal coordination, and hydrogen bonding **(Figure 8a)**. Moreover, when dopamine is exposed to base conditions (pH > 7), it changes to a quinone form **(Figure 8b)**. Quinone has a much lower surface affinity and hydrogen bond capability to form covalent bonds such as through Michael addition, Schiff base reaction, and dopa–quinone coupling **(Figure 8c)** (Zhang*, et al.*, 2020). In particular, the hydrophobic benzene ring can balance hydrophobic–hydrophilic balances,(Liu*, et al.*, 2022) stabilizing hydrogen bonds(Tamai*, et al.*, 1996) and repelling water at the surface of the substrate. Due to their rich and versatile chemistry, researchers have explored applying synthetic dopamine as an underwater adhesive. When dopamine molecules are introduced into the polymer, these various dopamine interactions can enable surface adhesion and enhance the cohesion of polymers.

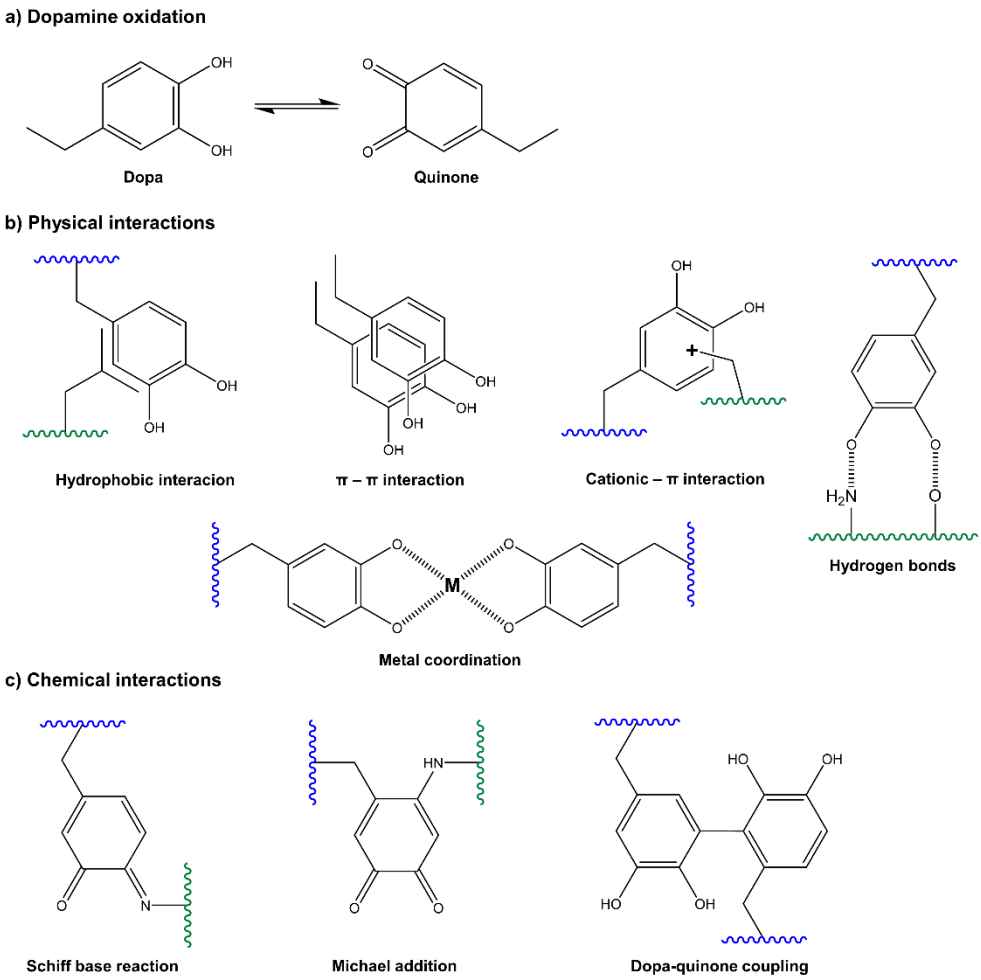

Figure 8. Chemical structure of a) dopamine and quinone. b) Physical interactions that dopamine can form. c) Chemical interactions that quinone can form.

1.3.2. Coacervation

Catechol in the mussel–foot protein is the main functional moiety affecting underwater adhesion **(Figure 9a)** (Wei*, et al.*, 2014). The adhesion process through catechol chemistry involves three synergistic processes; 1) surface spreading/drying, 2) coacervation, and 3) phase inversion (Yang*, et al.*, 2014). First, the water is spread on the surface by coacervation. Coacervation is liquid–liquid phase separation caused by the association (intermolecular interactions) of different molecules upon aqueous mixing. When a catechol–containing protein is submerged in water, hydrophobic, π– π stacking, π–cation interactions, and hydrogen bonding occur and promote coacervation **(Figure 9b)**. Second, catechol groups react with the target surface through intermolecular interactions such as hydrogen bonding, metal coordination, π– π stacking, and oxidation. The catechol group can instantly adhere to the target surface through these interactions. Finally, oxidation (i.e., dopamine–quinone coupling) and Michael addition reactions occur due to external stimuli such as pH change or the addition of a metal. These intermolecular interactions can solidify the catechol–containing materials, thereby leading to stronger adhesion.

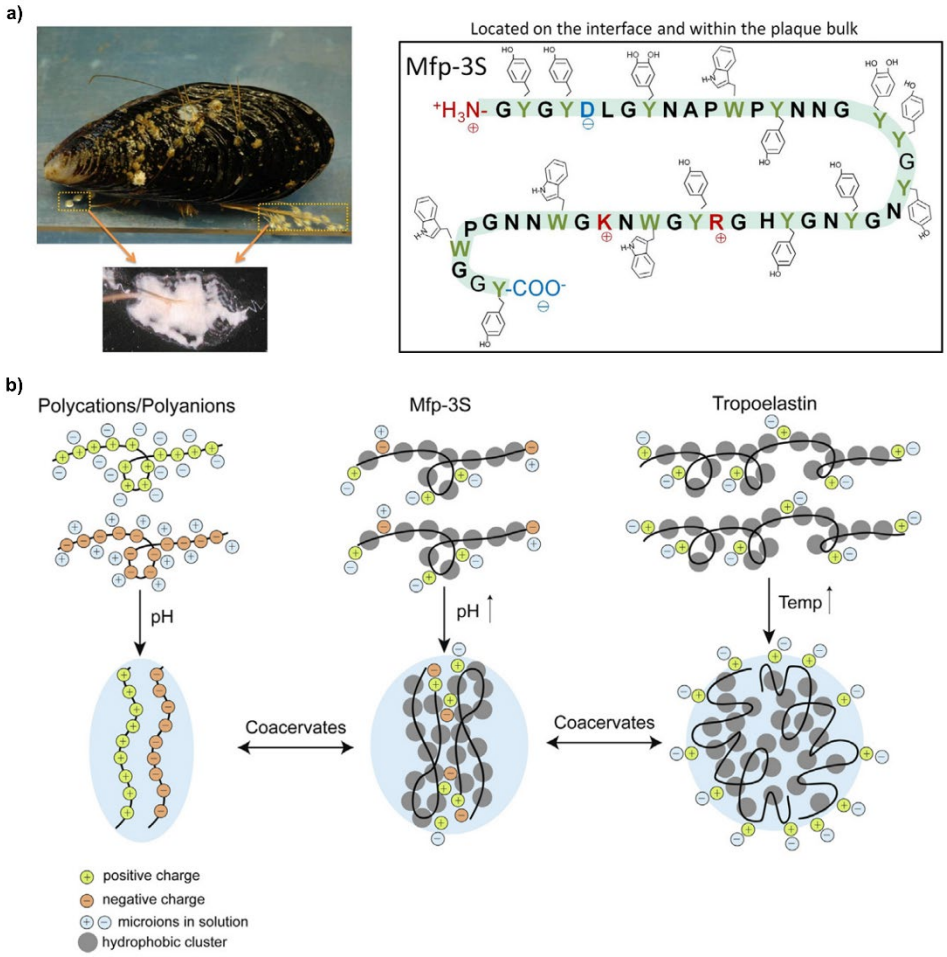

Figure 9. a) Images and chemical structure of mussel–foot protein. b) Schematic illustration of the coacervate formation process.

(Adapted from Wei, *et al*., 2014 with permission from Elsevier)

1.3.3. Catechol–Inspired Hydrogel Adhesives

Mussel–inspired hydrogel adhesives have drawn considerable attention as biological adhesives. These hydrogel adhesives can adhere to various surfaces in a moist environment and have favorable cell affinity. In recent years, dopamine–based stretchable and self–healable hydrogel adhesives have been reported using reversible intermolecular interactions of dopamine (Liu*, et al.*, 2022, Patil*, et al.*, 2015, Ryu*, et al.*, 2011, Xie*, et al.*, 2020). The dopamine network forms a physically crosslinked network, and this network dissipates and redistributes energy effectively when the strain is applied.

Dopamine is generally introduced into the polymer network in the form of polydopamine. Han et al. reported stretchable hydrogel adhesives by introducing polydopamine networks. They fabricate polydopamine networks by dopamine oxidation via O_2 (Han*, et al.*, 2017) **(Figure 10a)**. Yang et al. reported highly stretchable hydrogel adhesives using bacterial cellulose and polydopamine. They fabricated polydopamine networks through dopamine oxidation via ammonium persulfate (Yang*, et al.*, 2021) **(Figure 10b)**. Xue et al. introduced polydopamine networks by electrical oxidization. By using electrical oxidization methods, dopamine was oxidized without toxic oxidizing agents and the reaction was controlled (Xue*, et al.*, 2021) **(Figure 10c)**.

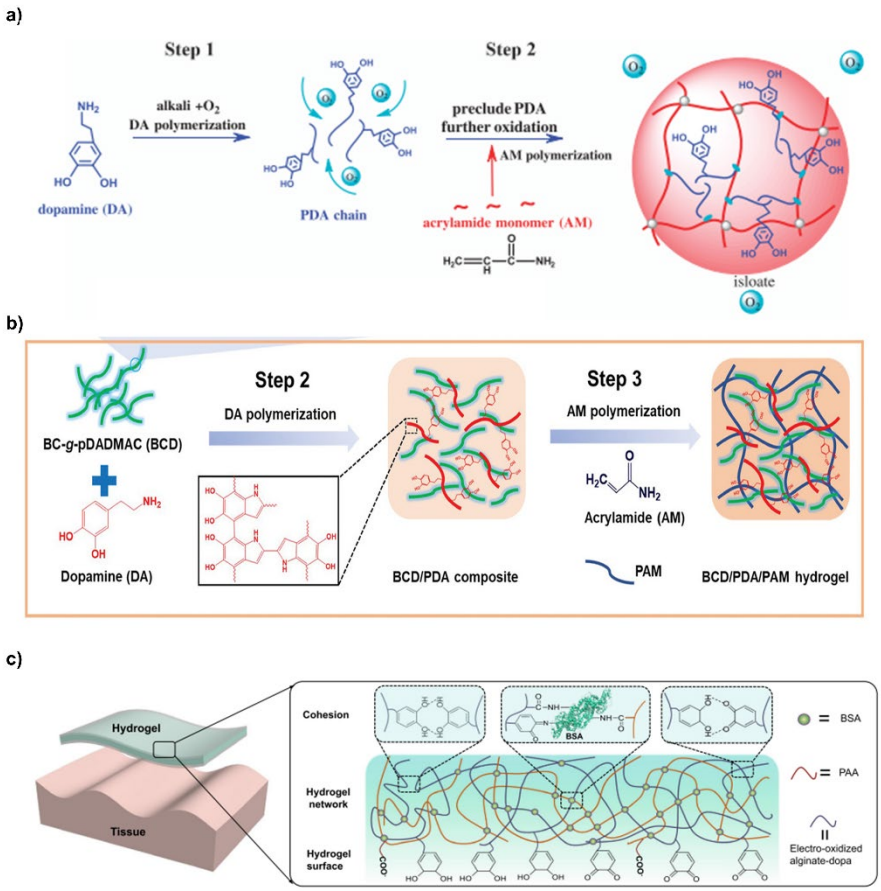

Figure 10. Hydrogel adhesives with polydopamine network. The polydopamine network is formed using a) alkali and O_2, b) ammonium persulfate, and c) electro oxidization.

(Adapted from Han, *et al*., 2017, Yang, *et al*., 2021, and Xue, *et al*., 2021, with permission from Springer Nature and John Wiley and Sons)

By adding nano clay or iron ions, dopamine networks can be fabricated without oxidizing agents. Liu et al. mixed Laponite with dopamine-grafted poly(ethylene glycol). The dopamine molecule forms a hydrogen bond and undergoes a dispersion interaction with the silica oxide of nanosilicate, resulting in the crosslinked networks (Liu*, et al.*, 2017) **(Figure 11a)**. Han et al. introduce polydopamine-intercalated clay nanosheets. Through the addition of clay nanosheets, dopamine was intercalated into clay nanosheets and limitedly oxidized between the layers (Han*, et al.*, 2017) **(Figure 11b)**. Hou et al. introduced ferric ions and dopamine. Dopamine forms a metal complex with ferric ions, and this complex is reversible according to pH (Holten-Andersen*, et al.*, 2011). Therefore, resultant hydrogel adhesives demonstrate re-formability and self-healability (Hou*, et al.*, 2015) **(Figure 11c)**. Another method to fabricate a dopamine network is grafting on the polymer backbone. Xie et al. grafted dopamine on carboxymethyl cellulose and the resultant hydrogel demonstrated high wet tissue adhesion (Xie*, et al.*, 2024) **(Figure 12a)**.Wang et al. reported self–healable hydrogel adhesives using dopamine–grafted dextran and poly(L–glutamic acid) (Wang*, et al.*, 2021) **(Figure 12b)**.

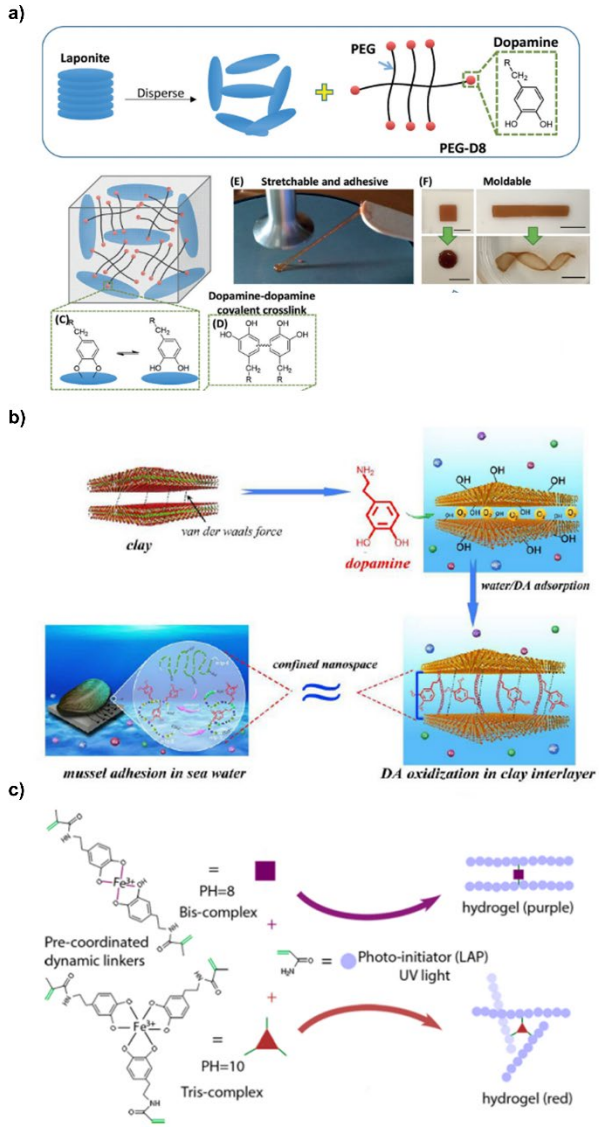

Figure 11. Hydrogel adhesives with polydopamine network. The polydopamine network is formed by the addition of a) Laponite, b) clay nanosheets, and c) ferric ions.

(Adapted from Liu, *et al*., 2017, Han, *et al*., 2017, and Hou, *et al*., 2015, with permission from John Wiley and Sons and American Chemical Society)

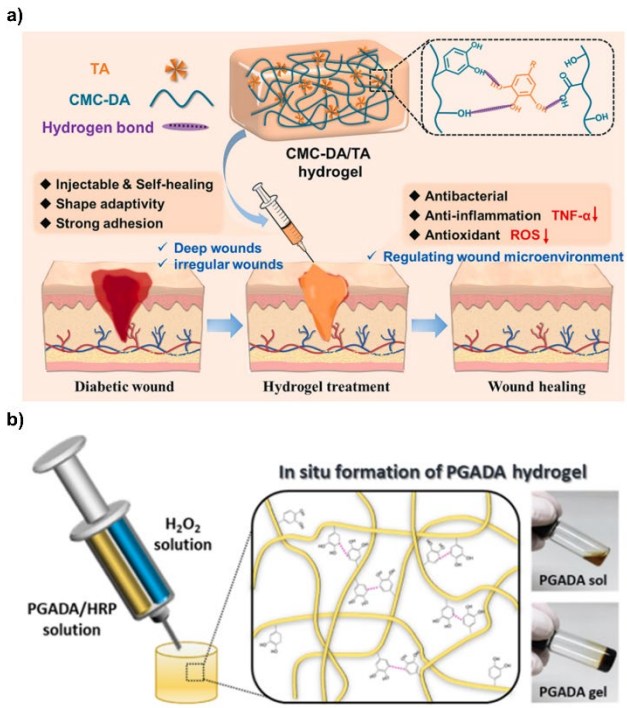

Figure 12. Hydrogel adhesives with dopamine-grafted polymers. The dopamine molecules grafted on a) carboxymethyl cellulose and b) poly(L–glutamic acid).

(Adapted from Xie, *et al*., 2024 and Wang, *et al*., 2021, with permission from Elsevier and American Chemical Society)

2. Objective

Recently, an attempt to replace suturing and stapling with hydrogel adhesives received significant attention due to their efficiency in the surgical process. Compared to conventional surgical methods, implanting hydrogel adhesives can save time and prevent secondary tissue damage. However, hydrogel adhesives have several limitations when applied to dynamic movable parts of the human body. Poor interface adhesion to the target substrate needs additional adhesive for fixation. A lack of flexibility cannot withstand dynamic movement and the large range of motion of a human body.

To overcome these issues, researchers use dopamine as a tissue adhesion functional group. Dopamine is one of the most promising materials that can interact with diverse functional groups and has favorable cell affinity. Recently, stretchable and self–healable hydrogel adhesives have been reported through the reversible intermolecular interactions of dopamine, such as hydrophobic interactions (π– π stacking), π–cation interactions, and hydrogen bonding. These previously reported dopamine–based hydrogel adhesives use oxidized dopamine or a dopamine–grafted polymer (Deng*, et al.*, 2021, Han*, et al.*, 2017). However, these hydrogel adhesives exhibit relatively low tissue adhesion and mechanical resilience due to uncontrollable reactions and relatively low dopamine content.

This study aimed to fabricate highly resilient hydrogel adhesives in a facile method. Inspired by the coacervation phenomenon of mussel–foot proteins (Cui*, et al.*, 2019, Wei*, et al.*, 2014), we designed a dopamine-modified oligomer and applied it as a crosslinking agent. By introducing dopamine molecules in crosslinking agents, a

high content of dopamine molecules can easily incorporated into the hydrogel. The resultant hydrogel adhesives will exhibit two major performances: 1) mechanical resilience and 2) robust tissue adhesion in a wet environment **(Figure 13)**. The fabricated hydrogel, using a dopamine-modified cross-linking agent, forms a densely associated network structure through the intermolecular interaction (hydrogen bonds, hydrophobic associations, π–π interactions) of the dopamine molecules. This associated network structure enables the hydrogel to exhibit high mechanical resilience. Moreover, the hydrophilic hydroxyl group of dopamine forms physical and chemical interactions (hydrogen bonds, hydrophobic interaction, and Schiff base reaction) with substrates. These interactions between dopamine and substrates enable the hydrogels to form robust tissue adhesion in wet environments.

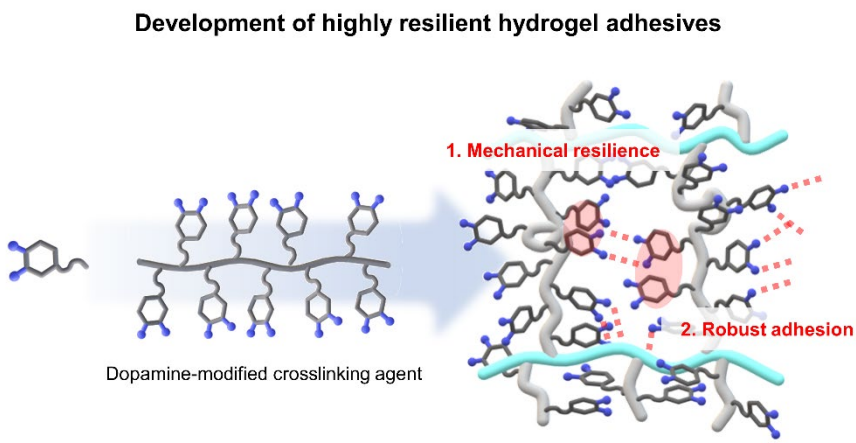

Figure 13. Schematic of dopamine–modified crosslinking agent and the synthesized hydrogel adhesive using it.

2.1. Design of Dopamine–Modified Crosslinking Agent for Hydrogel Adhesives

Crosslinking is essential for fabricating hydrogels and is formed through chemical and physical interactions. The mechanical properties of hydrogel are easily modified through the control of the crosslinking of hydrogel, such as crosslinking density and the length or volume of the crosslinking agent. Moreover, diverse functional hydrogels, such as those that are stretchable, self–healable, and biodegradable, can be fabricated by introducing functional groups or bonds in the crosslinking agent.

In this part, the linear acrylate functionalized and dopamine–modified crosslinking agent was designed to synthesize the highly resilient hydrogel adhesives. The dopamine–modified crosslinking agent was synthesized through the aza–Michael reaction between the amine group of dopamine and the acrylate group of a diacrylate monomer. The resultant dopamine–modified crosslinking agents exhibit the following three characteristics: 1) the end group of the crosslinking agent is functionalized with acrylate, 2) multiple dopamine molecules are incorporated with a short interval in the crosslinking agent, and 3) hydrolyzable ester bonds are incorporated into the crosslinking agent **(Figure 14a)**. First, the terminal acrylate group of the crosslinking agent can react with other acrylate monomers through free radical polymerization. As the linearly synthesized crosslinking agent has two acrylate groups, it can form a gel by crosslinking. Second, the short intervals between dopamine molecules enable crosslinking agents to be associated in the hydrogel network through the physical interactions of dopamine, such as hydrogen bonds and hydrophobic interactions. The associated structure formed by these physical interactions gives the hydrogel mechanical resilience. At the same time, the hydrophilic hydroxyl groups of dopamine are exposed to the surface of hydrogel and

form robust adhesion between substrates **(Figure 14b)**. Finally, hydrolyzable ester bonds in the dopamine–modified crosslinking agent enable hydrogel made using the dopamine–modified crosslinking agent to be degraded under physiological conditions **(Figure 14a)**.

Using acrylic acid, which can form additional intermolecular interactions, as the polymer base monomer, the dopamine–modified crosslinking agent was densely associated within the hydrogel matrix. Through these design strategies of the hydrogel matrix, the hydrogel adhesives synthesized using a dopamine–modified crosslinking agent exhibit robust tissue adhesion with high mechanical resilience.

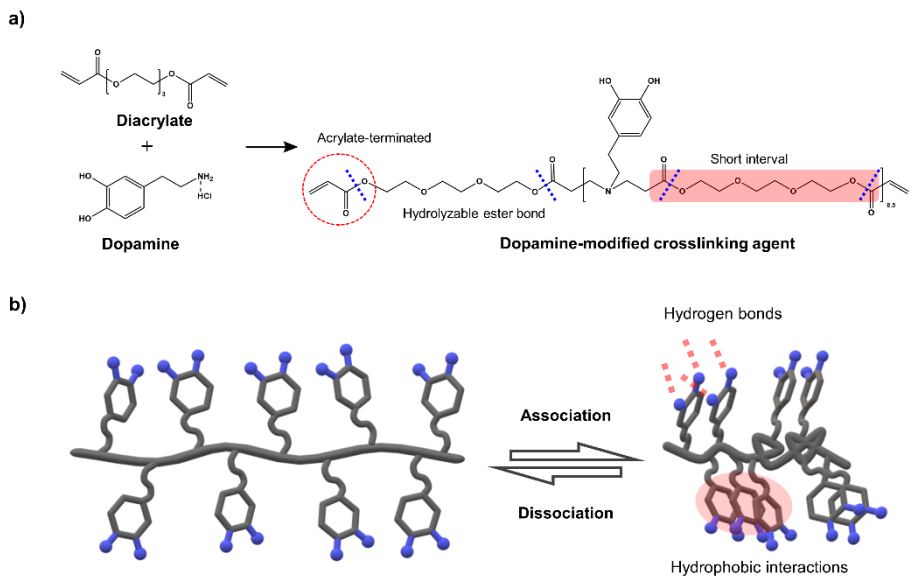

Figure 14. a) Chemical synthesis process of acrylate functionalized and dopamine–modified linear crosslinking agent. b) The associated structure of dopamine–modified crosslinking agent formed through physical interactions and its reversibility.

2.2. Modification of Hydrogel Network Structure for Enhancing Toughness

The mechanical properties of the hydrogel are greatly influenced by its network structure, which is determined by the type of polymer backbone and crosslinking agent. Traditionally, hydrogels have a single–network structure, and the composition and structure of the polymer backbone and crosslinking agent have controlled the mechanical properties of hydrogels. However, these kinds of single–network hydrogels had limitations in improving their mechanical properties. Therefore, multiple networks and functional polymeric materials, which have diverse physical and chemical interactable moieties, have been introduced to improve the mechanical properties of hydrogels.

In this part, the double network hydrogel adhesive using a dopamine–modified crosslinking agent was designed to enhance the toughness of hydrogel adhesives. The double network hydrogel adhesives were designed by following two strategies: 1) introducing a bulkier dopamine–modified crosslinking agent **(Figure 15a)**, and 2) a linear polymer **(Figure 15b)**. The backbone structure of the dopamine–modified crosslinking agent was modified to be bulkier to improve the stretchability of the hydrogel adhesive. A bulkier crosslinking agent forms a free volume in the hydrogel network. However, this free volume can decrease the modulus of hydrogel and weaken the associated structure of the dopamine–modified crosslinking agent. Therefore, these problems can be overcome by forming a double network structure by introducing a physically interactable linear cationic polymer. By introducing poly(vinyl imidazole), a second network was formed through additional intermolecular interactions such as chain entanglement, hydrogen bonds, cation-π interactions, hydrophobic interactions, and ionic interactions. The toughness of the

hydrogel is improved by forming a double network due to the addition of poly(1-vinyl imidazole).

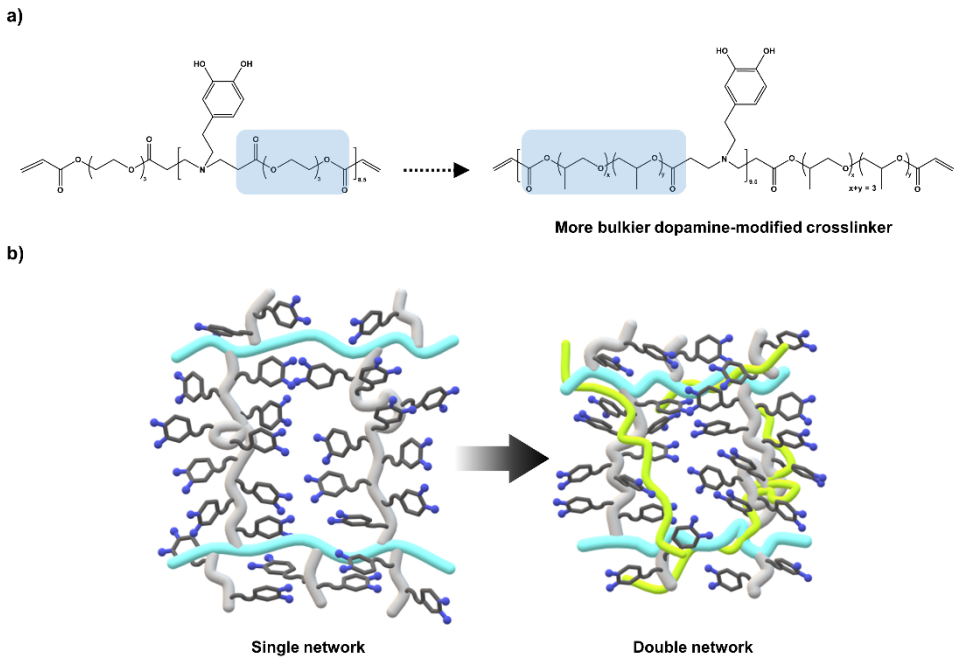

Figure 15. a) Change of chemical structure of the dopamine–modified crosslinking agent and b) network structure of hydrogel adhesive.

Chapter 1

Highly Resilient Hydrogel Adhesives

1. Introduction

Hydrogels are three–dimensional hydrophilic polymer networks infiltrated with water (Zhao*, et al.*, 2021). Owing to their easily controllable network structure and high water content, hydrogels are used as a functional material in various fields (Griffin*, et al.*, 2021, Han*, et al.*, 2020, Mo*, et al.*, 2021, Ye*, et al.*, 2022, Zhang*, et al.*, 2019). In particular, in biomedical fields, the high similarity to biological tissues of hydrogels makes them biocompatible materials used as drug delivery carriers, cell culture media, hemostatic agents, and wound dressing materials (Lee*, et al.*, 2001). Moreover, hydrogel exhibits various functionalities, such as hemostasis (Bu*, et al.*, 2019), cell adhesion (Vahedi*, et al.*, 2018), anti–microbial (GhavamiNejad*, et al.*, 2016), and anti–inflammatory (Mao*, et al.*, 2019) properties by introducing functional monomers or additives. Among them, hydrogel adhesives have received considerable attention due to their easy applicability and efficiency. Compared to traditional suturing and stapling, hydrogels prevent secondary tissue damage and do not need to be removed after use (Han*, et al.*, 2017). However, the low mechanical resilience of hydrogels limits wound dressing in movable parts, such as the knee, wrist, and ankle, where frequent and a large range of motion occur.

To overcome these issues, a dual–crosslinked network structure was proposed for the hydrogel system. Dual–crosslinked networks comprise a strong crosslink that maintains the hydrogel structure and a weak crosslink that dissipates energy (Chu*, et al.*, 2021). By introducing weak reversible sacrificial bonds in addition to strong bonds, the hydrogel can accommodate mechanical loading and prevent crack development (Ducrot*, et al.*, 2014). The weak reversible bonds are commonly composed of host–guest interactions (Wang*, et al.*, 2018), hydrophobic associations (Fang*, et al.*, 2020, Liu*, et al.*, 2020), polyampholytes (Huang*, et al.*, 2021, Sun*, et*

al., 2013), metal–ligand coordinations (Lin*, et al.*, 2015, Liu*, et al.*, 2022), and hydrogen bonding (Yu*, et al.*, 2020).

Dopamine, 3,4–dihydroxyphenylalanine, has a benzene ring with two hydroxyl side groups. The structural characteristic of dopamine enables diverse intermolecular interactions (such as hydrogen bonds, hydrophobic association, cation–π interaction, Michael addition reaction, and Schiff base reaction). Dopamine–based hydrogels can adhere to various surfaces in a moist environment (Xie*, et al.*, 2020, Ye*, et al.*, 2011), and exhibit stretchability (Montazerian*, et al.*, 2021, Yang*, et al.*, 2021) and self–healablility (Deng*, et al.*, 2021, Wang*, et al.*, 2021). Therefore, dopamine–based hydrogels have drawn considerable attention as biological adhesives (Pinnaratip*, et al.*, 2019, Suneetha*, et al.*, 2021, Zhou*, et al.*, 2020). However, the previously reported dopamine–based hydrogel requires a metal ion or an oxidizating agent that exhibits biotoxicity and weaker tissue adhesion than commercially available fibrin glue (~20 kPa) and cyanoacrylate glue (~60 kPa) (Bu*, et al.*, 2019, Chen*, et al.*, 2021, Wu*, et al.*, 2021, Zhou*, et al.*, 2021). Considering the moist physiological environment, ensuring high wet tissue adhesion of hydrogel is critical (Chen*, et al.*, 2021). Poor interface adhesion between a hydrogel and a wound increases the risk of infections and delays tissue regeneration (Hasani-Sadrabadi*, et al.*, 2020).

In this part, to fabricate a highly resilient hydrogel adhesive that can withstand a dynamic environment and accelerate wound healing, a dual crosslinkable dopamine–modified crosslinking agent was synthesized and applied to the hydrogel. The acrylate terminated and dopamine–modified crosslinking agent, tri (ethylene glycol) diacrylate–dopamine crosslinking agent (TDC), was synthesized through the aza–Michael reaction between the amine group of dopamine and the acrylate group of the tri(ethylene glycol) diacrylate monomer. Then, the hydrogel hydrogel was

synthesized via photopolymerization between acrylic acid (AA) and TDC. The covalent crosslink is formed through the photopolymerization of acrylates, and the non–covalent crosslinks are formed *via* intermolecular dopamine–dopamine and dopamine–poly(AA) interactions (hydrogen bonding, π– π stacking, and hydrophobic interaction). Moreover, the dopamine molecules in the acrylic acid–tri (ethylene glycol) diacrylate–dopamine (ATE) hydrogel can adhere strongly to tissues through hydrogen bonds, oxidation, and the Schiff–base reaction of dopamine (Xue*, et al.*, 2021, Yi*, et al.*, 2021). The ATE hydrogel accelerates wound healing by protecting wound sites and maintains a moist environment through robust tissue adhesion and absorbing excess exudates through pH–sensitive AA. This study provides an straightforward method to develop functional hydrogels using only a crosslinking agent, which is expected to potentially be applied to electronic skins, sensors, and tissue scaffolds beyond the wound dressing materials.

2. Experimental

2.1. Materials

Tri (ethylene glycol) diacrylate (TEGDA, average Mn 250) and 2–hydroxy–4′–(2–hydroxyethoxy)–2–methylpropiophenone (Irgacure 2959, 98%) were purchased from Sigma–Aldrich. Dopamine hydrochloride (99%) was purchased from Alfa Aesar. Acrylic acid (AA, 99.5%), 2,2′–azobisisobutyronitrile (AIBN, 98%), triethylamine (TEA, 99.0%), dimethyl sulfoxide (DMSO, 99.8%), tert–butyl methyl ether (MTBE, 98.5%), and sodium azide (99.0%) were purchased from Samchun Chemicals Co., Ltd. 10× phosphate–buffered saline (PBS) solution was purchased from Tech & Innovation. Dulbecco's modified Eagle's medium (DMEM, #SH3243.01) was purchased from Hyclone Laboratories, Inc.

2.2. Synthesis of Crosslinking Agent

Tri (ethylene glycol) diacrylate–dopamine crosslinking agent (TDC), was synthesized via an aza–Michael addition reaction **(Figure 16)** between diacrylate and dopamine hydrochloride. The molar ratio of the carbon double bond of diacrylate and the amine of dopamine hydrochloride was set as 1.1: 0.5 to make an acrylate–terminated crosslinking agent. Dopamine hydrochloride (1.84 g, 10 mmol) and TEGDA (2.25 g, 11 mmol) were added to DMSO (10.70 g) under N_2 purging and stirred at 25 °C for 20 min until the solution became clear. TEA (0.98 g, 10 mmol) was added to adjust the pH to 8, and the mixture was stirred at 80 °C for 5 h in the dark. After the reaction, the mixture was suction–filtered to remove TEA salt. The

filtered solution was washed with MTBE three times to remove DMSO and the unreacted monomer. Finally, the residual solvent was removed using a rotary evaporator at 60 °C for 6 h. The yellow–transparent liquid was then obtained and stored at −20 °C.

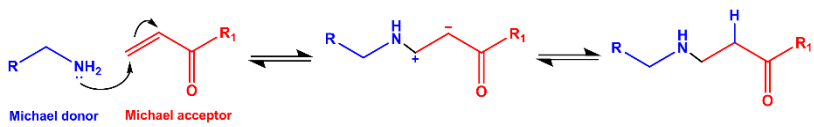

Figure 16. Reaction mechanism of Aza–Michael reaction.

2.3. Synthesis of Hydrogel

The acrylic acid–tri (ethylene glycol) diacrylate–dopamine (ATE) gels were synthesized in DMSO, due to the compatibility problem of dopamine–crosslinking agents. Then the hydrogel was obtained through solvent exchange by immersing the pre–gel in deionized water **(Figure 17)**. The ATE pre–gel was synthesized in DMSO through free radical photopolymerization. AA (2.0 g), TDC (0.75 g, 0.8 mole % of AA), and Irgacure 2959 (0.02 g, 1 wt. % of AA) were dissolved in DMSO (5.2 g, 35% solid content). The mixture was poured into a Teflon mold sized 12 × 75 × 0.5 mm^3 (W × L × T). The mixtures were covered with a silicon–coated PET film and subjected to UV irradiation for 5 min using a UV light–emitting diode lamp (365 nm, intensity = 17 mW/cm^2). After polymerization, the yellow–transparent pre–gel was obtained. The resulting ATE pre–gel was washed with DMSO and then immersed in cold DIW for 12 h, changing to fresh DIW every 2 h. After the solvent exchange, white–transparent ATE hydrogel was obtained and stored at −20 °C. The ATE hydrogels with different crosslinking agent contents (0.6, 0.7, 0.9, and 1.0 mol% of

TDC) were prepared following the same procedure. The hydrogel with 0.*x* mol% of TDC was denoted as the ATE*x* hydrogel. For samples without special mention, the ATE8 hydrogel was used.

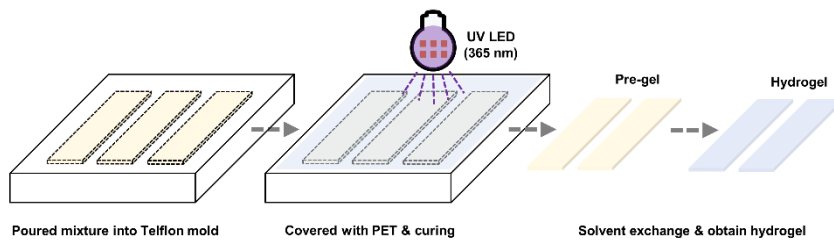

Figure 17. Schematic of the hydrogel preparation process.

2.4. Characterization of Crosslinking agent

The Aza–Michael reaction was monitored through Fourier transform infrared (FT–IR) spectroscopy. The IR spectra were recorded using an FT–IR spectrometer (Nicolet iS20, Thermo Fisher Scientific). All FT–IR samples were measured at 25 °C through the attenuated total reflection (ATR) mode. The obtained curves were normalized using the carbonyl ester bond band (1,720 cm^{-1}).

The molecular structure of synthesized crosslinking agents, linear polymers, and the released solvent was verified through a proton and carbon nuclear magnetic resonance (^{1}H and ^{13}C NMR) spectrometer (400–MHz, JNM–ECX400, JEOL). All NMR samples were measured at 25 °C, and tetramethylsilane (0.03% in DMSO–d6 and D2O) was used as an internal standard (δ = 0 ppm).

2.5. Solvent Exchange

The pre–gel was immersed in DIW to remove the DMSO in the pre–gel. To monitor the extracted solvent over time, 100 mg of pre–gel was immersed in 2 mL of D_2O for 12 h (fresh D_2O every 2 h). The extracted DMSO was confirmed through the ^1H NMR spectra, and the solvent–exchange ratio was calculated using the ^1H NMR spectra as well. (D_2O_n = 4.8 ppm peak integral at n h, $DMSO_n$ = 2.5 ppm peak integral at n h)

$$\text{Solvent extraction } (E_n) = \frac{DMSO_n}{D_2O_n}$$

$$\text{Extraction ratio } (\%) = \frac{E_n}{\sum E_n} \times 100$$

2.6. Swelling Ratio and Water Contents

The swelling ratio was measured using the pre–gel after immersion in DMSO and DIW at 25 °C for 24 h. A 12 × 12 (W × L) pre–gel sample was used, and the swelling ratio was calculated based on its weight and volume change. The weight and volume of the gel after being immersed in the solvent for n h were denoted $weight_n$ and $volume_n$, respectively.

$$\text{Swelling ratio } (\%) = \frac{weight,\ volume_{\,n}}{weight,\ volume\ of\ pre-gel} \times 100$$

The water content of the hydrogel was calculated based on the mass loss after lyophilization.

$$\text{Water Content (\%)} = \frac{wt.of\ hydrogel - wt.of\ lyophilized\ hydrogel}{wt.of\ hydrogel} \times 100$$

2.7. Small–Angle X–ray Scattering (SAXS)

The SAXS 1D profiles were obtained using an X–ray scattering spectrometer (Xeuss 2.0, Xenocs) using Cu Kα radiation (l = 1.54056 Å). The sample–to–detector distance was 2500 mm, and the irradiation time was set at 1800 s. The region $0.008 < Q < 0.014$ $Å^{-1}$ was used to determine the slope.

2.8. Tensile Test

The tensile test was conducted using a 30 mm length hydrogel. 10 mm of both ends of the hydrogel were covered with a corona–treated PET film to be used as a grip. The tensile test was conducted at a rate of 100 mm/min at 25 °C and 50 ± 10% RH using a Texture Analyzer (TA.XT plus, Stable Micro Systems).

2.9. Lap Shear Test

The tissue adhesion of hydrogel was measured through a lap shear test, and the wet porcine skin was used as a substrate due to its high similarity to human tissues **(Figure 18)**. The lap shear tests were conducted at a rate of 50mm/min at 25 °C and 50 ± 10% RH using a Texture Analyzer (TA.XT plus, Stable Micro Systems). Before attaching the hydrogel, the porcine skins were immersed in sodium azide solution (0.01 w/v% in DIW and 1× PBS solution) for hydration and to prevent degradation. Then, DIW/PBS solutions were sprayed to make a thoroughly wetted porcine skin surface. The hydrogel was attached through a pressure of 1 kPa for 10 s. The sample was stored in a covered stainless tray, and DIW/PBS solutions were sprayed to maintain a moist environment. Unless otherwise specified, the tests were conducted 3 h after adhesion.

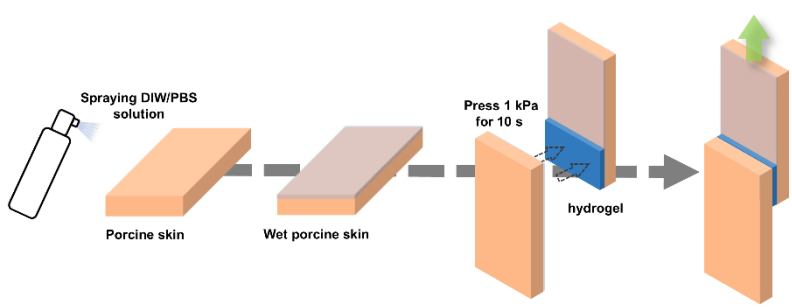

Figure 18 Schematic of lap shear test using wet porcine skin (Han, *et al.*, 2024).

2.10. Cyclic Tensile Test

Cyclic tensile tests were conducted using a Texture Analyzer (TA.XT plus, Stable Micro Systems) at 25 °C and 50 ± 10% RH. The tensile tests were conducted at a rate of 100 mm/min and repeated without rest. The residual strain, hysteresis energy loss (ΔU), and resilience values were calculated using the initial loading–unloading curve **(Figure 19)**.

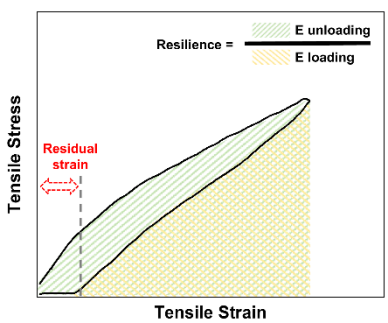

Figure 19. Schematic of tensile hysteresis curve (Han, *et al.*, 2024).

$$\Delta U = \int_{loading} \sigma d\varepsilon - \int_{unloading} \sigma d\varepsilon$$

$$\text{Resilience (\%)} = \frac{\int_{unloading} \sigma d\varepsilon}{\int_{loading} \sigma d\varepsilon} \times 100$$

2.11. Biodegradability Test

The lyophilized hydrogel (50 mg) was immersed in 1 × PBS solution (5 mL, pH 7.4) at 36 °C. After a specific time, the degraded hydrogel was washed with DIW and lyophilization. The degradation rate of the hydrogel was calculated using the mass loss of the gel.

2.12. Cell culture and In vitro Biocompatibility Tests

Cell Culture: To prepare hydrogel–treated DMEM media, the lyophilized hydrogel was immersed in DMEM at 37 ° C until hydrogel was degraded entirely (0.5 mg / 1 mL) **(Figure 20)**. STO cells were cultured in DMEM (10% FBS, 1% antibiotics) at 37 °C with 5 % CO_2. When the STO cells reached 80% confluence, the medium was replaced with hydrogel–treated DMEM and incubated. Pristine DMEM was used as the control.

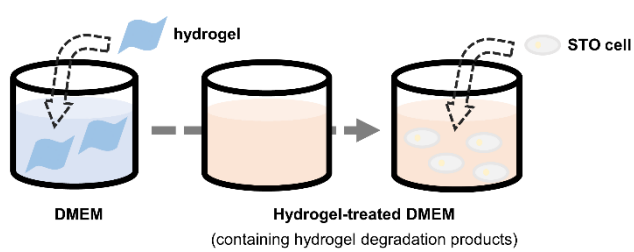

Figure 20. Schematic of in vitro biocompatibility process (Han, *et al.*, 2024).

Cell Viability: STO cells, with a seeding density of 1×10^5 cells, were seeded into 96–well cell culture plates and cultured for 72 h. STO cells were rinsed with PBS and incubated in 100 μL of 10% of the EZ–Cytox (DoGenBio) medium at 37 °C for 30 min. The cell viability was analyzed using a microplate spectrophotometer (Epoch 2, BioTek), and the absorbance at 450 nm was measured.

Cell Cytotoxicity: Cell cytotoxicity was evaluated by measuring the enzymatic activity of lactate dehydrogenase (LDH). The LDH release was evaluated using the EZ–LDH kit following the manufacturer's instruction. The supernatant was used to measure the released LDH. Cell cytotoxicity was analyzed using a microplate spectrophotometer (Epoch 2™, BioTek), and the absorbance at 450 nm was measured.

Cell Apoptosis: STO cells, with a seeding density of 1×10^5 cells were seeded in to 6–well cell culture plates and cultured for 48 h. The cultured STO cells were detached from the plates. After suspending the STO cells in a binding buffer, Annexin V–FITC/PI (BD Bioscience, #556547) was added and incubated for 15 min at 25 °C. Apoptotic cells were analyzed through cytometry (CytoFlex, Beckman Coulter).

Cell Live/Dead: The viability of STO cells was assessed using a Live/Dead™ Cell Imaging Kit (Thermo Fisher Scientific, #R37601) following the manufacturer's instruction. STO cells were seeded in μ-slide Chemotaxis 3D (IBIDI, Martinsried, Germany) and cultured for 72 h. Then, the Live Green and Dead Red reagents were added to the medium and incubated for 15 min at 25 °C. The live and dead cells were

analyzed using a confocal microscope system (LSM 710, Carl Zeiss, Oberkochen, Germany).

2.13. In vivo Biocompatibility Tests

Wound Healing Test: Six–week–old male Sprague Dawley rats were used for in vivo biocompatibility tests. The rats were anesthetized with a mixture of Alfaxan (80 mg/ kg) and xylazine HCl (10 mg/ kg). A 6 mm diameter circular wound was created on the rats' backs using a biopsy punch and wound sites were immobilized by suturing with a silicon wound splint. In the hydrogel–treated group, the hydrogel was implanted and dressed with a Tegaderm film. In the control group, only the Tegaderm film was implanted. Tissue regeneration and vasculogenesis were observed at different time points (0, 4, 8, and 11 d after implantation). The wounded skin was harvested 11 d after implantation for the histological analysis. All animal experiments were approved by the Institutional Animal Care and Use Committee of Seoul National University (SNU–210616–1–2).

Immunohistochemistry: The skin slides were fixed in 80% acetone solution for 20 min. The slides were rinsed with PBS and incubated in 5% normal goat serum for 30 min. The samples were incubated with the vascular endothelial growth factor (VEGF) antibody (sc–7269, Santa Cruz, 1:100 dilution) containing PBST (PBS with 0.1% Triton–X) medium for 2 h, followed by incubation in a VEGF antibody (1:100 dilution) containing the PBST medium for 1 h. Images were acquired using a confocal microscope (LSM 710, Carl Zeiss, Oberkochen, Germany).

Hematoxylin and Eosin (H&E) Staining*:* The skin samples were fixed in 4% paraformaldehyde (PFA) for 2 h and dehydrated in 30% sucrose for 24 h. The tissues with a 20 µm thick longitudinal section were obtained and fixed with 4% PFA for 5 min. The fixed samples were stained with H&E for 5 min. The stained samples were washed with ethanol three times and incubated in xylene for 5 min. All images were acquired using the SlideViewer software (3DHISTECH, Budapest, Hungary).

Masson's Trichrome Staining: Masson's trichrome staining was performed using VitroView™ Masson's Trichrome Stain Kit (Rockville, USA) following the manufacturer's instruction. All images were acquired using the Eclipse Ts2^{TM} fluorescence microscope (Nikon, Tokyo, Japan). Red represented keratin, muscle fibers, and the cytoplasm; blue represented collagen; and black represented the cell nuclei.

3. Results and Discussion

3.1. Preparation of Crosslinking Agent

The linear dopamine–modified crosslinking agent was synthesized using tri (ethylene glycol) diacrylate and dopamine hydrochloride *via* the aza–Michael reaction **(Figure 21a)**. The molar ratio of the C=C of acrylate to NH_2 of dopamine was set as 1.1: 0.5 to make the acrylate–terminated crosslinking agent. This crosslinking agent, the tri (ethylene glycol) diacrylate – dopamine crosslinking agent, was denoted as TDC. A reduction in the 810 cm^{-1} band (acrylate C=C bond) in the FT–IR spectra showed that the amine group dopamine fully reacted after 5 h **(Figure 21b)**.

a)

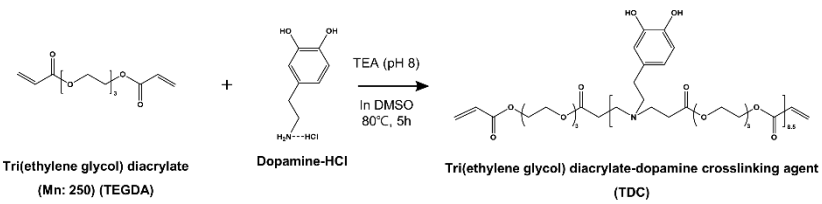

b)

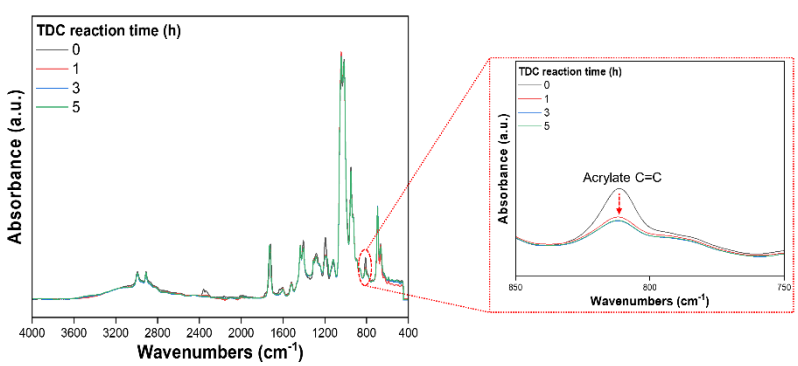

Figure 21. a) Chemical synthesis process of TDC. b) FT–IR spectra of TDC at different time points during the reaction (Han, *et al.*, 2022).

The end–group fidelity of the TDC was confirmed by the acrylate C=C bond proton peaks (5.9–6.4 ppm) in the ^{1}H NMR spectrum **(Figure 22)**. The molecular weight of TDC was calculated using the proton peak integral values between 5.9–6.0 ppm (acrylate C=C) and 6.55–6.75 ppm (benzene CH, adjacent to OH). The peak integral ratio of the 5.9–6.0 ppm peaks to 6.55–6.75 ppm peaks is 1 : 8.5, indicating the incorporation of approximately 8.5 dopamine molecules in each TDC. Hence, the average molecular weight of TDC was estimated to be 3,700.

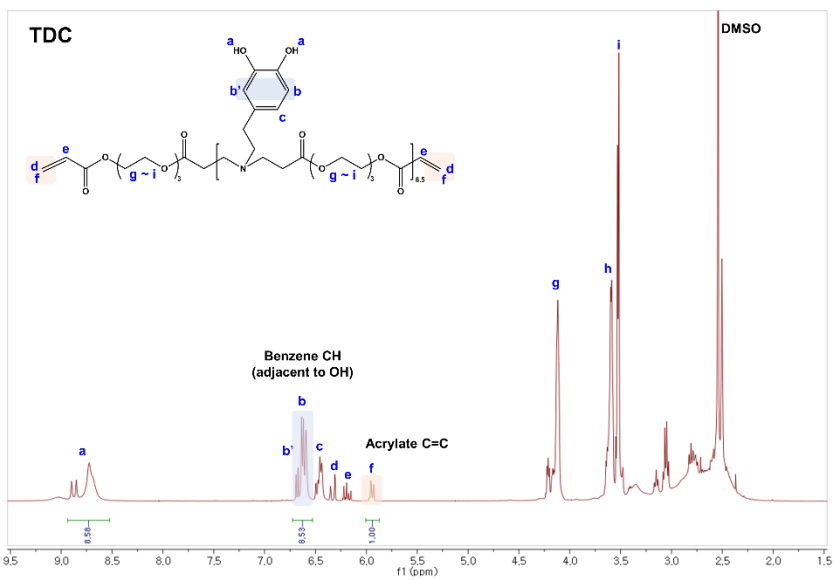

Figure 22. The ^{1}H NMR spectrum of TDC (Han, *et al.*, 2022).

3.2. Preparation of Hydrogels

The ATE hydrogel was prepared following two steps: 1) radical polymerization between the acrylate monomer AA and the crosslinking agent TDC, and 2) solvent exchange. First, the synthesized TDC was copolymerized with AA using DMSO as a solvent **(Figure 23)**. Next, the prepared organogel was immersed in cold DIW for 12 h to remove any unreacted monomers and DMSO. The unreacted monomers and DMSO were fully extracted after 3 h **(Figure 24)**. The ATE hydrogel was obtained after immersing the pre–gel in DIW for 12 h. The hydrogel with 0.*x* mol% of TDC was denoted as the ATE*x* hydrogel.

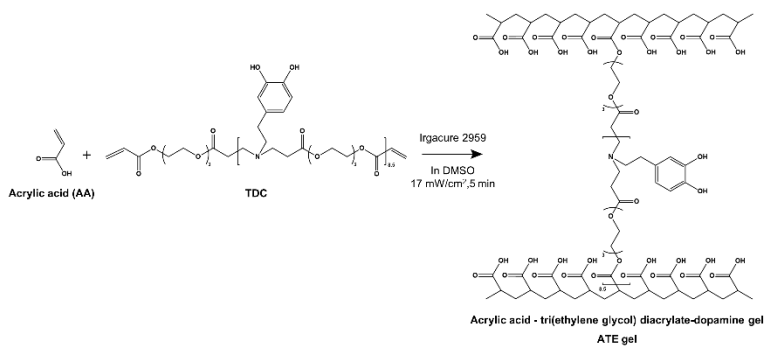

Figure 23. Chemical synthesis process of ATE gel. b) Schematic of the dual–crosslinked structure of ATE gel (Han, *et al.*, 2022).

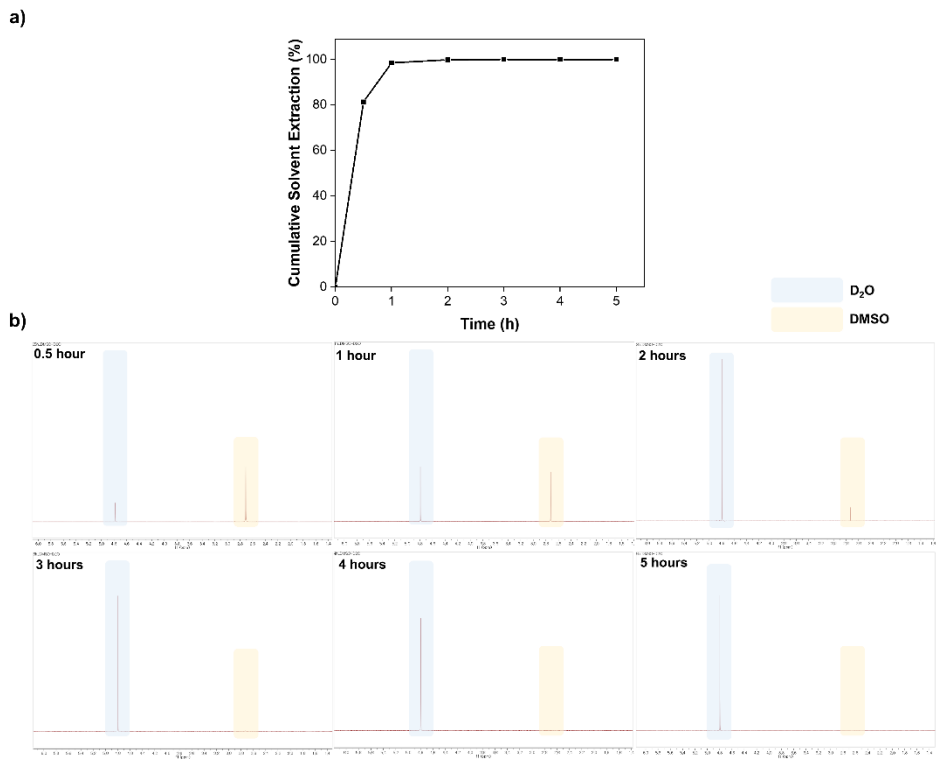

Figure 24. a) Solvent extraction ratio of ATE8 pre–gel and b) ^{1}H NMR spectrum of released DMSO when the ATE8 gel is immersed in D_2O at different time points (Han, *et al.*, 2022).

DMSO was used as a solvent for ATE gel synthesis. By using DMSO as a solvent, the radical scavenging effect caused by dopamine was reduced and the gel was successfully polymerized without protecting the hydroxyl group of dopamine. Polar aprotic solvents such as DMSO or DMF can form a hydrogen bond with the hydroxyl group of dopamine, thereby reducing the interaction between the propagating radical and the dopamine molecule during polymerization. Meanwhile, when a polar protic solvent such as methanol is used, hydrogen bonds are formed between the solvents, so the scavenging effect of dopamine cannot be reduced (Yang*, et al.*, 2015). The model test verified that using DMSO in our system successfully polymerized, i.e., gelation, was successful through free radical reaction without protecting the hydroxyl group of dopamine. In the model test, a linear polymer was synthesized through a precursor containing the same dopamine content as the ATE8 gel, and polymerization was confirmed through ^{1}H NMR measurement. As a result of the model test, the conversion of the precursor was approximately 98% **(Table 1 and Figure 25)**. Moreover, there was no acrylic acid release during the solvent exchange process (**Figure 24b)**. These results verify that the polymerization was successful without the radical scavenging effect of dopamine.

Table 1. Polymerization model test results.

Model Test		
	Formulation	
Mole %	Acrylic acid	Dopamine
	100	8
	^{1}H NMR integral ratio (%)	
Before polymerization	100	8
After polymerization	2.09	8
	Conversion: 98%	

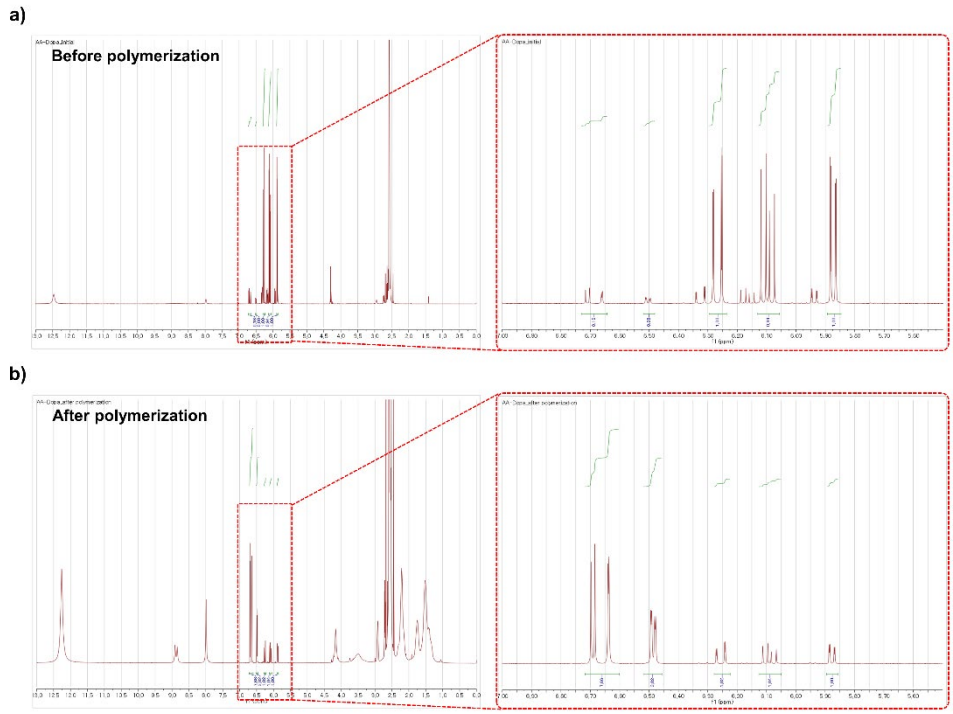

Figure 25. The ^{1}H NMR spectrum of precursor. a) Before polymerization and b) after polymerization.

3.3. Characterization

The prepared ATE hydrogel comprises a dual crosslinked network. The covalent crosslinks formed due to the acrylates, and the non–covalent crosslinks formed through the association of TDC by physical intermolecular dopamine–dopamine and dopamine–poly(AA) interactions (hydrogen bonding, π–π stacking, and hydrophobic interactions) **(Figure 26)**. To evaluate the effect of the non–covalent crosslinking of the ATE hydrogel, the ATE8 pre–gel (0.8 mole% TDC) was immersed in DIW and DMSO for 24 h, and volume change was observed. DMSO, an organic solvent composed of polar sulfoxide and nonpolar methyl groups, weakens physical intermolecular interactions through its amphiphilic nature (Mathis*, et al.*, 2018, Noack*, et al.*, 2010). Therefore, the effect of physical intermolecular interactions on the formation of non–covalent crosslinks can be verified based on the change in the volume when ATE pre–gel is immersed in each solvent. The ATE8 pre–gel contracted approximately up to 35% of its original volume when immersed in DIW. In contrast, the ATE8 pre–gel expanded by approximately 1100% of its original volume when immersed in DMSO **(Figure 27)**.

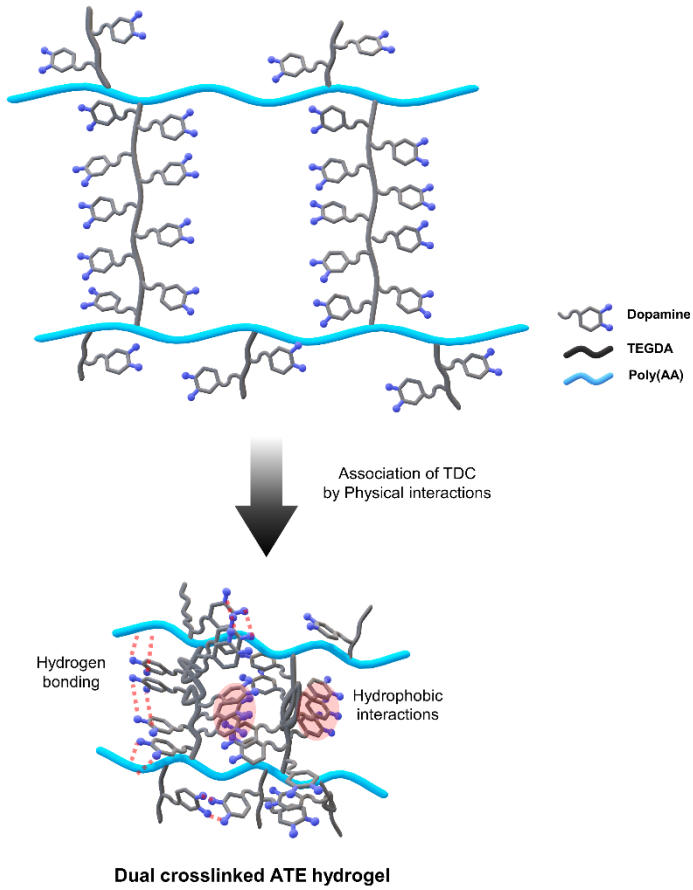

Figure 26. Illustration of the dual–crosslinked structure of ATE hydrogel.

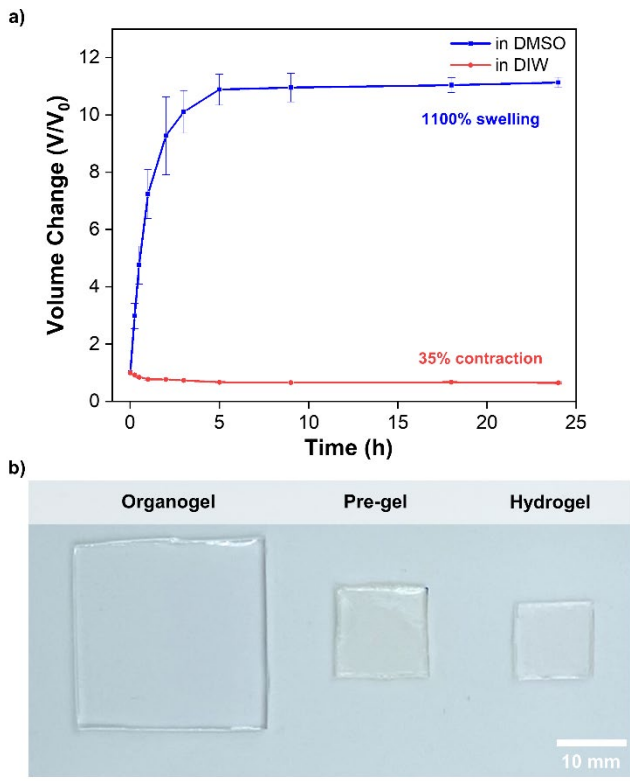

Figure 27. a) Swelling and contraction ratio of ATE8 gel when immersed in DMSO and DIW for 24 h. b) Images of ATE8 organogel, pre–gel, and hydrogel (Han, *et al.*, 2022).

Furthermore, the change in the network structure of the ATE hydrogel was verified using SAXS spectrum at the low Q region. The ATE8 organogel (immersed in DMSO) exhibited a steeper slope (slope: – 4.0) than the ATE hydrogel (immersed in DIW) (slope: – 2.5) **(Figure 28)**. This result suggests an increase the domain size of the ATE gel upon immersion in DMSO. The swelling test and SAXS results verified the effect of intermolecular interactions on the formation of the hydrogel structure.

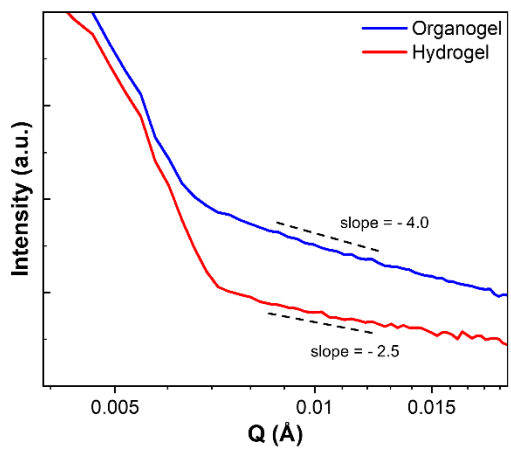

Figure 28. SAXS 1D profile of the ATE8 organogel and hydrogel (Han, *et al.*, 2022).

Then, the effect of the TDC contents on network structure formation was evaluated by the contraction ratio and water content of the ATE hydrogel in the equilibrium state with different TDC contents. As the TDC contents increased from 0.6% to 1.0%, the contraction ratio of the ATE hydrogel gradually increased from 25% (ATE6 hydrogel) to 43% (ATE10 hydrogel). The water content decreased from 58.4% (ATE6 hydrogel) to 42.9% (ATE10 hydrogel) **(Table 2)**. These results demonstrate that the increase of TDC content causes a greater association of TDC by increasing

the extent of physical intermolecular interactions, resulting in a denser hydrogel network structure.

Table 2. Contraction ratio and water content of ATE hydrogel with different TDC contents.

ATE*x* hydrogel	**TDC contents (mole%)**				
	0.6	**0.7**	**0.8**	**0.9**	**1.0**
Contraction ratio (%)	25.7	29.7	35.4	40.3	43.6
Water content (%)	58.4	54.8	49.0	46.9	42.9

3.4. Mechanical Performances

3.4.1. Tensile Property

The crosslinking density of the hydrogel greatly affects its mechanical properties; therefore, the changes in the mechanical properties of the hydrogel according to its TDC content were evaluated using a tensile test **(Figure 29a)**. As the TDC content increased from 0.6 to 1.0%, the tensile strength increased by approximately 50 kPa, from 71.3 kPa (ATE6 hydrogel) to 123.2 kPa (ATE10 hydrogel). Fracture elongation decreased by approximately 200%, from 422% (ATE6 hydrogel) to 224% (ATE10 hydrogel) **(Figure 29b and Table 3)**. The associated TDC in the ATE hydrogel network stretches and dissipates energy when mechanical loading is applied. The ATE hydrogel with a higher TDC content is expected to be more elongated owing to relatively more moieties that could be stretched. However, as the crosslinking density increases, increased chain entanglement restricts the movement of the polymer chain, resulting in a decrease in elongation.

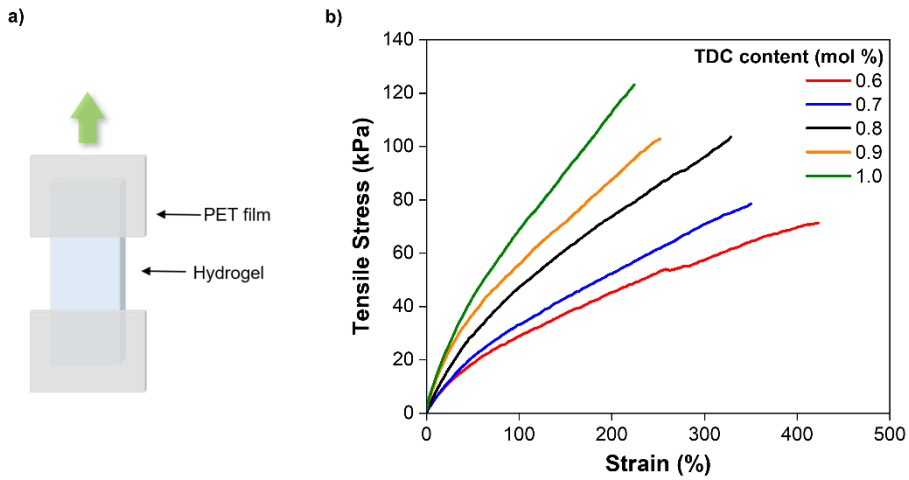

Figure 29. a) Schematic of tensile test. b) The strain–stress curve of ATE hydrogel with different TDC contents (Han, *et al.*, 2022).

Table 3. Tensile strength and fracture elongation of ATE hydrogel with different TDC contents.

ATE*x* hydrogel	**TDC contents (mole%)**				
	0.6	**0.7**	**0.8**	**0.9**	**1.0**
Tensile strength (kPa)	71.3	78.5	103.5	102.9	123.2
Fracture elongation (%)	422	350	328	252	224

3.4.2. Adhesion Property

The adhesion strength of the ATE hydrogel was measured through the lap shear test using porcine skin **(Figure 30a)**. The porcine skin was used as the model tissue because of its high similarity to human skin (Li*, et al.*, 2017). As the TDC content increased, the adhesion strength increased from 59.4 kPa (ATE6 hydrogel) to 82.9 kPa (ATE10 hydrogel) **(Table 4)**. When the associated structure of TDC was formed by physical interactions, the hydrophilic hydroxyl groups of dopamine were exposed to the surface of the hydrogel (Cui*, et al.*, 2019). These hydroxyl groups robustly adhered to biological tissues *via* hydrogen bonding, oxidation, and Schiff–base reaction between dopamine and the functional group of skins (amine, carboxylic acid, and hydroxyl groups) **(Figure 30b)** (Ma*, et al.*, 2021, Xu*, et al.*, 2021). In the case of the ATE hydrogel, dopamine molecules are incorporated in a crosslinking agent; therefore, the adhesion strength increases as the TDC content increases.

Table 4. Adhesion strength of ATE hydrogel with different TDC contents.

ATE*x* hydrogel	**TDC contents (mole%)**				
	0.6	**0.7**	**0.8**	**0.9**	**1.0**
Lap shear strength (kPa)	59.4	64.9	71.4	75.4	82.9

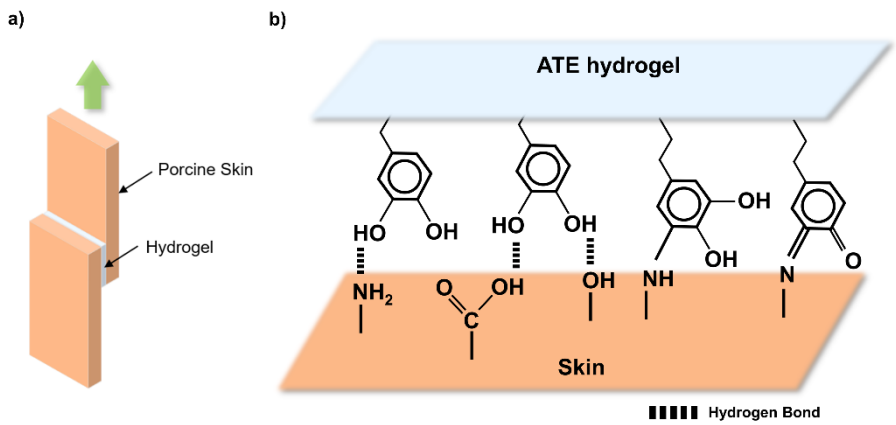

Figure 30. Schematic of lap shear test and b) the adhesion mechanism of ATE hydrogel (Han, *et al.*, 2022).

In our system, the mechanical properties of the ATE hydrogel varied depending on the TDC content used as a crosslinking agent. As the TDC content increased, the tensile strength, tissue adhesion, and contraction ratio increased, whereas the water content and fracture elongation decreased. Hydrogels with 0.8 mole% TDC exhibited optimal mechanical strength (103.5 kPa tensile strength, 328% fracture elongation), tissue adhesion (71.4 kPa), and water content (48.8%). Consequently, the ATE8 hydrogel was chosen for subsequent experiments.

3.4.3. Change in Adhesion Over Time

The adhesion strength of the hydrogel must be maintained in a moist environment because the wound environment is moist due to exudate produced by damaged skin, as well as a moist physiological environment (Zhang*, et al.*, 2020). The tissue adhesion performance of hydrogel in a moist environment is a vital factor for wound dressing and greatly affects its durability. Therefore, we observed the change in tissue adhesion over time (0, 1, 3, 6, 10, 24, and 48 h) under DIW and PBS solution (pH 7.4) treated conditions **(Figure 31)**. The DIW−treated condition simulated a generally moist environment, and the PBS−treated condition simulated a physiological condition in which body secretions were released. Both conditions were maintained by spraying DIW and PBS solutions every 12 h. For the DIW−treated condition, the maximum adhesion strength (71.4 kPa) was observed after 3 h, and for the PBS−treated condition, the maximum adhesion strength (59.6 kPa) was observed after 6 h. Over time, the adhesion strength under both conditions decreased, but the ATE hydrogel still exhibited excellent adhesion strength of over 30 and 10 kPa after 24 and 48 h, respectively, under both conditions.

The decrease in adhesion strength of the ATE hydrogel over time is attributed to the destruction of the associated TDC structure. Due to the ATE hydrogel containing the hydrolyzable TDC, the structure of the associated TDC was destroyed, and the ATE hydrogel was degraded over time. As the structure of the associated TDC is destroyed, the number of reactive sites on the hydrogel surface that interact with skin tissues decreases. Moreover, as the hydrogel degrades, the cohesion of the hydrogel decreases, thereby decreasing the adhesion strength. This phenomenon can be

indirectly confirmed through changes in the fracture state of the ATE hydrogel on the adhesion time **(Figure 32)**.

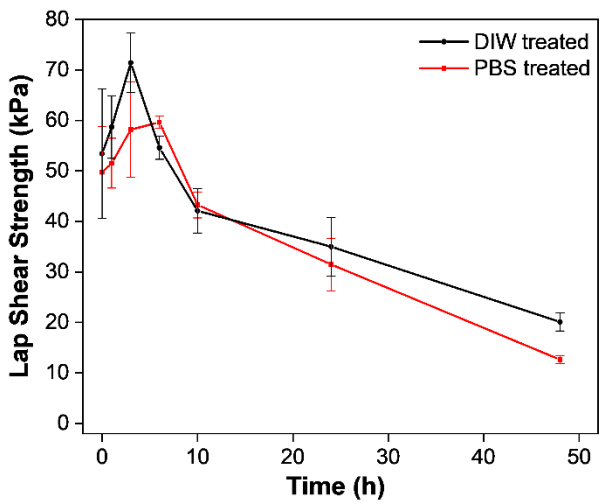

Figure 31. Tissue adhesion of the ATE8 hydrogel at different time points after adhesion under DIW and PBS–treated conditions (Han, *et al.*, 2022).

The overall adhesion strength under the PBS−treated condition was lower than that under the DIW−treated condition. This is pH–sensitive acrylic acid is used as the backbone, so the ATE hydrogel absorbs more water and degrades rapidly at higher pH conditions (Karnal, *et al.*, 2019). However, unlike the DIW−treated condition, the maximum adhesion strength under the PBS−treated condition was measured 6 h after adhesion and exhibited a higher adhesion strength. This result is caused by an additional interaction with porcine skin due to dopamine oxidation (Zhang, *et al.*, 2014).

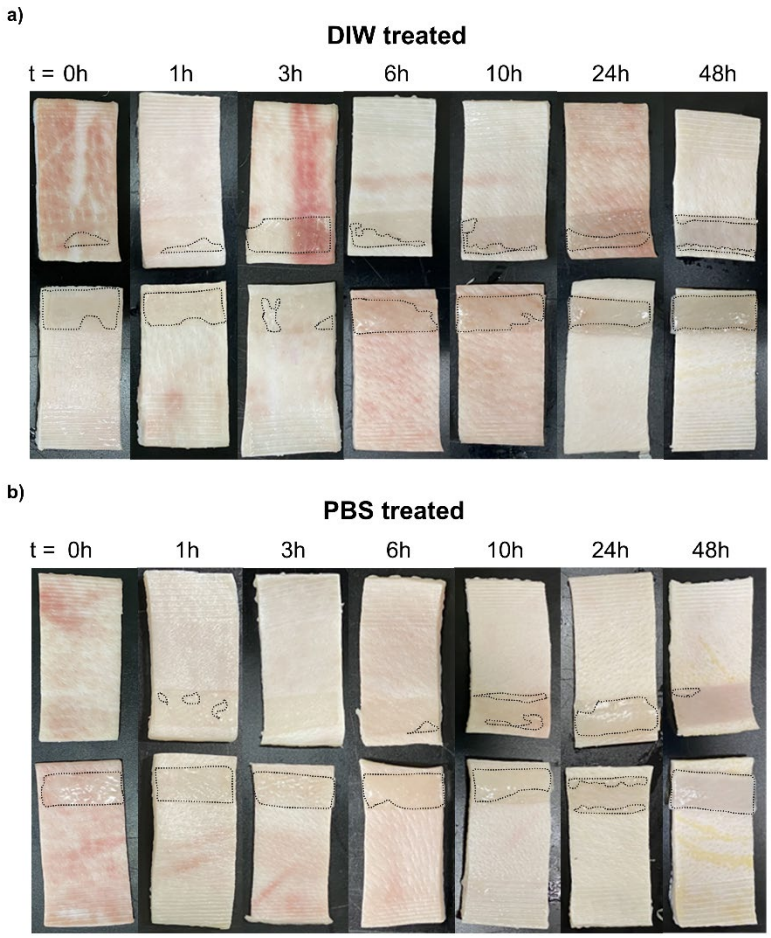

Figure 32. Failure mode after lap shear test and degradation profile of a) DIW– and b) PBS–treated samples at different time points after adhesion (Han, *et al.*, 2022).

3.4.4. Recovery Property

Movable parts, such as joints (knee, wrist, and ankle), have a frequent and large range of motion. Hence, the application of hydrogel on movable parts requires appropriate recovery properties against mechanical loading. A cyclic tensile test was conducted to evaluate the recovery properties of the ATE hydrogel. The residual strain, resilience, and hysteresis energy loss (ΔU) of the ATE hydrogel were calculated using the initial loading–unloading curves at different strain rates. No residual strain was observed at the 100 and 150% strain rates **(Figure 33a, b)**. At the 200 and 250% strain rates, the residual strain was observed to be approximately 3 and 8%, respectively **(Figure 33c, d)**. Below 200% strain, negligible hysteresis loop changes and high resilience (approximately 94 %) were observed. However, at 250% strain, the residual strain increased sharply, and the mechanical resilience decreased by approximately 90% **(Table 5)**.

Table 5. Residual strain and resilience of ATE8 hydrogel with different strain rates.

ATE8 hydrogel	**Strain rate (%)**			
	100	**150**	**200**	**250**
Residual strain (%)	–	4.4	4.8	7.6
Resilience (%)	93.7	94.3	94.1	90.9

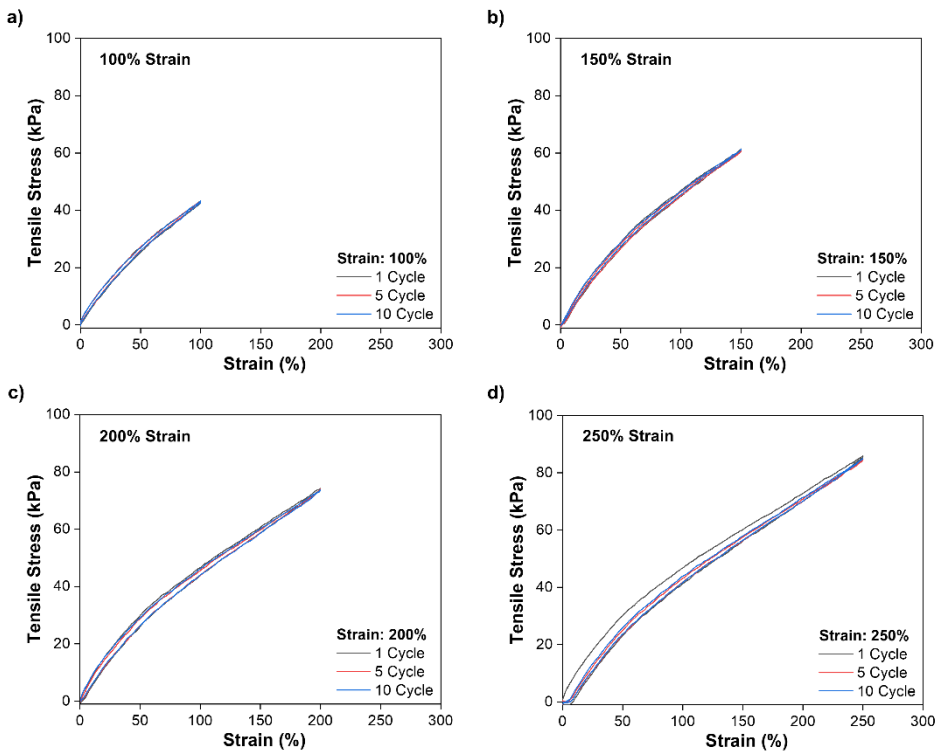

Figure 33. a) Cyclic tensile test of the ATE8 hydrogel at a) 100%, b) 15 %, c) 200%, and d) 250% strain (Han, *et al.*, 2022).

The ATE hydrogel demonstrated excellent recovery properties with high resilience and immediate recovery under 200% strain **(Figure 34a)**; these recovery properties are mainly attributed to the non–covalent crosslinked and associated TDC. When mechanical loading was applied to the ATE hydrogel, the associated TDC dissipated energy by dissociation **(Figure 34b)**. Therefore, the ATE hydrogel can withstand large mechanical deformations (Ducrot*, et al.*, 2014). Moreover, a reversible, non–covalent association of TDC enables the ATE hydrogel to return to its original state. However, the residual strain was observed at over 200% strain, suggesting that the

fully stretched TDC could no longer dissipate energy over 200% strain rates, and the covalent crosslinked site was destroyed.

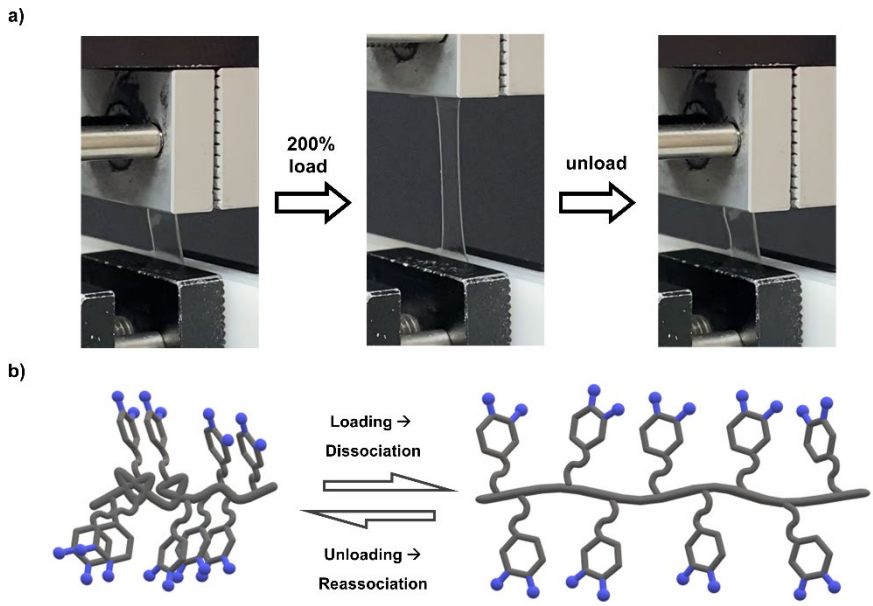

Figure 34. a) Image of the 200% strain rate cyclic tensile test for the ATE8 hydrogel. b) Mechanism of recovery property of ATE hydrogel (Han, *et al.*, 2022).

3.5. Biocompatibility of Hydrogel Adhesive

3.5.1. Biodegradation

The biodegradability of the ATE hydrogel was evaluated under physiological conditions by immersing the ATE hydrogel in a PBS solution (pH 7.4) at 37°C. The ATE hydrogel is degraded under physiological conditions due to the hydrolyzable ester bond in TDC **(Figure 35a)** (Browning, *et al.*, 2014). The ATE hydrogel was degraded by 51% after 36 h and completely degraded after 72 h **(Figure 35b, c)**.

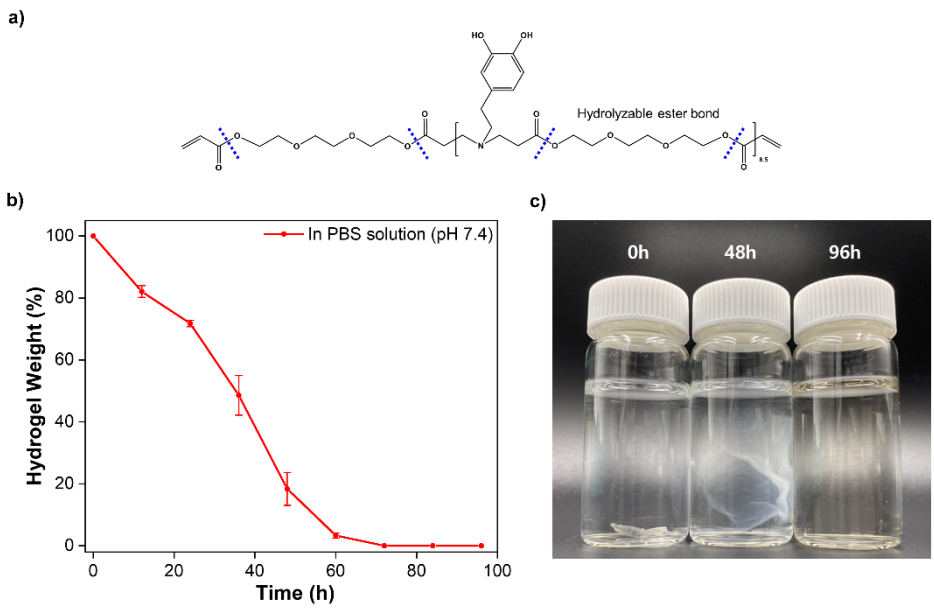

Figure 35. a) Degradation mechanism of TDC. b) In vitro biodegradation of the ATE hydrogel in PBS solution (pH 7.4) for 96 h. c) Image of ATE hydrogel at different time points (Han, *et al.*, 2022).

3.5.2. In vitro Biocompatibility Tests

The potential toxicity of the ATE hydrogel was evaluated using cell viability, cell cytotoxicity, apoptosis, and live/dead assays in a hydrogel–treated medium. The hydrogel–treated medium contained a degradation product of the ATE hydrogel. First, cell viability and cytotoxicity were measured using the WST–1 and LDH release assays over time. The effect of the hydrogel on apoptosis in STO cells was measured through Annexin V/PI staining and live/dead cell staining. Compared with the control group, the viability **(Figure 36a)**, cytotoxicity **(Figure 36b)**, apoptosis **(Figure 36c)**, and Live/Dead staining **(Figure 36d)** of STO cells in the hydrogel–treated medium exhibited a non–significant difference. These results indicate that the ATE degradation product is non–toxic and biocompatible.

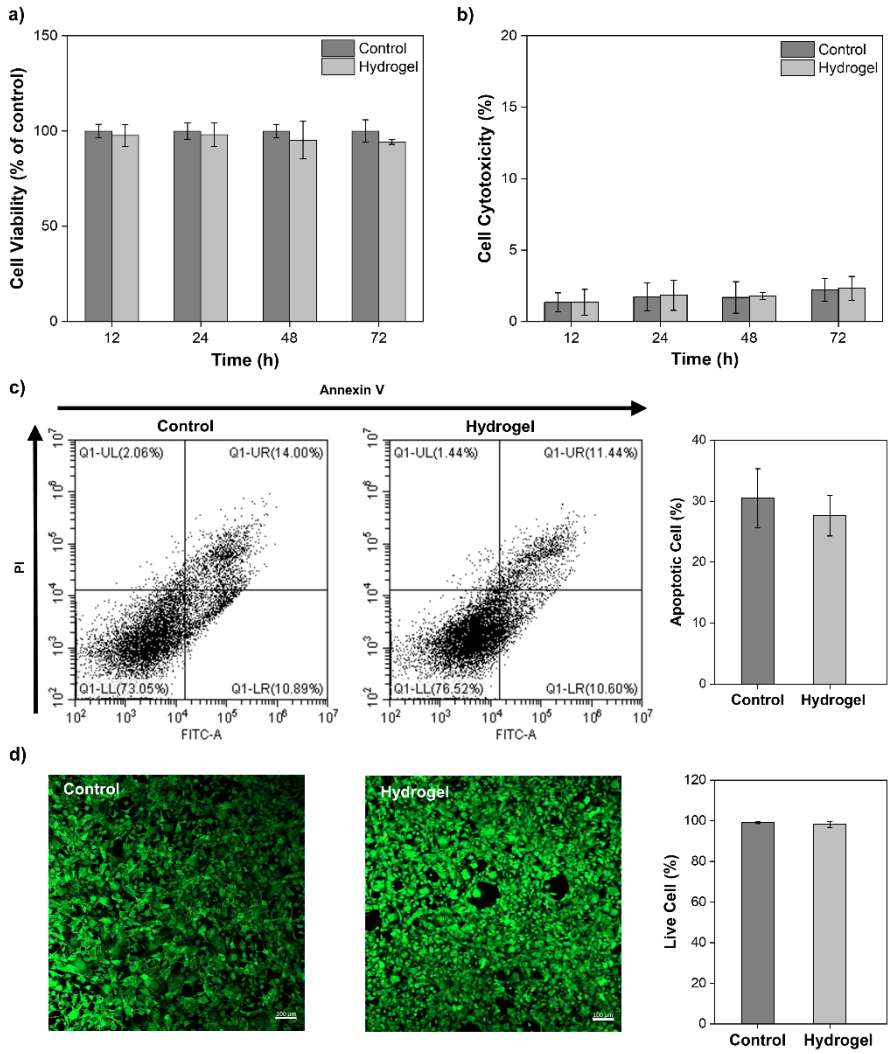

Figure 36. In vitro biocompatibility test of STO cells exposed to the hydrogel–treated medium. a) Effect of the ATE8 hydrogel degradation product on cell viability and b) potential toxicity and cell apoptosis. c) Annexin V–FITC/PI staining and d) Live/Dead cell staining 48 h after incubation (Han, *et al.*, 2022).

3.5.3. In vivo Wound Healing Tests

To evaluate the wound healing performance of the ATE hydrogel, quantitative (wound closure assay and vessel density) and histological analyses H&E and Masson's trichrome staining) were performed using rat models of skin wound healing. First, the change in wound size over time (0, 4, 8, and 10 days post–implantation) and vessel density (10 days post–implantation) in each group (control and hydrogel–treated groups) were observed. Compared to the control group (Tegaderm film–treated group) the ATE hydrogel–treated group exhibited faster healing **(Figure 37a, b)** and increased blood vessel formation around the wound site **(Figure 37c)**. Then to evaluate tissue regeneration, we compared the tissue thickness between the non–wounded (normal) and wounded (control and hydrogel–treated) groups **(Figure 38a)**. Compared to the normal group, we observed a significant thickening of the epidermal layer in the control group, which was twice as thick as that observed in the hydrogel–treated group **(Figure 38b)**. A thickening of the dermal layer around the wound sites was also observed, and it was thicker in the control group than in the hydrogel–treated group **(Figure 38c)**. Moreover, the hydrogel–treated group exhibited significantly higher collagen deposition **(Figure 38d)**. Collectively, these results suggest that the ATE hydrogel promotes tissue regeneration and accelerates wound healing (Loh*, et al.*, 2018) due to its pH–sensitive AA and high tissue adhesion in a moist environment. Excess exudates produced by wounds can be absorbed by AA, and the wound site can be protected by high tissue adhesion in a moist environment (Korting*, et al.*, 2011). Therefore, the ATE hydrogel maintains a moist environment at the wound site, accelerating wound healing.

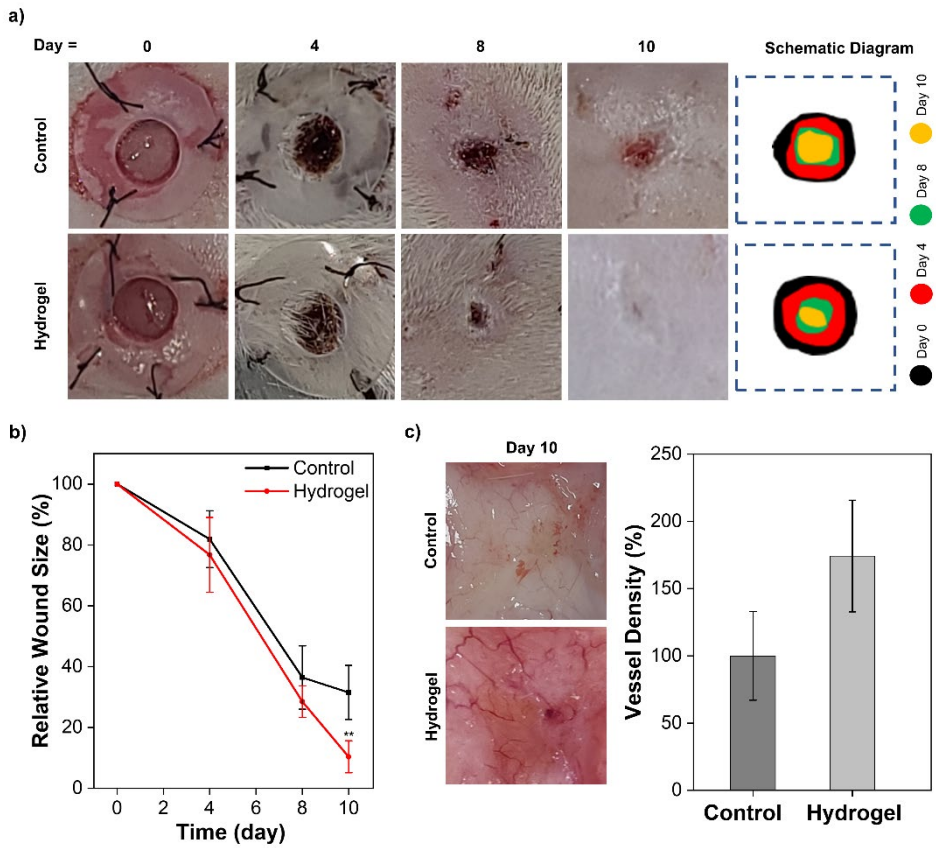

Figure 37. In vivo wound healing tests using rat models of skin wound healing. a) Effect of the ATE hydrogel on wound healing and b) change in wound size over time. c) Vasculogenesis around the wound site 10 days after wound healing (Han, *et al.*, 2022).

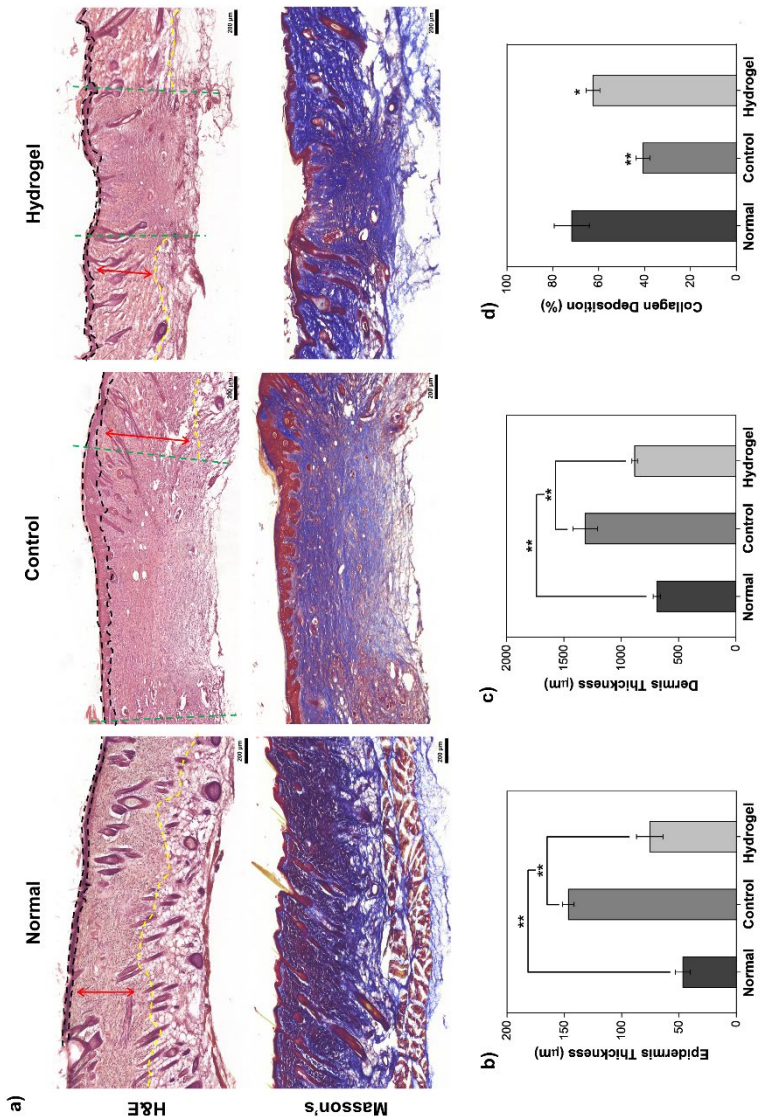

Figure 38. a) Hematoxylin and eosin staining and Masson's trichrome staining image. Black and green dashed lines represent the boundary of the epidermis and the wound site, respectively. Red arrows represent the dermis. Comparison of b) epidermis thickness, c) dermis thickness, and d) collagen deposition with the non–wounded (normal) and wounded (control and hydrogel–treated) groups. (** $p < 0.01$, * $p < 0.05$ vs normal) (Han, *et al.*, 2022)

4. Conclusion

In this part, the dopamine–modified crosslinking agent was designed, and a highly resilient hydrogel adhesive was manufactured using the dopamine–modified crosslinking agent. The linear and acrylate–terminated dopamine–modified crosslinking agent was successfully synthesized through the aza–Michael reaction between tri(ethylene glycol) diacrylate and dopamine, and approximately 8.5 dopamine molecules were incorporated in the crosslinking agent. The designed crosslinking agent forms a dual–crosslinked structure in the hydrogel network. Through this structure, the dopamine–modified crosslinking agent can be associated in the hydrogel network. The associated network structure and its reversibility enable hydrogel to withstand mechanical loading by dissociation of the crosslinking agent and recover (i.e., reassociation) its original shape without external stimuli. The resultant hydrogel adhesive exhibits high mechanical resilience with instant recovery, approximately 94% at a 200% strain rate.

Moreover, the association of crosslinking agents makes dopamine molecules in crosslinking agents exposed to the hydrogel surface, and they form robust tissue adhesion. The resultant hydrogel demonstrates 71.4 kPa maximum wet tissue adhesion and excellent adhesion maintenance in a moist environment (over 10 kPa after 48 h). Finally, the pH–sensitive AA backbone absorbs excess exudates and maintains a moist environment when applied at the wound site, and the ester bond incorporated in a dopamine–modified crosslinking agent enables hydrogel to hydrolyze under physiological conditions.

The dopamine–modified crosslinking agent makes hydrogel exhibit excellent elasticity with tissue adhesion. However, the resultant hydrogel is limited in stretchability compared to reported hydrogels. Therefore, further investigation is needed to enhance tensile elongation without a decrease in other mechanical properties.

Chapter 2

Toughness Enhanced Hydrogel Adhesives

1. Introduction

Hydrogel adhesives are widely used as wound closure patches due to their high similarity to living tissues (Yuk*, et al.*, 2022). Compared with surgical stitching, hydrogel adhesives can prevent secondary tissue damage and reduce time consumption (Deng*, et al.*, 2019, Han*, et al.*, 2023). However, hydrogel adhesives typically lack the adhesiveness and toughness required for securely holding and sealing wounds (Chen*, et al.*, 2022). In recent years, hydrogel adhesives with diverse functionalities, such as high toughness (Deng*, et al.*, 2021), stretchability (Mo*, et al.*, 2021, Yang*, et al.*, 2021), and self–healability (Chen*, et al.*, 2018, Hao*, et al.*, 2022) have been reported. However, most existing studies focus only on one specific property. Notably, to ensure the practical use of hydrogel adhesives as wound–sealing patches, a well–balanced combination of tissue adhesion, toughness, and mechanical resilience is required, posing a challenge due to the negative correlation among these characteristics (Yu*, et al.*, 2023).

The primary challenge in developing hydrogel adhesives is the simultaneous realization of strong wet tissue adhesion and high mechanical resilience. Wounded tissues produce large amounts of exudate, and joint areas and organs are frequently subjected to a wide range of motion (Hong*, et al.*, 2019, Xu*, et al.*, 2021, Zhao*, et al.*, 2023). For hydrogel adhesives to be used as wound–sealing patches, they must strongly adhere to wet tissues and adapt to dynamic movements without deformation (Chen*, et al.*, 2021, Wang*, et al.*, 2022). Insufficient adhesion and mechanical resilience of hydrogel adhesives can lead to poor contact with dynamic wound sites, which increases the risk of secondary infection (Xu*, et al.*, 2021) and limits their long–term use (Han*, et al.*, 2018).

Double network (DN) hydrogels can simultaneously achieve high toughness and mechanical resilience through their heterogeneous network structures (Chen, *et al.*, 2015). Specifically, DN hydrogels consist of a highly crosslinked first network that maintains a hydrogel shape and a slightly crosslinked/entangled second network that dissipates energy. When mechanical stress is applied, the second network redistributes energy, while the first network maintains the elasticity of the hydrogel (Slootman, *et al.*, 2022, Sun, *et al.*, 2013). Furthermore, if the applied stress exceeds the capacity of the first network, the fragments of the disrupted first network can act as crosslinking agents for the second network (Gong, 2010). As a result, DN hydrogels exhibit significantly increased toughness compared to single–network hydrogels. In recent years, the introduction of reversible bonds such as host–guest interactions (Dai, *et al.*, 2022), hydrophobic associations (Li, *et al.*, 2022), Schiff–base reactions (Zhou, *et al.*, 2021), interpenetrating structures (Li, *et al.*, 2015), and crystalline structures (Varshney, *et al.*, 2022) has enabled DN hydrogels to achieve high toughness with excellent elasticity.

Notably, toughness and adhesiveness are typically negatively correlated. As the toughness of an adhesive increases, its ability to wet the interface between substrates and adhesives decreases (Han, *et al.*, 2017). To address this trade–off relationship (Liu, *et al.*, 2022, Tobing, *et al.*, 2001), dopamine–modified crosslinking agents were introduced (Han, *et al.*, 2022). In this framework, acrylate–terminated and dopamine–modified crosslinking agents underwent covalent crosslinking with acrylate, and the dopamine molecules in the crosslinking agents generated reversible physical crosslinking and hydrogen bond with tissues. Although the hydrogel adhesives prepared using dopamine–modified crosslinking agents achieved high

mechanical resilience and strong tissue adhesion, their elongation was limited due to the hydrogel network being formed only by covalent bonds.

This part aimed to develop highly resilient DN hydrogel adhesives characterized by high wet tissue adhesion and toughness, enabling their application in dynamic environments. The DN structure was formed using a dopamine–modified crosslinking agent, tri(propylene glycol) diacrylate–dopamine crosslinking agent (TPDC), and linear poly(1–vinyl imidazole) (PVI). The first network was formed through the multiple crosslinking of TPDC, involving covalent bonds, hydrophobic associations, π–π stacking, and hydrogen bonds. The second network was established through additional intermolecular interactions induced by PVI addition, such as chain entanglement, cation–π interactions, and hydrogen bonds. The network structures were noncovalently associated by reversible physical interactions between poly(AA), TPDC, and PVI. The resulting acrylic acid–tri(propylene glycol) diacrylate–dopamine (ATP) hydrogel exhibited excellent stretchability and instant recovery properties through the noncovalently associated network structure. The hydroxyl group of dopamine and the amine group of PVI, exposed on the hydrogel surface, formed hydrogen bonds and participated in Schiff–base reactions with the wet tissue surface, ensuring the strong wet tissue adhesion of the ATP hydrogel. Moreover, the pH–sensitive AA allowed the hydrogel to maintain a moist environment by absorbing excess exudates from the wound site, promoting wound healing. Through these well–balanced mechanical characteristics, the ATP hydrogel can withstand successive cyclic loading and effectively seal damaged tissues. Consequently, ATP hydrogel has the potential to be utilized as a wound–sealing patch in dynamic tissues of the human body.

2. Experimental

2.1. Materials

1–vinyl imidazole (VI, 99%), and 2–hydroxy–4′–(2–hydroxyethoxy)–2–methylpropiophenone (Irgacure 2959, 98%) were purchased from Sigma–Aldrich. Tri (propylene glycol) diacrylate (TPGDA, average Mn 300) and tetraethyl thiuram disulfide (TETD, 97%) were purchased from Tokyo Chemical Industry Co., Ltd. Dopamine hydrochloride (99%) was purchased from Alfa Aesar. Acrylic acid (AA, 99.5%), 2,2′–azobisisobutyronitrile (AIBN, 98%), triethylamine (TEA, 99.0%), dimethyl sulfoxide (DMSO, 99.8%), *N*, *N*–dimethyl formamide (DMF, 99.5%), tert–butyl methyl ether (MTBE, 98.5%), ether (99.0%), and sodium azide (99.0%) were purchased from Samchun Chemicals Co., Ltd. 10× phosphate–buffered saline (PBS) solution was purchased from Tech & Innovation. Dulbecco's modified Eagle's medium (DMEM, #SH3243.01) was purchased from Hyclone Laboratories, Inc.

2.2. Synthesis of Crosslinking Agent

Tri(propylene glycol) diacrylate–dopamine crosslinking agent (TPDC), was synthesized via an aza–Michael addition reaction. The molar ratio of the carbon double bond of diacrylate and amine of dopamine hydrochloride was set as 1.1: 0.5 to make an acrylate–terminated crosslinking agent. Dopamine hydrochloride (1.89 g, 10 mmol) and TPGDA (3.30 g, 11 mmol) were added to DMSO (12.12 g) under N_2 purging and stirred at 25 °C for 20 min until the solution became clear. TEA (1.01 g, 10 mmol) was then added to adjust pH to 8, and the mixture was stirred at

80 °C for 12 h in the dark. After the reaction, TEA salt was removed through suction filtration. The filtered solution was washed with MTBE three times to remove DMSO and the unreacted monomer. Finally, the residual solvent was removed using a rotary evaporator at 60 °C for 6 h. A yellow–transparent liquid was obtained and stored at −20 °C.

2.3. Synthesis of Linear Cationic Polymer

Poly(1–vinyl imidazole) was synthesized via reversible addition−fragmentation chain-transfer polymerization. VI (4.7 g, 50 mmol), TETD (0.3 g, 1.0 mmol), and AIBN (0.32 g, 2 mmol) were added to DMF (20.0 g) under N_2 purging for 20 min. The solution reacted at 70 °C for 12 h. The reactants were washed by repeating the process of precipitating in ether and redissolving in DMF. Finally, the residual solvent was removed by vacuum evaporation at 25 °C.

2.4. Preparation of Hydrogels

The acrylic acid–tri(propylene glycol) diacrylate–dopamine (ATP) pre–gel was synthesized in DMSO by free radical photopolymerization. AA (2.0 g), TPDC (0.9 g, 0.7 mole% of AA), PVI (0.04 g, 2 wt.% of AA), and Irgacure 2959 (0.02 g, 1 wt.% of AA) were dissolved in DMSO (6.8 g, 30% solid content). The mixture was poured into a Teflon mold with dimensions of 12 × 75 × 0.5 mm^3 (W × L × T). The mixtures were covered with a silicon–coated PET film and subjected to UV irradiation for 5 min using a UV light–emitting diode lamp (365 nm, intensity = 17mW/cm^2). After polymerization, a yellow–transparent pre–gel was obtained. The resulting ATP pre–

gel was washed with DMSO and then immersed in cold DIW for 12 h, changing to fresh DIW every 2 h. After the solvent exchange, a white–opaque ATP hydrogel was obtained and stored at −20 °C. The ATP hydrogels with different PVI contents (0, 1, 3, and 4 wt.%) were prepared following the same procedure. The hydrogel with *x* wt.% of PVI was denoted as the ATP*x* hydrogel. For samples without special mention, the ATP2 hydrogel was used.

2.5. Characterization

The Aza–Michael reaction was monitored through Fourier transform infrared (FT–IR) spectroscopy. The IR spectra were recorded using an FT–IR spectrometer (Nicolet iS20, Thermo Fisher Scientific). All FT–IR samples were measured at 25 °C using the attenuated total reflection (ATR) mode. The obtained curves were normalized using the carbonyl ester bond band (1,720 cm^{-1}).

The molecular structure of synthesized crosslinking agents, the linear polymer, and the released solvent was verified using a proton and carbon nuclear magnetic resonance (^{1}H and ^{13}C NMR) spectrometer (400–MHz, JNM–ECX400, JEOL). All NMR samples were measured at 25 °C, and tetramethylsilane (0.03% in DMSO–d6 and D2O) was used as an internal standard (δ = 0 ppm).

2.6. Solvent Exchange

The pre–gel was immersed in DIW to remove the DMSO in the pre–gel. To monitor the extracted solvent over time, 100 mg of pre–gel was immersed in 2 mL of D_2O for 12 h (fresh D_2O every 2 h). The extracted DMSO was confirmed using the ^1H NMR spectra, and the solvent–exchange ratio was calculated using the spectra as well. (D_2O_n = 4.8 ppm peak integral at n h, $DMSO_n$ = 2.5 ppm peak integral at n h)

$$\text{Solvent extraction } (E_n) = \frac{DMSO_n}{D_2O_n}$$

$$\text{Extraction ratio } (\%) = \frac{E_n}{\sum E_n} \times 100$$

2.7. Swelling Ratio and Water Content

The swelling ratio was measured using the pre–gel after immersion in DMSO and DIW at 25 °C for 24 h. A 12 × 12 (W × L) pre–gel sample was used, and the swelling ratio was calculated based on its weight and volume change. The weight and volume of the gel after being immersed in the solvent for n h were denoted $weight_n$ and $volume_n$, respectively.

$$\text{Swelling ratio } (\%) = \frac{weight,\ volume_n}{weight,\ volume\ of\ pre-gel} \times 100$$

The water content of the hydrogel was calculated based on the mass loss after lyophilization.

$$\text{Water Content (\%)} = \frac{wt.of\ hydrogel - wt.of\ lyophilized\ hydrogel}{wt.of\ hydrogel} \times 100$$

2.8. X–ray Photoelectron Spectroscopy (XPS)

The surface chemical composition of the hydrogel was obtained using an XPS spectrometer (K–Alpha, Thermo Scientific) by recording X–ray photoelectron spectra. The lyophilized hydrogel was used for XPS analysis. A monochromatic Al Kα X–ray (hν = 1,486.6 eV) source was used, operating at 12 kV and 72 W. The neutral C1s peak was used as a reference (set at 284.6 eV).

2.9. Tensile Test

The tensile test was conducted using 30 mm length hydrogel. 10 mm of both ends of the hydrogel were covered with a corona–treated PET film to be used as a grip. For the crack tip tensile test, 1 mm of crack was generated at the center of the hydrogel **(Figure 39)**. A tensile test was conducted at a rate of 100 mm/min at 25 °C and 50 ± 10% RH using a Texture Analyzer (TA.XT plus, Stable Micro Systems).

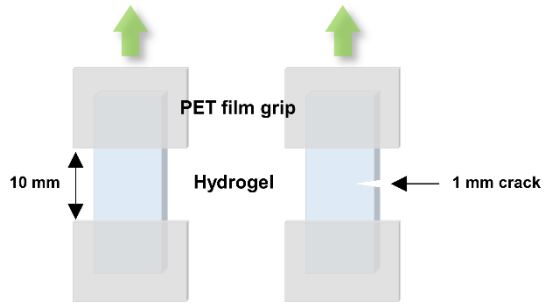

Figure 39. Schematic of tensile test and crack tip tensile test process.

2.10. Lap Shear Test

The tissue adhesion of hydrogel was measured through a lap shear test, and the wet porcine skin was used as a substrate due to its high similarity to human tissues. The lap shear tests were conducted at a rate of 50mm/min at 25 °C and 50 ± 10% RH using a Texture Analyzer (TA.XT plus, Stable Micro Systems). Before attaching the hydrogel, the porcine skins were immersed in sodium azide solution (0.01 w/v% in DIW and 1× PBS solution) for hydration and to prevent degradation. Then, DIW/PBS solutions were sprayed to make a thoroughly wetted porcine skin surface. The hydrogel was attached with 1 kPa pressure for 10 s. The sample was stored in a covered stainless tray, and DIW/PBS solutions were sprayed to maintain a moist environment. Unless otherwise specified, the tests were conducted 3 h after adhesion.

2.11. Cyclic Tensile Test

Cyclic tensile tests were conducted using a Texture Analyzer (TA.XT plus, Stable Micro Systems) at 25 °C and 50 ± 10% RH. The tensile tests were conducted at a rate of 100 mm/min and repeated without rest. The residual strain, hysteresis energy loss (ΔU), and resilience values were calculated using the initial loading–unloading curve.

$$\Delta U = \int_{loading} \sigma d\varepsilon - \int_{unloading} \sigma d\varepsilon$$

$$\text{Resilience (\%)} = \frac{\int_{unloading} \sigma d\varepsilon}{\int_{loading} \sigma d\varepsilon} \times 100$$

2.12. Burst Pressure Test

A 4 mm hole was introduced in the porcine skin using a biopsy punch. Before attaching the hydrogel, the porcine skin was sprayed with DIW. Then, a 1 × 1 mm^2 (W × L) hydrogel was adhered to the hole. The porcine skin was then placed in a customized apparatus with an airflow of 50 cc/min. The pressure was measured using a manometer **(Figure 40)**.

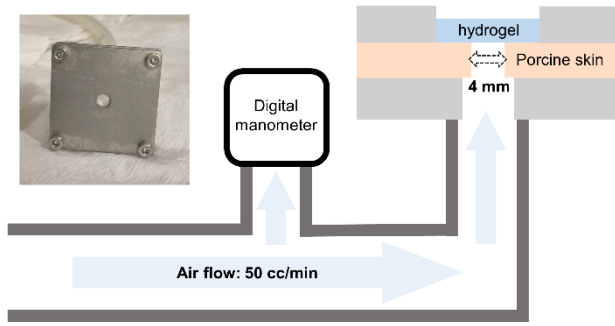

Figure 40. Schematic of the burst pressure test process (Han, *et al.*, 2024).

2.13. Biodegradability Test

The lyophilized hydrogel (50 mg) was immersed in 1 × PBS solution (5 mL, pH 7.4) at 36 °C. After a specific time, the degraded hydrogel was washed with DIW and lyophilization. The degradation rate of the hydrogel was calculated using the mass loss of the gel.

2.14. Cell culture and In vitro Biocompatibility Tests

Cell Culture: To prepare hydrogel–treated DMEM media, the lyophilized hydrogel was immersed in DMEM at 37 ° C until hydrogel was degraded entirely (0.5 mg / 1 mL). STO cells were cultured in DMEM (10% FBS, 1% antibiotics) at 37 °C with 5 % CO_2. When the STO cells reached 80% confluence, the medium was replaced with hydrogel–treated DMEM and incubated. Pristine DMEM was used as the control.

Cell Viability: STO cells, with a seeding density of 1×10^5 cells, were seeded into 96–well cell culture plates and cultured for 72 h. STO cells were rinsed with PBS and incubated in 100 μL of the 10% EZ–Cytox (DoGenBio) medium at 37 °C for 30 min. Cell viability was analyzed using a microplate spectrophotometer (Epoch 2, BioTek), and the absorbance at 450 nm was measured.

Cell Cytotoxicity: Cell cytotoxicity was evaluated by measuring the enzymatic activity of lactate dehydrogenase (LDH). The LDH release was evaluated using the EZ–LDH kit following the manufacturer's instructions. The supernatant was used to measure the released LDH. Cell cytotoxicity was analyzed using a microplate spectrophotometer (Epoch 2^{TM}, BioTek), and the absorbance at 450 nm was measured.

Cell Live/Death: The viability of STO cells was assessed using a Live/Dead^{TM} Cell Imaging Kit (Thermo Fisher Scientific, #R37601) following the manufacturer's instructions. STO cells were seeded in μ-slide Chemotaxis 3D (IBIDI, Martinsried, Germany) and cultured for 72 h. Then, the Live Green and Dead Red reagents were added to the medium and incubated for 15 min at 25 °C. The live and dead cells were analyzed using a confocal microscope system (LSM 710, Carl Zeiss, Oberkochen, Germany).

2.15. In vivo Biocompatibility Tests

Wound Healing Test: Six–week–old male Sprague Dawley rats were used for in vivo biocompatibility tests. Rats were anesthetized with a mixture of Alfaxan (80 mg/ kg) and xylazine HCl (10 mg/ kg). A 6 mm diameter circular wound was created on the rats' backs using a biopsy punch and wound sites were immobilized by suturing with a silicon wound splint. In the hydrogel–treated group, the hydrogel was implanted and dressed with a Tegaderm film. In the control group, only the Tegaderm film was implanted. Tissue regeneration and vasculogenesis were observed at different time points (0, 4, 8, and 11 d after implantation). The wounded skin was harvested 11 d after implantation for the histological analysis. All animal experiments were approved by the Institutional Animal Care and Use Committee of Seoul National University (SNU–230127–1)

Immunohistochemistry: The skin slides were fixed in 80% acetone solution for 20 min. The slides were rinsed with PBS and incubated in 5% normal goat serum for 30 min. The samples were incubated with the VEGF antibody (sc–7269, Santa Cruz, 1:100 dilution) containing the PBST (PBS with 0.1% Triton–X) medium for 2 h, followed by incubation in a VEGF antibody (1:100 dilution) containing the PBST medium for 1 h. Images were acquired using a confocal microscope (LSM 710, Carl Zeiss, Oberkochen, Germany).

Hematoxylin and Eosin (H&E) Staining*:* The skin samples were fixed in 4% paraformaldehyde (PFA) for 2 h and dehydrated in 30% sucrose for 24 h. The tissues with a 20 μm thick longitudinal section were obtained and fixed with 4% PFA for 5 min. The fixed samples were stained with H&E for 5 min. The stained samples were

washed with ethanol three times and incubated in xylene for 5 min. All images were acquired using the SlideViewer software (3DHISTECH, Budapest, Hungary).

Masson's Trichrome Staining: Masson's trichrome staining (VitroView™ Masson's Trichrome Stain Kit, Rockville, USA) was conducted following the manufacturer's instructions. All images were acquired using the Eclipse Ts2™ fluorescence microscope (Nikon, Tokyo, Japan). Red represented keratin, muscle fibers, and the cytoplasm; blue represented collagen; and black represented the cell nuclei.

3. Results and Discussion

3.1. Preparation of Crosslinking Agent

The linear dopamine–modified crosslinking agent was synthesized using tri (propylene glycol) diacrylate and dopamine hydrochloride *via* the aza–Michael reaction **(Figure 41a)**. The molar ratio of the C=C of acrylate to the NH_2 of dopamine was set as 1.1: 0.5 to make the acrylate–terminated crosslinking agent. This crosslinking agent, tri (propylene glycol) diacrylate – dopamine crosslinking agent, was denoted as TPDC. A reduction in the 810 cm^{-1} band (acrylate C=C bond) in the FT–IR spectra showed that the amine group dopamine fully reacted after 9 h **(Figure 41b)**.

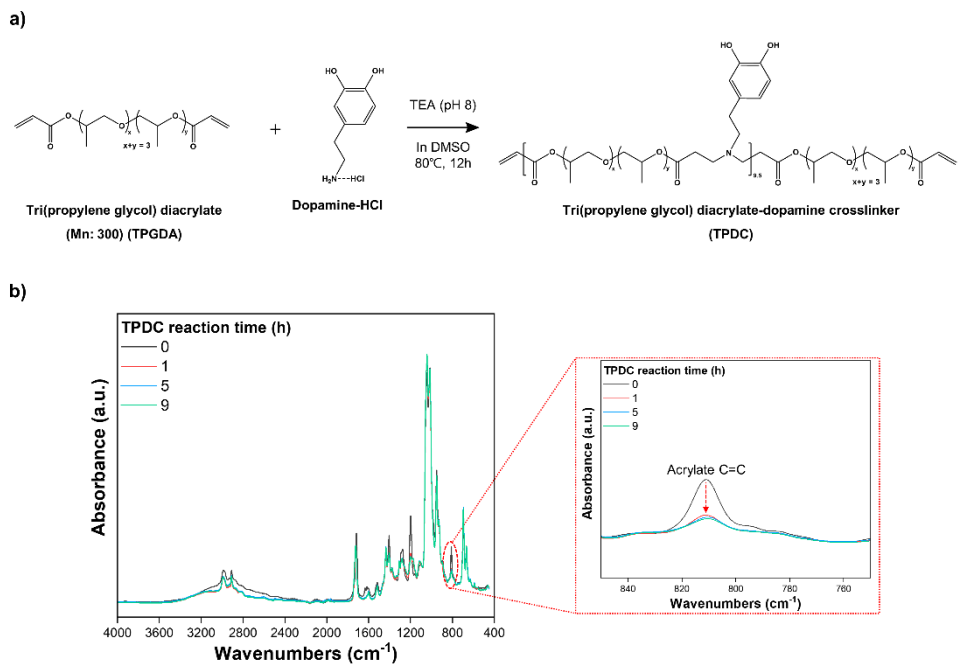

Figure 41. a) Chemical synthesis process of TPDC. b) FT–IR spectra of TPDC at different time points during the reaction (Han, *et al.*, 2024).

The end–group fidelity of the TPDC was confirmed by the acrylate C=C bond proton peaks (5.9–6.4 ppm) in the ^{1}H NMR spectrum **(Figure 42)**. The molecular weight of TPDC was calculated using the proton peak integral values between 5.9–6.0 ppm (acrylate C=C) and 6.55–6.75 ppm (benzene CH, adjacent to OH). The peak integral ratio of the 5.9–6.0 ppm peaks to 6.55–6.75 ppm peaks is 1 : 9.5, indicating the incorporation of approximately 9.5 dopamine molecules in each TPDC. Hence, the average molecular weight of TPDC was estimated to be 4,600.

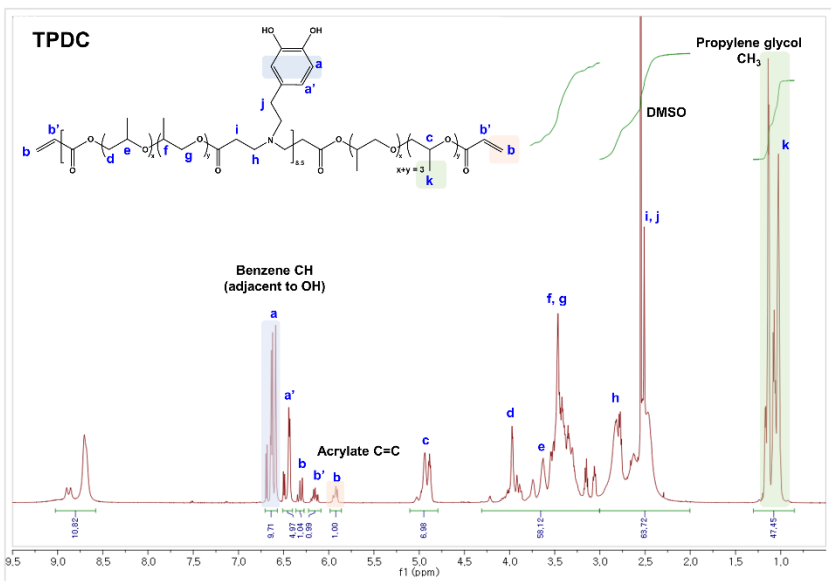

Figure 42. The ^{1}H NMR spectrum of TPDC (Han, *et al.*, 2024).

3.2. Preparation of Linear Polymer

Linear PVI to form a second network through physical interactions was synthesized through reversible addition−fragmentation chain–transfer polymerization **(Figure 43a)**. The target number average molecular weight of PVI was set at 38.6 kDa. The reaction was confirmed by the disappearance of the vinyl C=C bond proton peaks (4.8–5.6 ppm) of ^{1}H NMR spectroscopy **(Figure 43b)**.

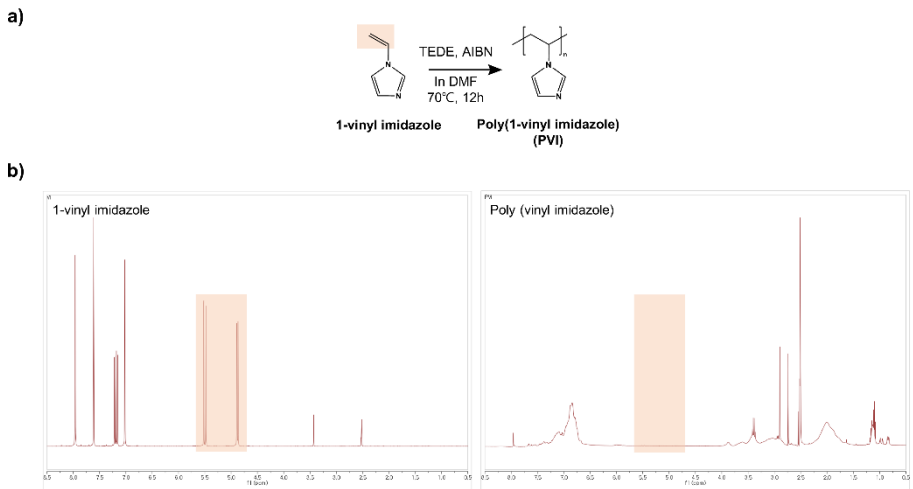

Figure 43. a) Chemical synthesis process of PVI and b) the ^{1}H NMR spectrum of VI and PVI (Han, *et al.*, 2024).

3.3. Preparation of Hydrogel Adhesives

The ATP double network hydrogel was prepared by following two steps: 1) radical polymerization between the acrylate monomer AA and the crosslinking agent TPDC, and 2) solvent exchange. First, the synthesized TPDC was copolymerized with AA using DMSO as a solvent. In this step, PVI was used to form the second network by physical intermolecular interactions in the prepared hydrogel network (**Figure 44**). Next, the prepared organogel was immersed in cold DIW for 12 h to remove any unreacted monomers and DMSO. The release of unreacted monomers and DMSO was monitored using ^{1}H NMR spectroscopy, and the monomers were fully extracted after 7 h (**Figure 45**). The ATP hydrogel was obtained after immersing the pre–gel in DIW for 12 h. The hydrogel with *x* wt.% of PVI was denoted as the ATP*x* hydrogel.

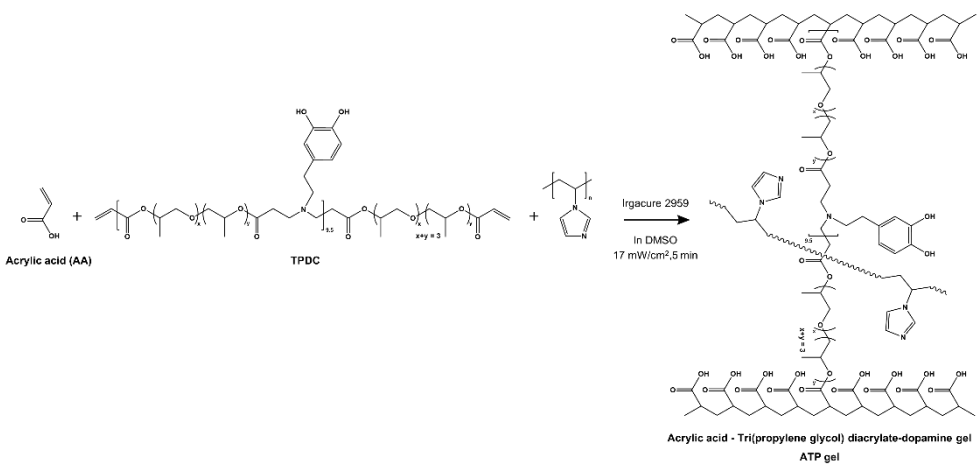

Figure 44. Chemical synthesis process of ATP gel (Han, *et al.*, 2024).

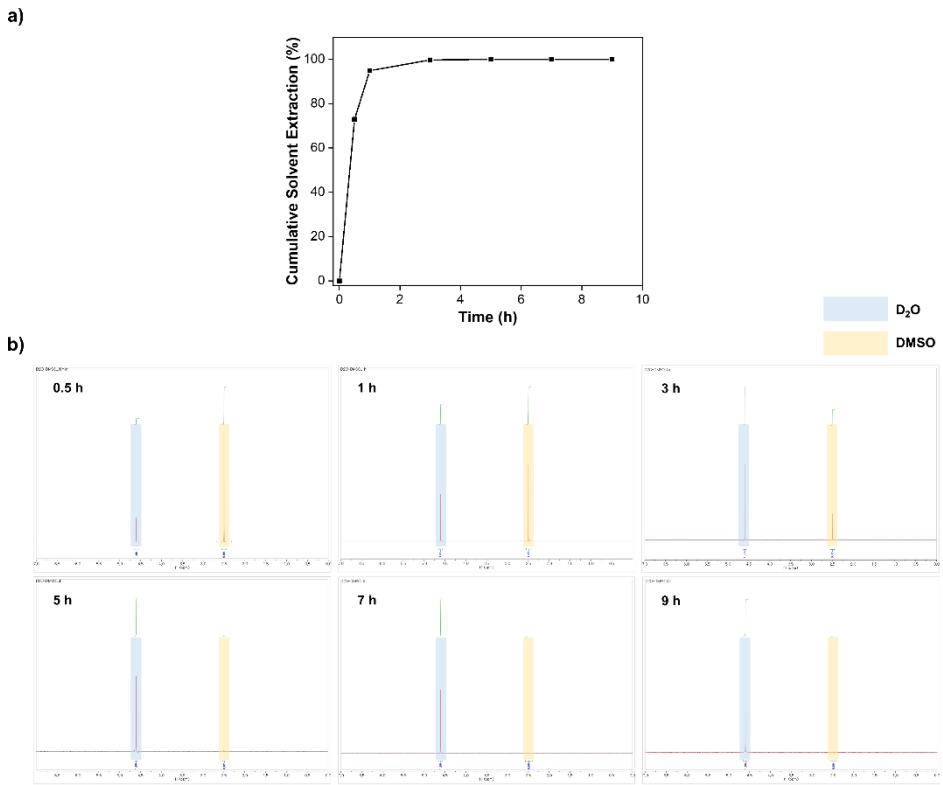

Figure 45. Solvent extraction ratio of ATP2 pre–gel and b) ^{1}H NMR spectrum of released DMSO when the ATP2 gel is immersed in D_2O at different time points (Han, *et al.*, 2024).

3.4. Characterization of Hydrogel Adhesives

The ATP hydrogel comprises two networks. The first network involves the covalent crosslinking between AA and TPDC, along with noncovalent bonds, such as hydrophobic associations (propylene glycol and dopamine) and hydrogen bonds [poly(AA) and dopamine] (**Figure 46a**). The second network involves the non–covalent crosslinking induced by the PVI (**Figure 46b**). Linear PVI forms physical crosslink through chain entanglement and intermolecular interactions such as hydrogen bonding, hydrophobic interactions, π–π stacking, and cation–π interactions.

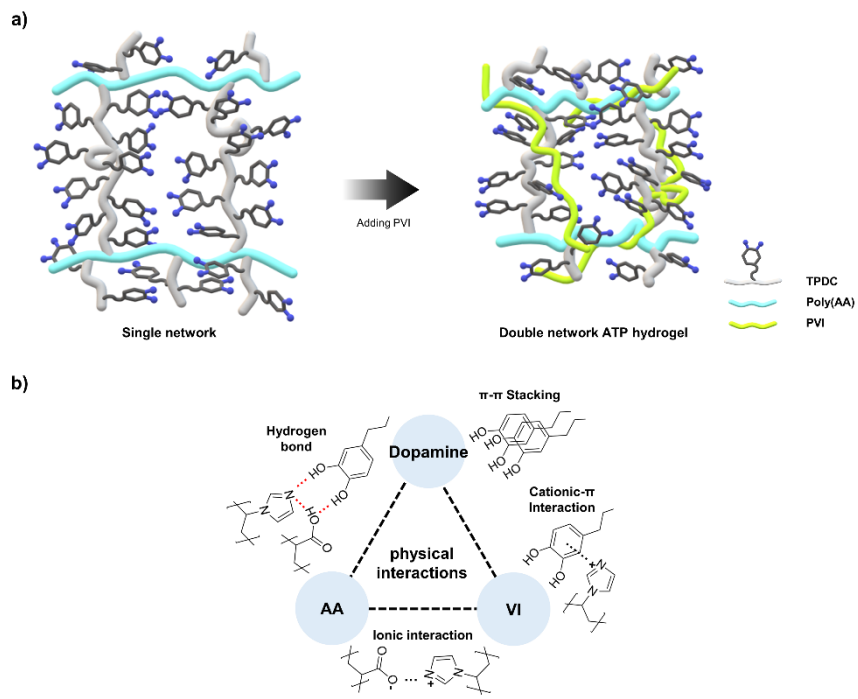

Figure 46. a) Scheme of the ATP hydrogel network structure. b) The physical intermolecular interactions formed in ATP hydrogel (Han, *et al.*, 2024).

The effect of PVI on the formation of the second network was confirmed by variations in the swelling ratio and surface atomic ratio of the ATP hydrogel with changes in the PVI content (**Table 6**). The ATP0 hydrogel (without PVI) swelled by approximately 30%, whereas the other hydrogels (with various PVI contents) contracted. As the PVI content increased, the hydrogel contraction ratio gradually increased from approximately 20% (ATP1 hydrogel) to 50% (ATP4 hydrogel), and the water content correspondingly decreased from approximately 76% (ATP0 hydrogel) to 38% (ATP4 hydrogel). The surface atomic ratios of the ATP hydrogels were determined through X–ray photoelectron spectroscopy (XPS) (**Figure 47**). As the PVI content increased, the proportion of C–O bonds increased from 17.0% (ATP0 hydrogel) to 26.2% (ATP4 hydrogel). Specifically, as intermolecular interactions such as hydrogen bonds, hydrophobic associations, cation–π interactions, and chain entanglements increased, the hydrophilic moieties (hydroxyl group of dopamine and amine group of imidazole) became more exposed to the hydrogel surface as the hydrophobic moieties (propylene glycol and benzene ring of dopamine) became more associated within the hydrogel network. In other words, the addition of PVI enhanced the intermolecular interactions in the bulk layer, resulting in the formation of a denser network structure of the ATP hydrogel.

Table 6. Swelling and contraction properties of ATP hydrogel with different PVI contents.

ATP*x* hydrogel	**PVI contents (wt. %)**				
	0	**1**	**2**	**3**	**4**
Weight change (%)	121.2	79.6	54.3	53.0	50.5
Volume change (%)	132.7	83.1	62.5	57.4	52.3
Water content (%)	76.3	65.3	46.4	41.0	38.1
Atomic ratio (C–O %)	17.0	19.9	22.9	24.3	26.2

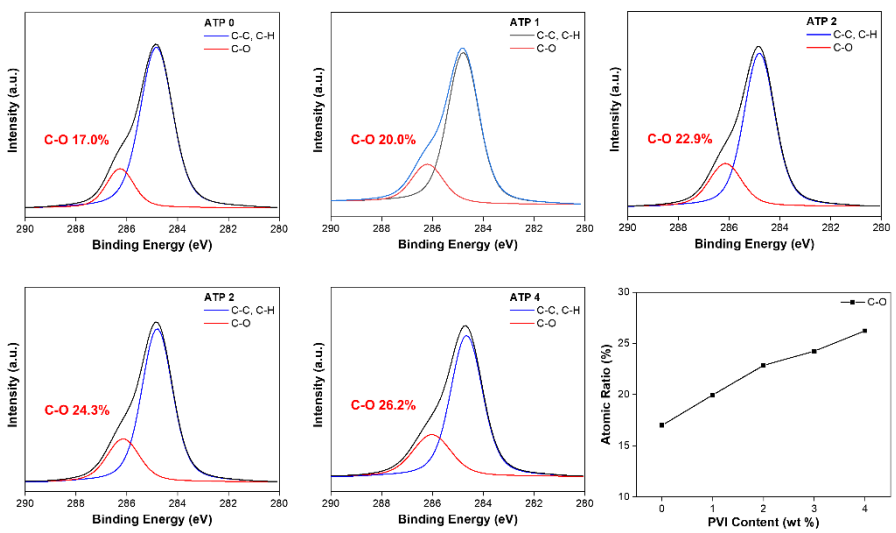

Figure 47. Peak–fitting XPS spectra of a) ATP0, b) ATP1, c) ATP2, d) ATP3, and e) ATP4 hydrogels (Han, *et al.*, 2024).

The ATP hydrogel network consisted of two main types of bonds: covalent bonds formed between AA and TPDC, and noncovalent bonds formed between poly(AA), TPDC, and PVI. To evaluate the effect of these noncovalent intermolecular interactions such as hydrogen bonds, hydrophobic associations, cation–π interactions, π –π interactions, and chain entanglements on the formation of the hydrogel network, the ATP2 pre–gel was immersed in DMSO and DIW for 24 h, and the weight change of the pre–gel was observed. The weight of the ATP2 pre–gel increased and decreased by approximately 2,100 and 55% with respect to its original weight when immersed in DMSO and DIW, respectively (**Figure 48a**). Moreover, comparing the gels immersed in each solvent,the ATP hydrogel is opaque, and the ATP organogel is transparent (**Figure 48b**). This difference in light transmittance is caused by the association of polymer network structures forming light scattering centers. These results demonstrate that noncovalent intermolecular interactions between poly(AA), TPDC, and PVI influence the formation of the hydrogel network, making it denser (Eklund*, et al.*, 2020, Zhou*, et al.*, 2018).

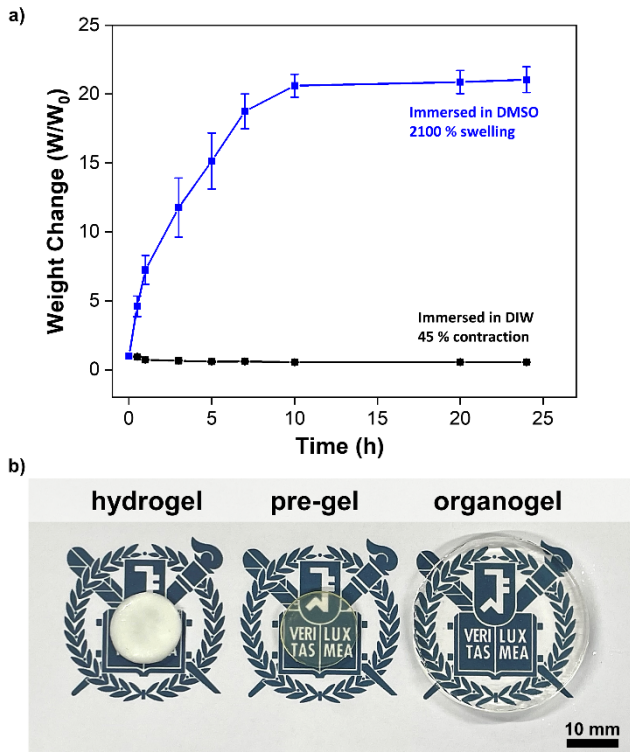

Figure 48. a) Swelling and contraction ratio of ATP2 pre–gel when immersed in DMSO and DIW for 24 h. b) Images of ATP2 organogel, pre–gel, and hydrogel (Han, *et al.*, 2024).

3.5. Tensile Property

Because the mechanical properties of hydrogels are affected by the corresponding hydrogel network structure, tensile tests were conducted to examine the change in the mechanical properties with varying PVI contents (0 wt.% to 5 wt.%). The addition of PVI, which formed the second network through physical crosslinking, increased the fracture elongation and tensile strength of the ATP hydrogels. The fracture elongation and tensile strength of the ATP0 hydrogel were 510% and 80 kPa, respectively, whereas the corresponding values for the ATP4 hydrogel dramatically increased to 910% and 310 kPa, respectively (**Figure 49a and Table 7**). The physically crosslinked networks of the hydrogel dissociated under mechanical stress, resulting in energy dissipation and redistribution energy, therefore, the fracture elongation and tensile strength increased with the increase in PVI content.

Table 7. Tensile strength and fracture elongation of ATP hydrogel with different PVI contents.

ATP*x* hydrogel	**PVI contents (wt.%)**				
	0	**1**	**2**	**3**	**4**
Tensile strength (kPa)	79.4	121.4	213.7	240.1	318.9
Fracture elongation (%)	518	678	883	854	919

The fracture elongation limit of the PVI–containing hydrogels (ATP2–4 hydrogels) was observed to be 900%, beyond which the network structure could no longer withstand mechanical loading. At elongations exceeding 600%, fluctuations in the strain–stress curve were observed in the PVI–containing ATP hydrogels (ATP1–4 hydrogels). These fluctuations were attributable to the occurrence of necking and

crack generation in the hydrogel as the first network was destroyed, which intensified with further stretching of the hydrogel (**Figure 49c**) (Gong, 2010).

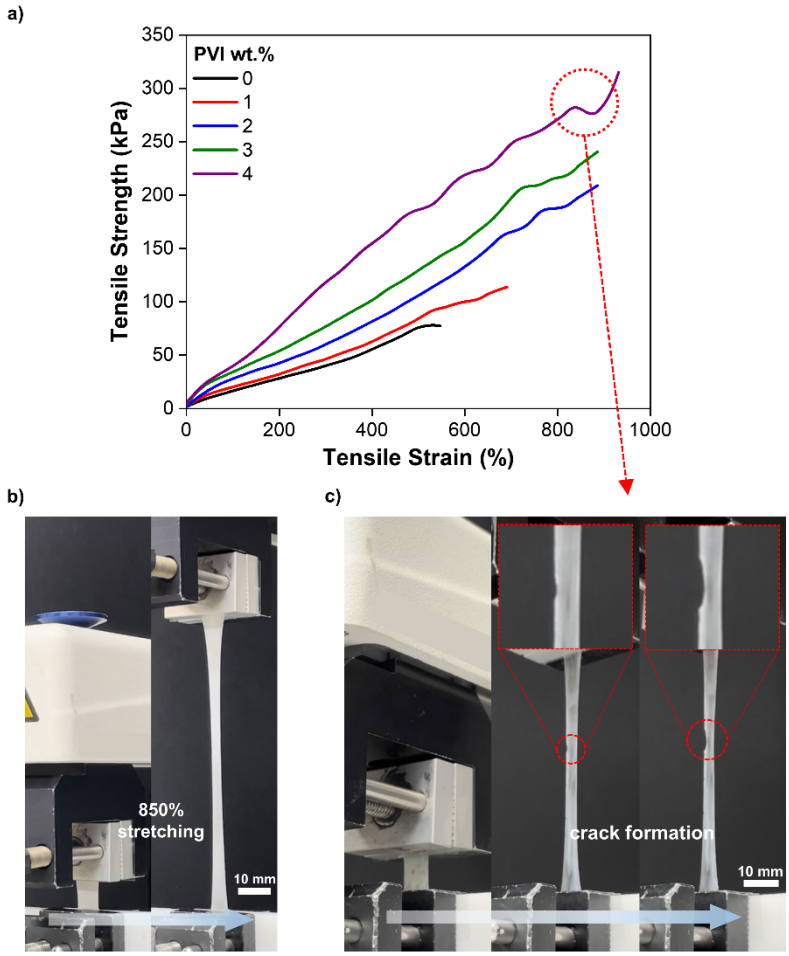

Figure 49. a) Strain–stress curves of the ATP hydrogels with different PVI contents. b) Photographs of the stretched ATP2 and c) ATP4 hydrogel (Han, *et al.*, 2024).

The effect of the DN structure on the mechanical properties of the ATP hydrogels was evaluated through crack tip tests. The PVI–containing DN hydrogel (ATP2 hydrogel) was approximately 150% more elongated than the single–network hydrogel (ATP0 hydrogel). The higher crack propagation resistance of the ATP2 hydrogel was attributable to the effective redistribution of stress around the crack tip by the DN network (**Figure 50a, b**) (Slootman*, et al.*, 2022).

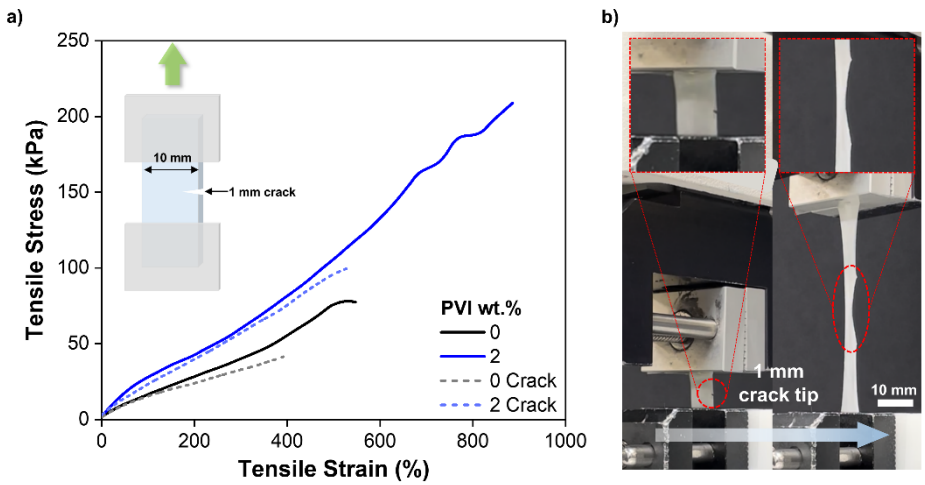

Figure 50. Stress–strain curve of notched ATP0 and ATP2 hydrogels and e) photographs of notched and stretched ATP2 hydrogels (Han, *et al.*, 2024).

3.6. Adhesion Property

The adhesion strength of the ATP hydrogels was evaluated by conducting a lap shear test and observing the failure mode of the ATP hydrogels. The failure mode of an adhesive is determined by the balance between its adhesion and cohesion forces. Analyzing the adhesion strength and failure modes reveals the mechanical performance of the adhesive (**Figure 51**).

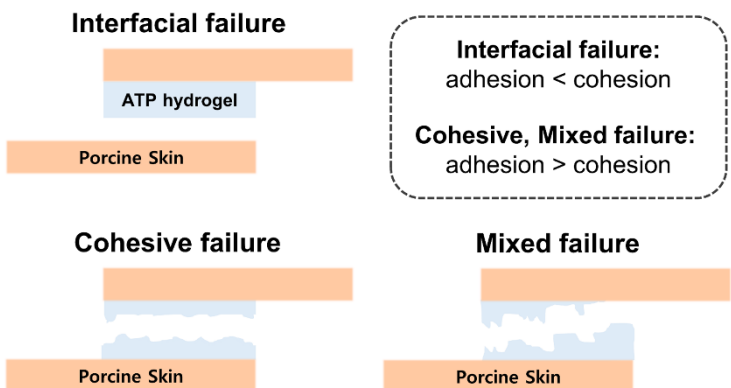

Figure 51. The failure mode of adhesive (Han, *et al.*, 2024).

Porcine skin was selected as the model tissue owing to its similarity to human skin (Sullivan*, et al.*, 2001). To simulate a wet physiological environment, the ATP hydrogels were attached to fully wetted porcine skin and stored in wet conditions. The addition of PVI significantly increased the adhesion strength from 16.2 kPa (ATP0 hydrogel) to 42.1 kPa (ATP1 hydrogel) with a linear progression to 45.5 kPa (ATP2 hydrogel) up to an added content of 2 wt.% (**Figure 52a**). Specifically, the addition of PVI increased the amount of the amine group of imidazole and promoted the exposure of the hydroxyl group of dopamine to the hydrogel surface **(Figure 53)**.

Therefore, the adhesion strength was expected to increase with the PVI content. However, when the PVI addition content exceeded 3 wt.%, the adhesion strength of the hydrogel decreased to 31.7 kPa (ATP4 hydrogel). This phenomenon occurred because the hydrogen bonds, hydrophobic associations, cation–π interactions, and chain entanglements were intensified by the addition of PVI, which increased the modulus of the hydrogel. The elevated modulus led to reduced wettability, resulting in the decreased adhesion strength of the hydrogel (Tobing and Klein, 2001). The increase in the modulus was confirmed by the strain–stress curve of the ATP hydrogels and the failure modes. As the PVI content increased, the failure modes of the hydrogel changed from a mixed failure mode (ATP0–2 hydrogels) to interfacial failure (ATP3 and ATP4 hydrogels) (**Figure 52b**). These results demonstrate that ATP hydrogels robustly adhere to biological tissues, and adhesion strength varies with the PVI content as the modulus of the hydrogel changes.

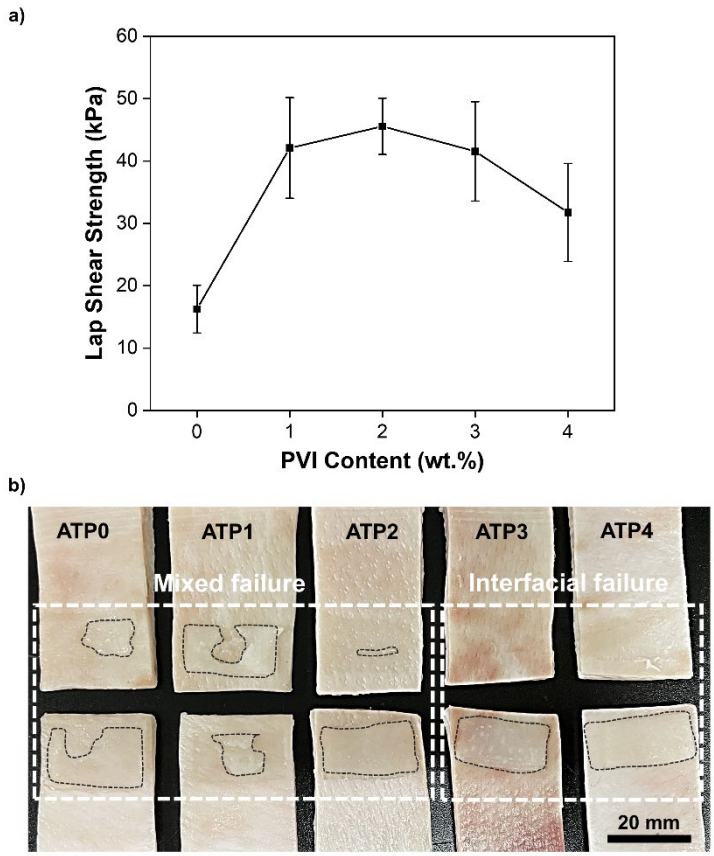

Figure 52. a) Tissue adhesion strength of ATP hydrogels with different PVI contents. b) Failure mode of the ATP hydrogels after lap shear tests with different PVI contents. Grey dashed lines represent the residual ATP hydrogels on the porcine skin after lap shear test (Han, *et al.*, 2024).

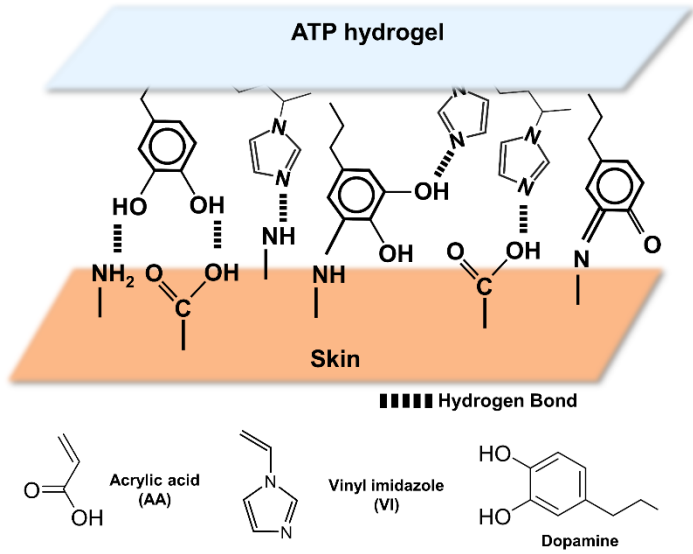

Figure 53. The adhesion mechanism of ATP hydrogel (Han, *et al.*, 2024).

3.7. Change in Adhesion Strength Over Time

When a hydrogel is implanted in the human body, it is exposed to wet conditions induced by the exudate produced by damaged skin and sweat from everyday activities. Therefore, hydrogel adhesives must maintain adhesion in wet environments to ensure durability. To evaluate the adhesion maintenance of the ATP hydrogel, the change in the tissue adhesion over time (0, 1, 3, 6, 10, and 24 h) under wet conditions was observed using the ATP2 hydrogel, which exhibited the highest adhesion strength among the prepared hydrogels. The initial adhesion strength was 24.8 kPa, and gradually increased to a peak value of 45.5 kPa 3 h after adhesion (**Figure 54a**). The exposed hydroxyl group of dopamine and the amine group of PVI formed hydrogen bonds with the functional groups present in the skin, such as the amine, carboxylic acid, and hydroxyl groups. Therefore, the ATP hydrogel exhibited high tissue adhesion in the initial stages. Over time, oxidation and Schiff–base reactions of dopamine occurred, resulting in the formation of strong bonds between the skin and increased adhesion strength **(Figure 53)** (Saiz-Poseu*, et al.*, 2019). Within 1 h post–adhesion, insufficient interactions occurred between the ATP hydrogel and skin, leading to interfacial failure of the hydrogel (**Figure 54b**). However, as the interactions between the ATP hydrogel and skin intensified up to 3 h after adhesion, the failure mode of the ATP hydrogel transitioned to a mixed failure mode. As the attachment duration exceeded 3 h, the adhesion strength decreased (e.g., 27.6 kPa after 10 h). Nevertheless, the ATP hydrogel exhibited adhesion strengths of over 20 kPa even after 24 h of adhesion. The decrease in adhesion strength is attributable to the decrease in the cohesion of the ATP hydrogel owing to water absorption and hydrogel degradation. As the adhesion time increases, additional interactions between the ATP hydrogel and substrate are formed, but these interactions also weaken the existing interactions within the ATP hydrogel network (Zhang*, et al.*, 2022). Therefore, the dissociation of the network structure occurred

as adhesion duration increased, resulting in the cohesion of the ATP hydrogel, which is the strength itself, decreasing. As the adhesion strength is determined by a combination of cohesive and adhesive forces, a decrease in cohesion results in a decrease in adhesion strength (Han*, et al.*, 2024). This phenomenon (dissociation of the ATP hydrogel network structure) can be indirectly observed by the change in transparency of the ATP hydrogel according to adhesion time. The ATP hydrogel changes from opaque to transparent due to the disappearance of the light scattering center caused by the dissociation of the ATP hydrogel network structure.

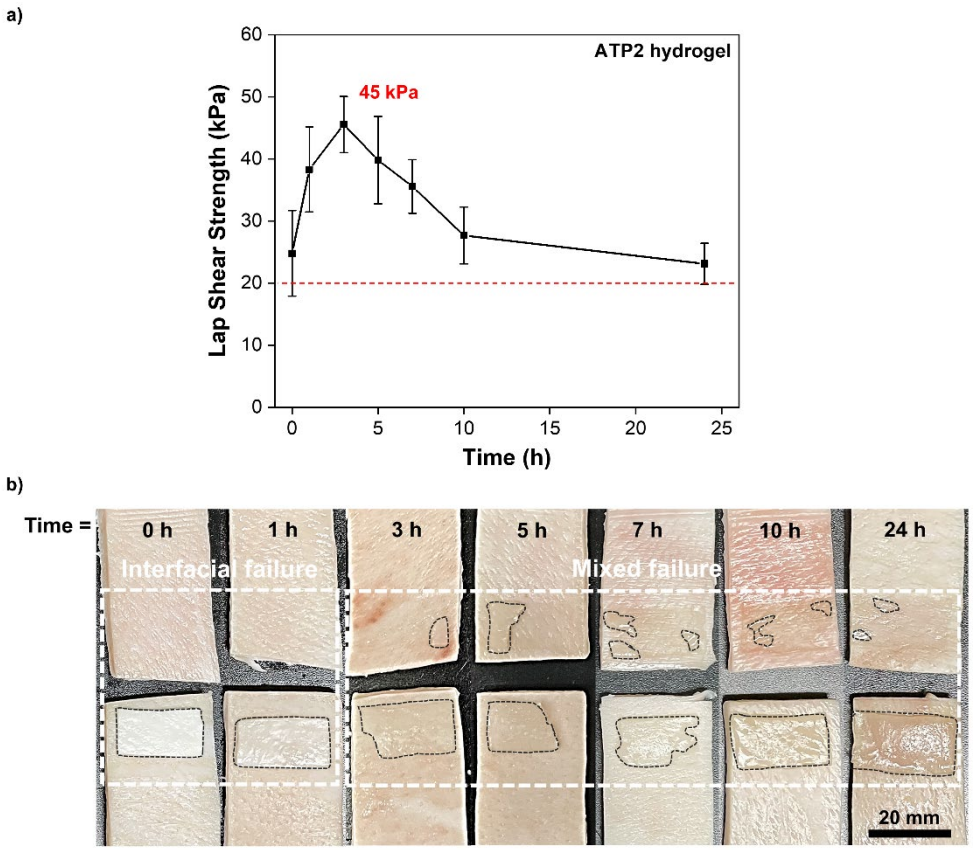

Figure 54. a) Change in tissue adhesion strength of ATP2 hydrogel over time. b) Failure mode of the ATP2 hydrogel at different time points after adhesion. Grey dashed lines represent the residual ATP hydrogels on the porcine skin after lap shear test (Han, *et al.*, 2024).

3.8. Recovery Property

The human body contains numerous mobile components: joints such as the knee, wrist, and ankle exhibit a wide range of motion, and organs such as the lungs, heart, and tendons repeatedly contract and relax. Hence, hydrogels must exhibit high mechanical resilience to withstand dynamic mechanical loadings (Jeong*, et al.*, 2023, Mengüç*, et al.*, 2014). To evaluate the recovery property of the ATP2 hydrogel in dynamic environments, a cyclic tensile test was conducted without rest. The residual strain and resilience were calculated using the initial loading–unloading curves at different strain rates. The ATP2 hydrogel exhibited a low residual strain (approximately 35%) and high mechanical resilience (approximately 63%) at strain rates of 200 and 400% (**Figure 55a, b**). At strain rates exceeding 600%, i.e., 700%, the mechanical resilience decreased to 53%, and the residual strain increased to 85% (**Figure 55c, d**). The recovery performance of the ATP hydrogel was attributable to the associated TPDC and entangled PVI: the associated TPDC can reversibly reassociate when mechanical stress is removed, and entangled PVI can enhance the elasticity of the hydrogel (Kim*, et al.*, 2021). Owing to its noncovalently associated DN structure, the ATP hydrogel demonstrated excellent recovery properties even without external stimuli. Notably, at strain rates exceeding 600%, the resilience significantly decreased, and the residual strain increased owing to the irreversible destruction of the covalently crosslinked network structure (**Table 8)**. However, even after the destruction of the first network (covalent crosslinking), its fragments functioned as crosslinking agents of the second network (Gong, 2010), and hydrogen bonds, hydrophobic associations, cation–π interactions, and chain entanglements induced by PVI contributed to the elasticity of the ATP hydrogel to a certain extent. Therefore, the ATP hydrogel exhibited excellent recovery properties even at high strain rates.

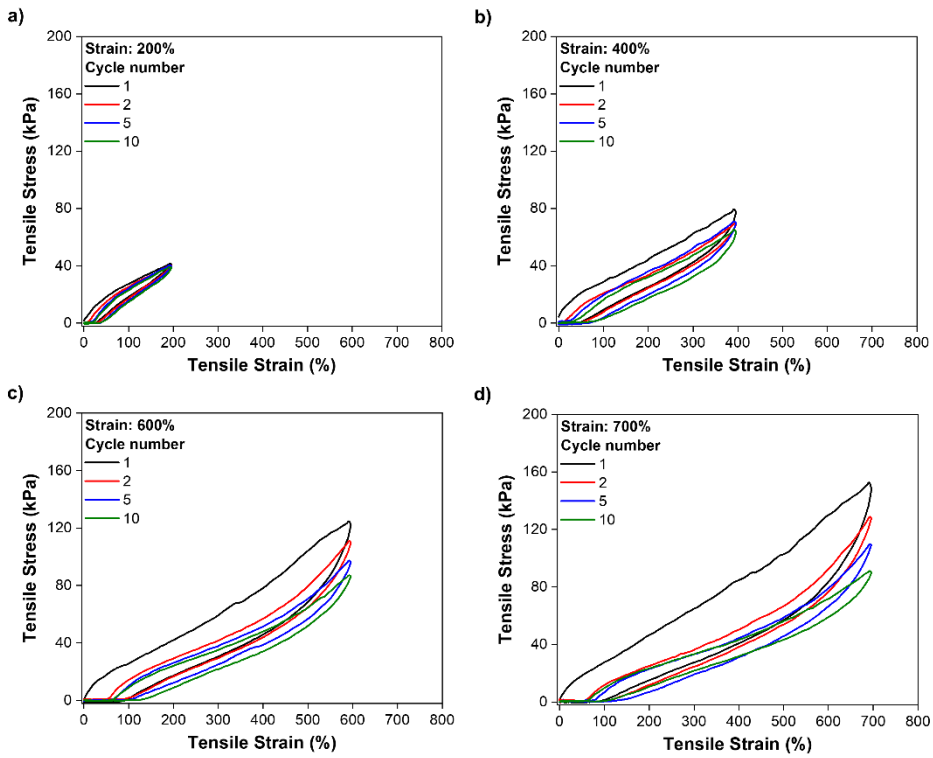

Figure 55. a) Cyclic tensile test of the ATP2 hydrogel at a) 200%, b) 400%, c) 600%, and d) 700% strain (Han, *et al.*, 2024).

Table 8. Residual strain and resilience of ATP2 hydrogel with different strain rates.

ATP2 hydrogel	**Strain rate (%)**			
	200	**400**	**600**	**700**
Residual strain (%)	27.2	41.2	71.3	91.3
Resilience (%)	35.0	63.4	57.1	53.0

Finally, a successive cycle tensile test was conducted to demonstrate the applicability of the ATP hydrogel in joint areas. The strain rate was set at 100%, considering the maximum strain rates of human motions (Jeong and Wang, 2023, Ying*, et al.*, 2020), and the test was conducted for 200–cycles. The ATP2 hydrogel could withstand 200–cycles at a strain rate of 100% (**Figure 56a**) and exhibited high mechanical resilience even after 200–cycles (**Figure 56b**). These results demonstrate the stability of the ATP2 hydrogel in dynamic environments.

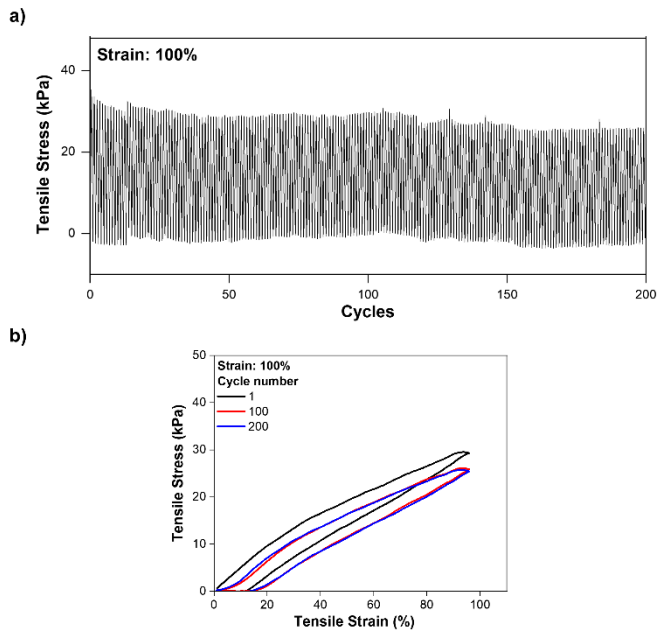

Figure 56. a) Successive cycle tensile test of ATP2 hydrogel at 100% strain rate and h) stress−strain curves of its 1st, 100th, and 200th cycles (Han, *et al.*, 2024).

3.9. Burst Pressure Test

The burst pressure test is an effective method for evaluating the robustness of hydrogel adhesives against dynamic pressure and their adhesiveness at wound sites (Wang*, et al.*, 2023). As the PVI content increased, the burst pressure of the ATP hydrogel increased from 114 mmHg (ATP0 hydrogel) to 236 mmHg (ATP4 hydrogel) **(Figure 57)**. A higher PVI content increases the toughness of the ATP hydrogel, leading to enhanced burst pressure strength. The burst pressure of the ATP hydrogel was higher than that of commercial sealing adhesives (under 50 mmHg) (Chen*, et al.*, 2022, Hong*, et al.*, 2019). Considering normal human arterial blood pressure (typically 120 mmHg), PVI–containing ATP hydrogels (ATP1–4 hydrogels) exhibited excellent pressure resistance, exceeding 160 mmHg.

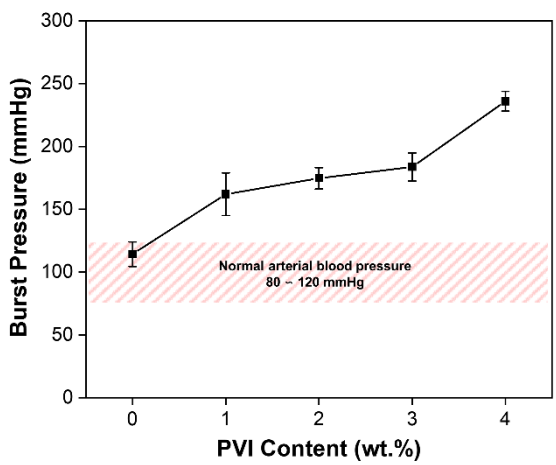

Figure 57. Burst pressure of ATP hydrogel with different PVI contents (Han, *et al.*, 2024).

A water/air sealing test using an ex vivo porcine model was conducted to evaluate the potential applications of the hydrogel. Perforations were created in the porcine small intestine and lung, and water and air flow were introduced, respectively. The damaged areas were then sealed using the ATP2 hydrogel. The ATP2 hydrogel effectively sealed the damaged spots even when water and air were still flowing, owing to its strong tissue adhesion and high toughness (**Figure 58a, b**). Furthermore, the sealing performance of the ATP2 hydrogel under physiological conditions was evaluated using a porcine small intestine. The perforated porcine small intestine sealed with the ATP2 hydrogel was immersed in a PBS solution (pH 7.4) for 48 h. The inside of the small intestine was filled with red PBS solution stained with Direct Red 80 dye for visual effect. The high wet tissue adhesion of the ATP hydrogel sealed the perforation effectively in a moist environment. Over time, due to the pH–sensitive AA and the hydrolyzable ester bond in TPDC, the ATP2 hydrogel swelled and was degraded. However, no liquid leakage was observed over 36 h due to the ATP2 hydrogel robustly adhering at the interface of the hydrogel and biological tissues (**Figure 58c)**. These results demonstrate the sealing performance and stability in a physiological environment of the ATP2 hydrogel.

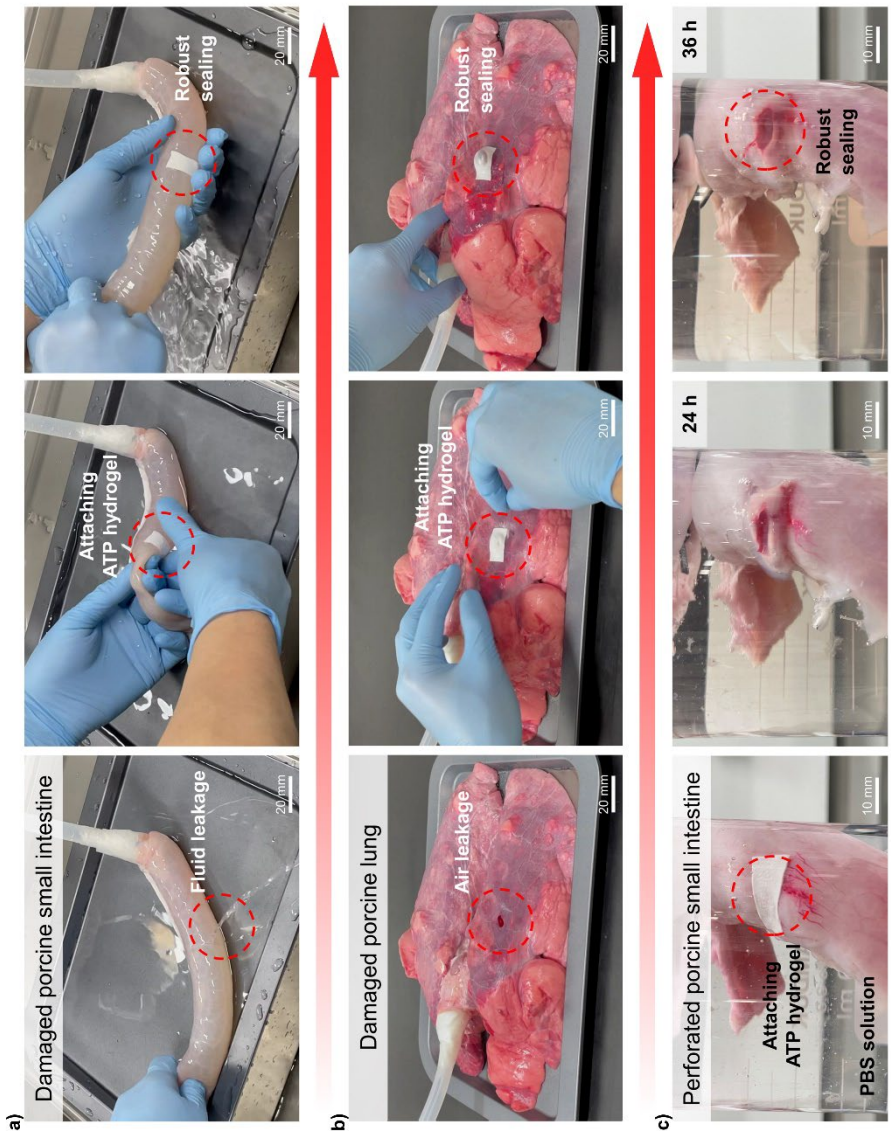

Figure 58. Photographs of a) fluid leakage sealing and b) air leakage sealing tests using the ATP2 hydrogel. c) Photographs of sealing performance tests of the ATP2 hydrogel (Han, *et al.*, 2024).

3.10. Biodegradation

The biodegradability was assessed by immersing the ATP hydrogel in a PBS solution at 36 °C. The ATE hydrogel was degraded under physiological conditions due to the hydrolyzable ester bond in TPDC **(Figure 59a)**. The ATP2 hydrogel exhibited 49% degradation after 36 h and completely degraded after 72 h (**Figure 59b**).

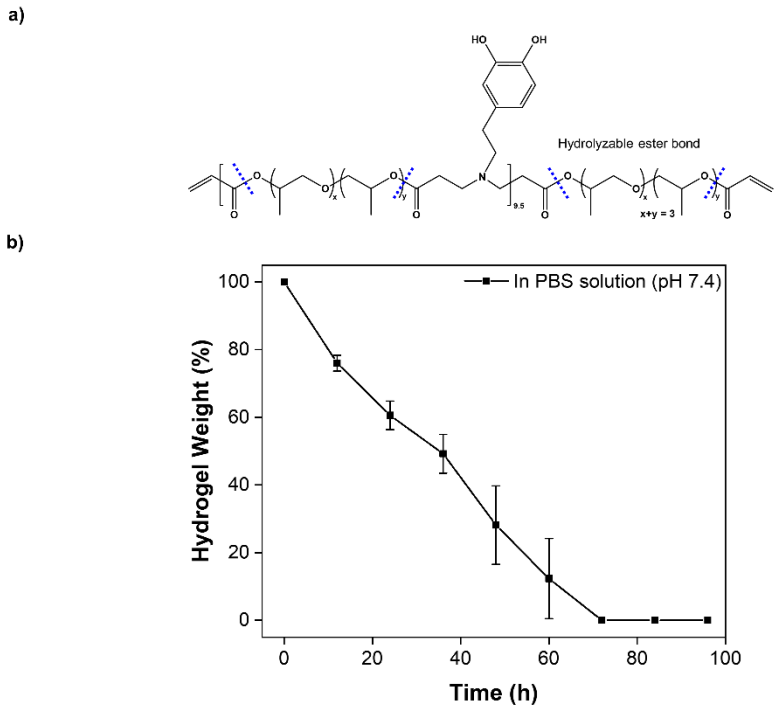

Figure 59. Degradation mechanism of TPDC. b) In vitro biodegradation of the ATP hydrogel in PBS solution (pH 7.4) for 96 h (Han, *et al.*, 2024).

3.11. In vitro Biocompatibility Tests

To assess the potential toxicity of the ATP hydrogel, the impact of the degradation products of ATP hydrogel on STO cells was observed. Compared to the control group, the hydrogel–treated group exhibited no significant difference in cell viability (**Figure 60a, c**) and cytotoxicity (**Figure 60b**). In summary, the ATP hydrogel degrades under physiological conditions, and its degradation products do not harm the cells.

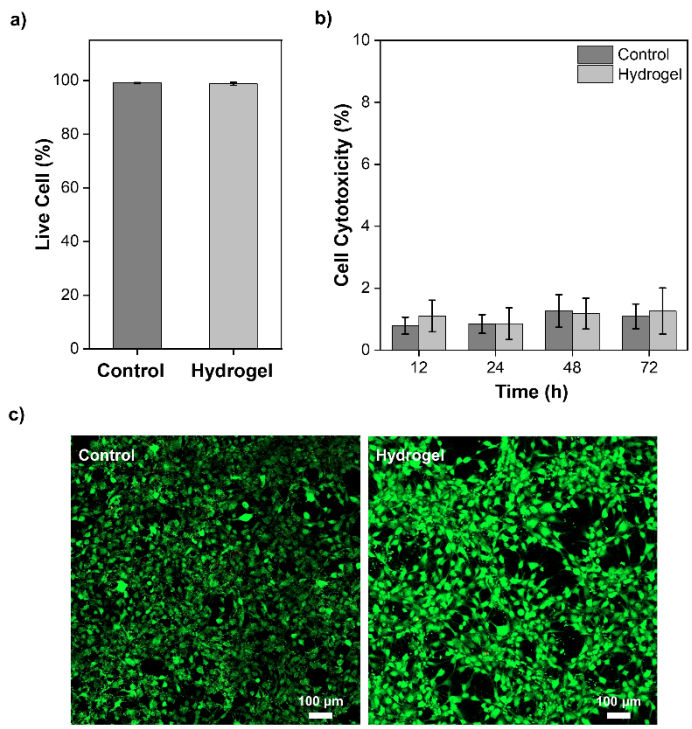

Figure 60. In vitro biocompatibility test of STO cells exposed to the hydrogel–treated medium. a) Effect of the ATP2 hydrogel degradation product on cell viability and b) potential toxicity. c) Live/Dead cell staining 72 h after incubation (Han, *et al.*, 2024).

3.12. In vivo Wound Healing Tests

The wound healing performance of the ATP hydrogel was assessed using a rat wound model, monitoring changes in wound size over time (0, 4, 8, and 11 d post–implantation). Subsequently, histological analyses (immunohisto-chemistry (IHC), hematoxylin–eosin (H&E), and Masson's trichrome staining) were conducted 11 d post–implantation to evaluate tissue regeneration. Compared to the control group, the hydrogel–treated group exhibited accelerated healing **(Figure 61a, b)** and a significantly higher level of the angiogenesis marker, vascular endothelial growth factor (VEGF) **(Figure 61c)**.

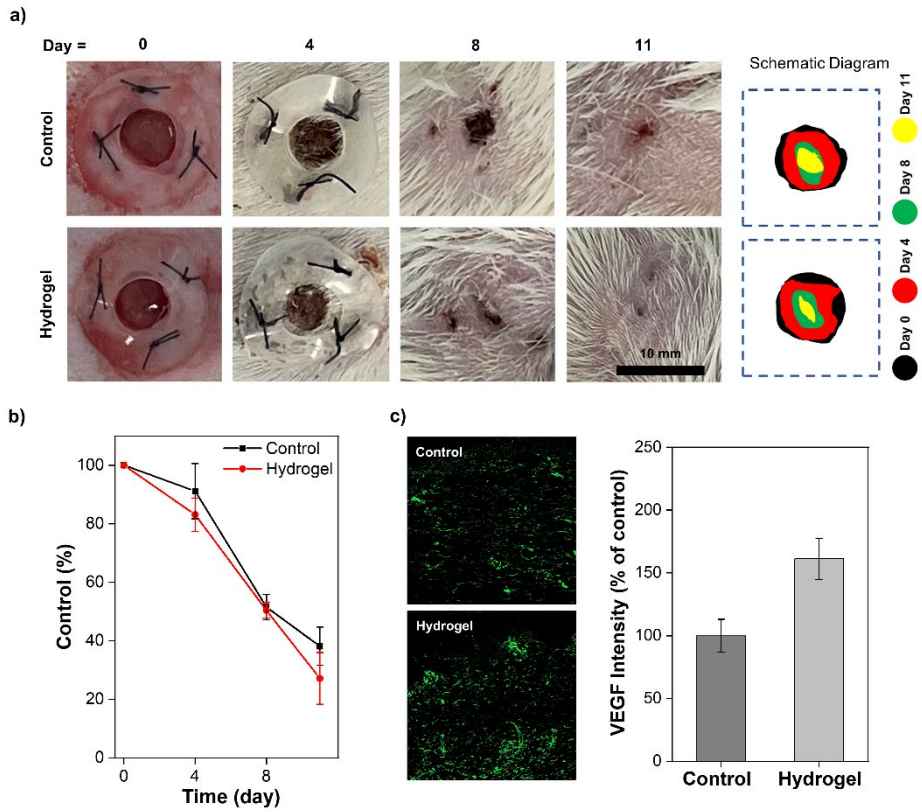

Figure 61. a) Effect of the ATP2 hydrogel on wound healing and remaining wound size over time. b) Immunohistochemistry staining images and VEGF antibody expression ratio (Han, *et al.*, 2024).

In H&E staining tests, the hydrogel–treated group demonstrated tissue (epidermis and dermis) thickness similar to that of the normal (non–wounded) group, while the control group exhibited significant tissue thickening (**Figure 62a, c**). Masson's staining analysis revealed a significantly higher collagen deposition in the hydrogel–treated group than in the control group (**Figure 62b, d**). Collectively, these results demonstrate that the ATP hydrogel promotes tissue regeneration at the wound site (Loh*, et al.*, 2018). The pH–sensitive AA can absorb excess exudates produced by the wounds. Furthermore, due to its robust tissue adhesion, the ATP hydrogel can securely adhere to the wound and stabilize the wound site. This capability enables the ATP hydrogel to protect the wound site, maintaining a moist environment and thereby accelerating wound healing (Korting*, et al.*, 2011).

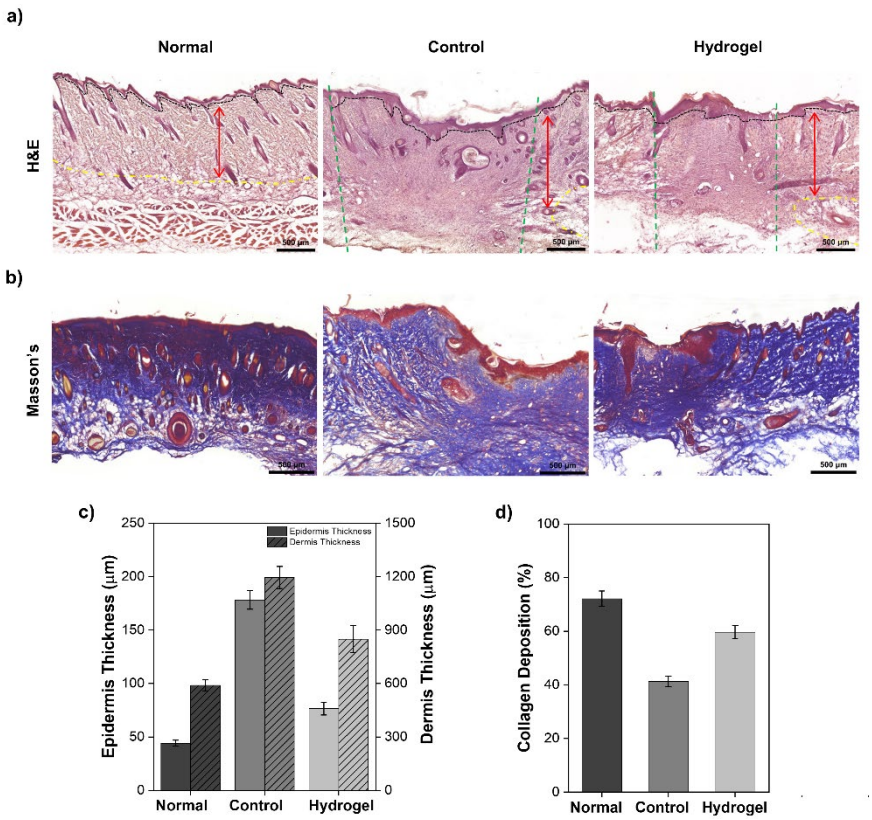

Figure 62. a) H&E staining images. Black and green dashed lines represent the boundary of the epidermis and wound site, respectively. Red arrows represent the dermis. b) Masson's trichrome staining images. Comparison of c) epidermis and dermis thickness values of non–wounded (normal) and wounded (control and hydrogel–treated) groups. Comparison of d) collagen deposition in non–wounded (normal) and wounded (control and hydrogel–treated) groups (Han, *et al.*, 2024).

4. Conclusion

In this part, the double network hydrogel adhesive was designed using an acrylate–terminated dopamine–modified crosslinking agent and linear polymer. To enhance the stretchability and toughness of hydrogel, the propylene glycol backbone dopamine–modified crosslinking agent, which has more free volume than ethylene glycol, and the physical interactable linear PVI were introduced, respectively. The first network was formed through covalent bonding between acrylates, and the second network was generated through noncovalent intermolecular interactions such as hydrogen bonds, hydrophobic associations, cation–π interactions, π –π interactions, and chain entanglement. These covalent and noncovalent intermolecular interactions led to associated network structures, resulting in a hydrogel with remarkable toughness and mechanical resilience. The polar groups of dopamine and imidazole within the ATP hydrogel formed strong bonds with tissues, ensuring robust adhesion even in wet conditions.

By introducing a noncovalently associated double network structure, the resultant hydrogel adhesive exhibited robust wet tissue adhesion (45.5 kPa) and significant tensile properties (883.5% fracture elongation and 213.8 kPa tensile strength) along with high mechanical resilience (53% resilience at 700% strain rate). Through these well–balanced and exceptional mechanical performances, the ATP hydrogel exhibited high burst pressure resistance (174.7 kPa), thereby exhibiting perforation sealing performances. Furthermore, the pH–sensitive AA promoted wound healing by maintaining a moist environment.

Summary

1. Overall Conclusion

This study aimed to develop a wound-sealing patch that can be applied in movable parts where frequent and a large range of motion occur. Therefore, this study aimed to enhance the three physical properties of hydrogel: weak wet tissue adhesion, low mechanical resilience, and low elongation. These properties were achieved through the dopamine-containing and acrylate-terminated linear oligomer, which can act as the crosslinking agent of the hydrogel. The designed dopamine–modified crosslinking agents in this study have three structural characteristics: the presence of 1) acrylate end groups, 2) multiple dopamine molecules with a short interval, and 3) hydrolyzable ester bonds. These structural properties of dopamine-modified crosslinking agents enable the fabrication of hydrogels that can be degraded under physiological conditions. Furthermore, dopamine-modified crosslinking agents form an associated structure through intermolecular interactions, allowing the hydrogel to exhibit high tissue adhesion and mechanical elasticity. Then, by adding a physically interactable cationic linear polymer, the stretchability of the hydrogel dramatically increased.

This study presents a straightforward method for fabricating highly resilient hydrogel adhesives with adjustable mechanical properties using a functional crosslinking agent. Manufactured hydrogel adhesives in this study demonstrate strong tissue adhesion, enhanced toughness, and high mechanical resilience. The hydrogels in this study demonstrate well-balanced mechanical properties compared to commercially available fibrin, poly(ethylene glycol), cyanoacrylate glues, and previously reported hydrogel adhesives **(Figure 63)**. Moreover, their applicability to living organisms was corroborated through biocompatibility tests and porcine organ model tests. Collectively, this study successfully manufactured a wound-sealing

patch that can be applied in movable parts, and these results provide the possibility of developing functional materials that could be used in the biomedical industry.

1.1 Dopamine–Modified Crosslinking Agent for Highly Resilient Hydrogel Adhesives

The linear acrylate-terminated and dopamine-contained crosslinking agent was successfully synthesized. Then, the hydrogels were fabricated following two steps. 1) Photopolymerization between acrylic acid and the dopamine-modified crosslinking agent in DMSO. 2) Solvent exchange to DIW. During the solvent exchange, intermolecular interactions between dopamine-dopamine and dopamine-poly(AA) (hydrogen bond, hydrophobic interaction, and π– π stacking) were formed, and a hydrogel adhesive having an associated network structure was obtained. The formation of the associated network structure was corroborated by the swelling test and SAXS analyses. Through this associated network structure and high dopamine content, the resultant hydrogel adhesive exhibited high mechanical resilience with instant recovery under cyclic loading (94% at a 200% strain rate) and high wet tissue adhesion (71.4 kPa), respectively. Moreover, the pH–sensitive acrylic acid backbone and ester bond in the crosslinking agent enabled the hydrogel adhesive to maintain moist environments and degrade under physiological conditions, respectively. Based on these results, the applicability of the resultant hydrogel to living organisms was evaluated, and it demonstrated that it could be utilized as a wound healing patch.

1.2. Double Network Structure for Toughness Enhanced Hydrogel Adhesives

The double-network hydrogel adhesive was fabricated using a dopamine-modified crosslinking agent and linear cationic polymer. By modifying the backbone of the dopamine-modified crosslinking agent from ethylene glycol to propylene glycol, the elongation of hydrogel dramatically increased. Moreover, by adding a physically interactable cationic polymer, PVI, a toughness enhanced double network hydrogel adhesive was obtained. Using PVI resulted in additional intermolecular interactions, such as chain entanglement and cation–π interaction, which led to the formation of a non-covalently associated double network structure. The formation of the associated network structure was corroborated by the swelling test and XPS analyses. Through this non-covalently associated double network structure, the resultant hydrogel adhesive exhibited dramatically enhanced toughness (883.5% fracture elongation and 213.8 kPa tensile strength), maintaining wet tissue adhesion (45.5 kPa) and mechanical resilience 53% resilience at 700% strain rate). Through these well–balanced mechanical performances, the resultant hydrogel adhesive demonstrated wound sealing performances with high burst pressure resistance (174.7 kPa).

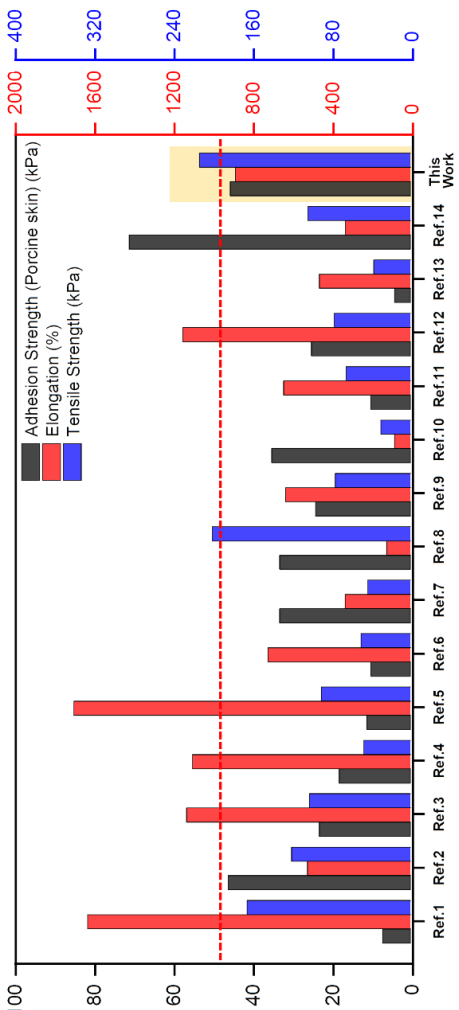

Figure 63. Comparison of adhesion strength, elongation, and tensile strength of ATP2 hydrogel adhesive with existing hydrogel adhesives (Han, *et al.*, 2024).

(Bian, *et al.*, 2022, Chen, *et al.*, 2021, Chen, *et al.*, 2023, Han, *et al.*, 2022, Jiang, *et al.*, 2023, Li, *et al.*, 2022, Pei, *et al.*, 2020, Wang, *et al.*, 2020, Yan, *et al.*, 2022, Yang, *et al.*, 2021, Zhang, *et al.*, 2022, Zhang, *et al.*, 2021, Zhao, *et al.*, 2022, Zhou, *et al.*, 2021).

References

References

Adams, J. C., 2023, Passing The Post: Roles of Posttranslational Modifications In The Form And Function of Extracellular Matrix, *American Journal of Physiology-Cell Physiology*, **324** (5): C1179

Ahmed, E. M., 2015, Hydrogel: Preparation, characterization, and applications: A review, *J Adv Res*, **6** (2): 105

Bertsch, P., Diba, M., Mooney, D. J. and Leeuwenburgh, S. C. G., 2022, Self-Healing Injectable Hydrogels for Tissue Regeneration, *Chemical Reviews*, **123** (2): 834

Bian, S., Hao, L., Qiu, X., Wu, J., Chang, H., Kuang, G. M., Zhang, S., Hu, X., Dai, Y., Zhou, Z., Huang, F., Liu, C., Zou, X., Liu, W., Lu, W. W., Pan, H. and Zhao, X., 2022, An Injectable Rapid-Adhesion and Anti-Swelling Adhesive Hydrogel for Hemostasis and Wound Sealing, *Advanced Functional Materials*, **32** (46): 2207741

Browning, M. B., Cereceres, S. N., Luong, P. T. and Cosgriff-Hernandez, E. M., 2014, Determination of The in Vivo Degradation Mechanism of PEGDA Hydrogels, *Journal of Biomedical Materials Research Part A*, **102** (12): 4244

Bu, Y., Zhang, L., Sun, G., Sun, F., Liu, J., Yang, F., Tang, P. and Wu, D., 2019, Tetra-PEG Based Hydrogel Sealants for In Vivo Visceral Hemostasis, *Advanced Materials*, **31** (28): 1901580

Cascone, S. and Lamberti, G., 2020, Hydrogel-Based Commercial Products for Biomedical Applications: A Review, *International Journal of Pharmaceutics*, **573**: 118803

Chen, K., Feng, Y., Zhang, Y., Yu, L., Hao, X., Shao, F., Dou, Z., An, C., Zhuang, Z., Luo, Y., Wang, Y., Wu, J., Ji, P., Chen, T. and Wang, H., 2019, Entanglement-Driven Adhesion, Self-Healing, and High Stretchability of Double-Network PEG-Based Hydrogels, *ACS Applied Materials & Interfaces*, **11** (40): 36458

Chen, K., Wu, Z., Liu, Y., Yuan, Y. and Liu, C., 2021, Injectable Double-Crosslinked Adhesive Hydrogels with High Mechanical Resilience and Effective Energy Dissipation for Joint Wound Treatment, *Advanced Functional Materials*, **32** (12): 2109687

Chen, Q., Chen, H., Zhu, L. and Zheng, J., 2015, Fundamentals of Double Network Hydrogels, *Journal of Materials Chemistry B*, **3** (18): 3654

Chen, T., Chen, Y., Rehman, H. U., Chen, Z., Yang, Z., Wang, M., Li, H. and Liu, H., 2018, Ultratough, Self-Healing, and Tissue-Adhesive Hydrogel for Wound Dressing, *ACS Applied Materials & Interfaces*, **10** (39): 33523

Chen, X., Zhang, J., Chen, G., Xue, Y., Zhang, J., Liang, X., Lei, I. M., Lin, J., Xu, B. B. and Liu, J., 2022, Hydrogel Bioadhesives with Extreme Acid-Tolerance for Gastric Perforation Repairing, *Advanced Functional Materials*, **32** (29): 2270168

Chen, Y., Fan, X., Lu, J., Liu, X., Chen, J. and Chen, Y., 2023, Mussel-Inspired Adhesive, Antibacterial, and Stretchable Composite Hydrogel for Wound Dressing, *Macromolecular Bioscience*, **23** (1): e2200370

Cheng, S., Wang, H., Pan, X., Zhang, C., Zhang, K., Chen, Z., Dong, W., Xie, A. and Qi, X., 2022, Dendritic Hydrogels with Robust Inherent Antibacterial Properties for Promoting Bacteria-Infected Wound Healing, *ACS Applied Materials & Interfaces*, **14** (9): 11144

Choi, Y., Kang, K., Son, D. and Shin, M., 2022, Molecular Rationale for the Design of Instantaneous, Strain-Tolerant Polymeric Adhesive in a Stretchable Underwater Human-Machine Interface, *ACS Nano*, **16** (1): 1368

Chu, W., Nie, M., Ke, X., Luo, J. and Li, J., 2021, Recent Advances in Injectable Dual Crosslinking Hydrogels for Biomedical Applications, *Macromolecular Bioscience*, **21** (7): e2100109

Cintron-Cruz, J. A., Freedman, B. R., Lee, M., Johnson, C., Ijaz, H. and Mooney, D. J., 2022, Rapid Ultratough Topological Tissue Adhesives, *Advanced Materials*, **34** (35): 2205567

Cui, C., Fan, C., Wu, Y., Xiao, M., Wu, T., Zhang, D., Chen, X., Liu, B., Xu, Z., Qu, B. and Liu, W., 2019, Water-Triggered Hyperbranched Polymer Universal Adhesives: From Strong Underwater Adhesion to Rapid Sealing Hemostasis, *Advanced Materials*, **31** (49): 1905761

Dai, W., Zhang, L., Yu, Y., Yan, W., Zhao, F., Fan, Y., Cao, C., Cai, Q., Hu, X. and Ao, Y., 2022, 3D Bioprinting of Heterogeneous Constructs Providing Tissue-Specific Microenvironment Based on Host–Guest Modulated Dynamic Hydrogel Bioink for Osteochondral Regeneration, *Advanced Functional Materials*, **32** (23): 2200710

Dai, X., Zhang, Y., Gao, L., Bai, T., Wang, W., Cui, Y. and Liu, W., 2015, A Mechanically Strong, Highly Stable, Thermoplastic, and Self-Healable Supramolecular Polymer Hydrogel, *Advanced Materials*, **27** (23): 3566

Deng, J., Tang, Y., Zhang, Q., Wang, C., Liao, M., Ji, P., Song, J., Luo, G., Chen, L., Ran, X., Wei, Z., Zheng, L., Dang, R., Liu, X., Zhang, H., Zhang, Y. S., Zhang, X. and Tan, H., 2019, A Bioinspired Medical Adhesive Derived from Skin Secretion of Andrias davidianus for Wound Healing, *Advanced Functional Materials*, **29** (31): 1809110

Deng, X., Huang, B., Wang, Q., Wu, W., Coates, P., Sefat, F., Lu, C., Zhang, W. and Zhang, X., 2021, A Mussel-Inspired Antibacterial Hydrogel with High Cell Affinity, Toughness, Self-Healing, and Recycling Properties for Wound Healing, *ACS Sustainable Chemistry & Engineering*, **9** (8): 3070

Ducrot, E., Chen, Y., Bulters, M., Sijbesma, R. P. and Creton, C., 2014, Toughening Elastomers with Sacrificial Bonds and Watching Them Break, *Science*, **344** (6180): 186

Eklund, A., Zhang, H., Zeng, H., Priimagi, A. and Ikkala, O., 2020, Fast Switching of Bright Whiteness in Channeled Hydrogel Networks, *Advanced Functional Materials*, **30** (28): 2000754

El-Sherbiny, I. M., Khalil, I. A. and Ali, I. H., Updates on Stimuli-Responsive Polymers: Synthesis Approaches and Features, 2018, in *Polymer Gels*, Springer

Fan, H. and Gong, J. P., 2021, Bioinspired Underwater Adhesives, *Advanced Materials*, **33** (44): e2102983

Fang, X., Li, Y., Li, X., Liu, W., Yu, X., Yan, F. and Sun, J., 2020, Dynamic Hydrophobic Domains Enable the Fabrication of Mechanically Robust and Highly Elastic Poly(vinyl alcohol)-Based Hydrogels with Excellent Self-Healing Ability, *ACS Materials Letters*, **2** (7): 764

Freedman, B. R., Uzun, O., Luna, N. M. M., Rock, A., Clifford, C., Stoler, E., Ostlund-Sholars, G., Johnson, C. and Mooney, D. J., 2021, Degradable and Removable Tough Adhesive Hydrogels, *Advanced Materials*, **33** (17): 2008553

GhavamiNejad, A., Park, C. H. and Kim, C. S., 2016, In Situ Synthesis of Antimicrobial Silver Nanoparticles within Antifouling Zwitterionic Hydrogels by Catecholic Redox Chemistry for Wound Healing Application, *Biomacromolecules*, **17** (3): 1213

Gong, J. P., 2010, Why Are Double Network Hydrogels So Tough?, *Soft Matter*, **6** (12): 2583

Griffin, D. R., Archang, M. M., Kuan, C. H., Weaver, W. M., Weinstein, J. S., Feng, A. C., Ruccia, A., Sideris, E., Ragkousis, V., Koh, J., Plikus, M. V., Di Carlo, D., Segura, T. and Scumpia, P. O., 2021, Activating an Adaptive Immune Response From a Hydrogel Scaffold Imparts Regenerative Wound Healing, *Nature Materials*, **20** (4): 560

Han, G.-Y., Kwack, H.-W., Kim, Y.-H., Je, Y. H., Kim, H.-J. and Cho, C.-S., 2024, Progress of Polysaccharide-Based Tissue Adhesives, *Carbohydrate Polymers*, **327**: 121634

Han, G. Y., Park, J. Y., Lee, T. H., Yi, M. B. and Kim, H. J., 2022, Highly Resilient Dual-Crosslinked Hydrogel Adhesives

Based on a Dopamine-Modified Crosslinker, *ACS Applied Materials & Interfaces*, **14** (32): 36304

Han, G. Y., Hwang, S. K., Cho, K. H., Kim, H. J. and Cho, C. S., 2023, Progress of Tissue Adhesives Based on Proteins and Synthetic Polymers, *Biomaterials Research*, **27** (1): 57

Han, G. Y., Park, J. Y., Back, J. H., Yi, M. B. and Kim, H. J., 2024, Highly Resilient Noncovalently Associated Hydrogel Adhesives for Wound Sealing Patch, *Adv Healthc Mater*: e2303342

Han, L., Lu, X., Liu, K., Wang, K., Fang, L., Weng, L. T., Zhang, H., Tang, Y., Ren, F., Zhao, C., Sun, G., Liang, R. and Li, Z., 2017, Mussel-Inspired Adhesive and Tough Hydrogel Based on Nanoclay Confined Dopamine Polymerization, *ACS Nano*, **11** (3): 2561

Han, L., Yan, L., Wang, K., Fang, L., Zhang, H., Tang, Y., Ding, Y., Weng, L.-T., Xu, J., Weng, J., Liu, Y., Ren, F. and Lu, X., 2017, Tough, Self-Healable and Tissue-Adhesive Hydrogel with Tunable Multifunctionality, *NPG Asia Materials*, **9** (4): e372

Han, L., Liu, K., Wang, M., Wang, K., Fang, L., Chen, H., Zhou, J. and Lu, X., 2018, Mussel-Inspired Adhesive and Conductive Hydrogel with Long-Lasting Moisture and Extreme Temperature Tolerance, *Advanced Functional Materials*, **28** (3): 1704195

Han, L., Yan, L., Wang, M., Wang, K., Fang, L., Zhou, J., Fang, J., Ren, F. and Lu, X., 2018, Transparent, Adhesive, and Conductive Hydrogel for Soft Bioelectronics Based on Light-Transmitting Polydopamine-Doped Polypyrrole Nanofibrils, *Chemistry of Materials*, **30** (16): 5561

Han, Z., Wang, P., Mao, G., Yin, T., Zhong, D., Yiming, B., Hu, X., Jia, Z., Nian, G., Qu, S. and Yang, W., 2020, Dual pH-Responsive Hydrogel Actuator for Lipophilic Drug Delivery, *ACS Applied Materials & Interfaces*, **12** (10): 12010

Hao, Y., Yuan, C., Deng, J., Zheng, W., Ji, Y. and Zhou, Q., 2022, Injectable Self-Healing First-Aid Tissue Adhesives with Outstanding Hemostatic and Antibacterial Performances for Trauma Emergency Care, *ACS Applied Materials & Interfaces*, **14** (14): 16006

Hasani-Sadrabadi, M. M., Sarrion, P. P., S., Chau, Y., Ansari, S., Li, S. A., T. and Moshaverinia, A., 2020, An Engineered Cell-Laden Adhesive Hydrogel Promotes Craniofacial Bone Tissue Regeneration in Rats, *Science translational medicine*, **12** (534): eaay6853

Hofman, A. H., van Hees, I. A., Yang, J. and Kamperman, M., 2018, Bioinspired Underwater Adhesives by Using the Supramolecular Toolbox, *Advanced Materials*, **30** (19): 1704640

Holten-Andersen, N., Harrington, M. J., Birkedal, H., Lee, B. P., Messersmith, P. B., Lee, K. Y. and Waite, J. H., 2011, Ph-Induced Metal-Ligand Cross-Links Inspired By Mussel Yield Self-Healing Polymer Networks With Near-Covalent Elastic Moduli, *Proceedings of the National Academy of Sciences*, **108** (7): 2651

Hong, Y., Zhou, F., Hua, Y., Zhang, X., Ni, C., Pan, D., Zhang, Y., Jiang, D., Yang, L., Lin, Q., Zou, Y., Yu, D., Arnot, D. E., Zou, X., Zhu, L., Zhang, S. and Ouyang, H., 2019, A Strongly Adhesive Hemostatic Hydrogel for The Repair of Arterial and Heart Bleeds, *Nature Communications*, **10** (1): 2060

Hou, S. and Ma, P. X., 2015, Stimuli-Responsive Supramolecular Hydrogels With High Extensibility And Fast Self-Healing Via Precoordinated Mussel-Inspired Chemistry, *Chemistry of Materials*, **27** (22): 7627

Huang, Y., Xiao, L., Zhou, J., Liu, T., Yan, Y., Long, S. and Li, X., 2021, Strong Tough Polyampholyte Hydrogels via the Synergistic Effect of Ionic and Metal–Ligand Bonds, *Advanced Functional Materials*, **31** (37): 2103917

Jeong, H. and Wang, W. D., 2023, Self-Adaptive Detachable Pneumatic Soft Actuators Using Uniformly Distributed Temporary-Bonding-Fasteners for Wearable Applications, *Sensors and Actuators A: Physical*, **349**: 114083

Jiang, L., Li, Y., Zou, F., Gan, D., Gao, M., Yuan, L., Zhang, Q. and Lu, X., 2023, Highly Self-Adhesive, Compressible, Stretchable, All Hydrogel-Based Supercapacitor for Wearable/Portable Electronics, *Materials Today Physics*, **33**: 101046

Karnal, P., Jha, A., Wen, H., Gryska, S., Barrios, C. and Frechette, J., 2019, Contribution of Surface Energy to pH-Dependent Underwater Adhesion of an Acrylic Pressure-Sensitive Adhesive, *Langmuir*, **35** (15): 5151

Kim, J., Zhang, G., Shi, M. and Suo, Z., 2021, Fracture, Fatigue, and Friction Of Polymers in Which Entanglements Greatly Outnumber Cross-Links, *Science*, **374** (6564): 212

Korting, H. C., Schollmann, C. and White, R. J., 2011, Management of Minor Acute Cutaneous Wounds: Importance of Wound Healing in a Moist Environment, *Journal of the*

European Academy of Dermatology and Venereology, **25** (2): 130

Lee, K. Y. and Mooney, D. J., 2001, Hydrogels for Tissue Engineering, *Chemical Reviews*, **101** (7): 1869

Li, G., Zhang, H., Fortin, D., Xia, H. and Zhao, Y., 2015, Poly(vinyl alcohol)-Poly(ethylene glycol) Double-Network Hydrogel: A General Approach to Shape Memory and Self-Healing Functionalities, *Langmuir*, **31** (42): 11709

Li, J., Celiz, A. D., Yang, J., Yang, Q., Wamala, I., Whyte, W., Seo, B. R., Vasilyev, N. V., Vlassak, J. J., Suo, Z. and Mooney, D. J., 2017, Tough Adhesives for Diverse Wet Surfaces, *Science*, **357** (6349): 378

Li, J., Yang, Z., Jiang, Z., Ni, M. and Xu, M., 2022, A Self-Healing and Self-Adhesive Chitosan Based Ion-Conducting Hydrogel Sensor by Ultrafast Polymerization, *International Journal of Biological Macromolecules*, **209**: 1975

Li, S., Liu, G., Wen, H., Liu, G., Wang, H., Ye, M., Yang, Y., Guo, W. and Liu, Y., 2022, A Skin-Like Pressure- and Vibration-Sensitive Tactile Sensor Based on Polyacrylamide/Silk Fibroin Elastomer, *Advanced Functional Materials*, **32** (19): 2111747

Li, W., Zheng, S., Zou, X., Ren, Y., Liu, Z., Peng, W., Wang, X., Liu, D., Shen, Z., Hu, Y., Guo, J., Sun, Z. and Yan, F., 2022, Tough Hydrogels with Isotropic and Unprecedented Crack Propagation Resistance, *Advanced Functional Materials*, **32** (43): 2207348

Lin, P., Ma, S., Wang, X. and Zhou, F., 2015, Molecularly Engineered Dual-Crosslinked Hydrogel with Ultrahigh Mechanical Strength, Toughness, and Good Self-Recovery, *Advanced Materials*, **27** (12): 2054

Liu, H., Qin, S., Liu, J., Zhou, C., Zhu, Y., Yuan, Y., Fu, D. a., Lv, Q., Song, Y., Zou, M., Wang, Z. and Wang, L., 2022, Bio-Inspired Self-Hydrophobized Sericin Adhesive with Tough Underwater Adhesion Enables Wound Healing and Fluid Leakage Sealing, *Advanced Functional Materials*, **32** (32): 2201108

Liu, J., Lin, S., Liu, X., Qin, Z., Yang, Y., Zang, J. and Zhao, X., 2020, Fatigue-Resistant Adhesion of Hydrogels, *Nature Communications*, **11** (1): 1071

Liu, T., Xie, Z., Chen, M., Tang, S., Liu, Y., Wang, J., Zhang, R., Wang, H., Guo, X., Gu, A., Yuan, Y. and Wang, N., 2022, Mussel-Inspired Dual-Crosslinked Polyamidoxime Photothermal Hydrogel with Enhanced Mechanical Strength for Highly Efficient and Selective Uranium Extraction from Seawater, *Chemical Engineering Journal*, **430**: 133182

Liu, X., He, X., Yang, B., Lai, L., Chen, N., Hu, J. and Lu, Q., 2020, Dual Physically Cross-Linked Hydrogels Incorporating Hydrophobic Interactions with Promising Repairability and Ultrahigh Elongation, *Advanced Functional Materials*, **31** (3): 2008187

Liu, X., Wu, J., Qiao, K., Liu, G., Wang, Z., Lu, T., Suo, Z. and Hu, J., 2022, Topoarchitected Polymer Networks Expand The Space Of Material Properties, *Nature Communications*, **13** (1): 1622

Liu, Y., Meng, H., Qian, Z., Fan, N., Choi, W., Zhao, F. and Lee, B. P., 2017, A Moldable Nanocomposite Hydrogel Composed of a Mussel-Inspired Polymer and a Nanosilicate as a Fit-to-Shape Tissue Sealant, *Angewandte Chemie International Edition*, **56** (15): 4224

Loh, E. Y. X., Mohamad, N., Fauzi, M. B., Ng, M. H., Ng, S. F. and Mohd Amin, M. C. I., 2018, Development of a Bacterial Cellulose-Based Hydrogel Cell Carrier Containing Keratinocytes and Fibroblasts for Full-Thickness Wound Healing, *Scientific Reports*, **8** (1): 2875

Ma, R. and Shi, L., 2014, Phenylboronic Acid-Based Glucose-Responsive Polymeric Nanoparticles: Synthesis and Applications in Drug Delivery, *Polymer Chemistry*, **5** (5): 1503

Ma, Y., Yao, J., Liu, Q., Han, T., Zhao, J., Ma, X., Tong, Y., Jin, G., Qu, K., Li, B. and Xu, F., 2020, Liquid Bandage Harvests Robust Adhesive, Hemostatic, and Antibacterial Performances as a First-Aid Tissue Adhesive, *Advanced Functional Materials*, **30** (39):

Ma, Z., Bao, G. and Li, J., 2021, Multifaceted Design and Emerging Applications of Tissue Adhesives, *Advanced Materials*, **33** (24): 2007663

Mansuri, S., Kesharwani, P., Jain, K., Tekade, R. K. and Jain, N. K., 2016, Mucoadhesion: A Promising Approach in Drug Delivery System, *Reactive and Functional Polymers*, **100**: 151

Mao, X., Cheng, R., Zhang, H., Bae, J., Cheng, L., Zhang, L., Deng, L., Cui, W., Zhang, Y., Santos, H. A. and Sun, X., 2019,

Self-Healing and Injectable Hydrogel for Matching Skin Flap Regeneration, *Advanced Science*, **6** (3): 1801555

Mathis, L., Chen, Y. and Shull, K. R., 2018, Tuning the Viscoelasticity of Hydrogen-Bonded Polymeric Materials through Solvent Composition, *Macromolcules*, **51** (11): 3975

Mengüç, Y., Park, Y.-L., Pei, H., Vogt, D., Aubin, P. M., Winchell, E., Fluke, L., Stirling, L., Wood, R. J. and Walsh, C. J., 2014, Wearable Soft Sensing Suit for Human Gait Measurement, *The International Journal of Robotics Research*, **33** (14): 1748

Mo, J., Dai, Y., Zhang, C., Zhou, Y., Li, W., Song, Y., Wu, C. and Wang, Z., 2021, Design of Ultra-Stretchable, Highly Adhesive and Self-Healable Hydrogels via Tannic Acid-Enabled Dynamic Interactions, *Materials Horizons*, **8** (12): 3409

Montazerian, H., Baidya, A., Haghniaz, R., Davoodi, E., Ahadian, S., Annabi, N., Khademhosseini, A. and Weiss, P. S., 2021, Stretchable and Bioadhesive Gelatin Methacryloyl-Based Hydrogels Enabled by in Situ Dopamine Polymerization, *ACS Applied Materials & Interfaces*, **13** (34): 40290

Nam, S. and Mooney, D., 2021, Polymeric Tissue Adhesives, *Chemical Reviews*, **121** (18): 11336

Noack, K., Kiefer, J. and Leipertz, A., 2010, Concentration-Dependent Hydrogen-Bonding Effects on The Dimethyl Sulfoxide Vibrational Structure in The Presence of Water, Methanol, and Ethanol, *Chemphyschem*, **11** (3): 630

Patil, N., Falentin-Daudré, C., Jérôme, C. and Detrembleur, C., 2015, Mussel-Inspired Protein-Repelling Ambivalent Block Copolymers: Controlled Synthesis and Characterization, *Polymer Chemistry*, **6** (15): 2919

Pei, X., Zhang, H., Zhou, Y., Zhou, L. and Fu, J., 2020, Stretchable, Self-Healing and Tissue-Adhesive Zwitterionic Hydrogels as Strain Sensors for Wireless Monitoring of Organ Motions, *Materials Horizons*, **7** (7): 1872

Pinnaratip, R., Bhuiyan, M. S. A., Meyers, K., Rajachar, R. M. and Lee, B. P., 2019, Multifunctional Biomedical Adhesives, *Advanced Healthcare Materials*, **8** (11): 1801568

Ren, K., Cheng, Y., Huang, C., Chen, R., Wang, Z. and Wei, J., 2019, Self-Healing Conductive Hydrogels Based on Alginate, Gelatin and Polypyrrole Serve as A Repairable Circuit and A Mechanical Sensor, *Journal of Materials Chemistry B*, **7** (37): 5704

Ryu, J. H., Lee, Y., Kong, W. H., Kim, T. G., Park, T. G. and Lee, H., 2011, Catechol-Functionalized Chitosan/Pluronic Hydrogels for Tissue Adhesives and Hemostatic Materials, *Biomacromolecules*, **12** (7): 2653

Saiz-Poseu, J., Mancebo-Aracil, J., Nador, F., Busque, F. and Ruiz-Molina, D., 2019, The Chemistry behind Catechol-Based Adhesion, *Angewandte Chemie International Edition*, **58** (3): 696

Salazar, P., Martín, M. and González-Mora, J. L., 2016, Polydopamine-Modified Surfaces in Biosensor Applications, *Polymer science: research advances, practical applications and educational aspects. Formatex Research Center SL*: 385

Scognamiglio, F., Travan, A., Rustighi, I., Tarchi, P., Palmisano, S., Marsich, E., Borgogna, M., Donati, I., de Manzini, N. and Paoletti, S., 2016, Adhesive and Sealant Interfaces for General Surgery Applications, *Journal of Biomedical Materials Research Part B: Applied Biomaterials*, **104** (3): 626

Shin, M., Park, S. G., Oh, B. C., Kim, K., Jo, S., Lee, M. S., Oh, S. S., Hong, S. H., Shin, E. C., Kim, K. S., Kang, S. W. and Lee, H., 2017, Complete Prevention of Blood Loss with Self-Sealing Haemostatic Needles, *Nature Materials*, **16** (1): 147

Shokrani, H., Shokrani, A., Seidi, F., Munir, M. T., Rabiee, N., Fatahi, Y., Kucinska-Lipka, J. and Saeb, M. R., 2022, Biomedical Engineering of Polysaccharide-Based Tissue Adhesives: Recent Advances and Future Direction, *Carbohydrate Polymers*, **295**: 119787

Singh, M., Teodorescu, D. L., Rowlett, M., Wang, S. X., Balcells, M., Park, C., Bernardo, B., McGarel, S., Reeves, C., Mehra, M. R., Zhao, X., Yuk, H. and Roche, E. T., 2024, A Tunable Soft Silicone Bioadhesive for Secure Anchoring of Diverse Medical Devices to Wet Biological Tissue, *Advanced Materials*, **36** (3): e2307288

Slootman, J., Yeh, C. J., Millereau, P., Comtet, J. and Creton, C., 2022, A Molecular Interpretation of The Toughness of Multiple Network Elastomers at High Temperature, *Proceedings of the National Academy of Sciences*, **119** (13): e2116127119

Sullivan, T. P., Eaglstein, W. H., Davis, S. C. and Mertz, P., 2001, The Pig as A Model for Human Wound Healing, *Wound Repair and Regeneration*, **9** (2): 66

Sun, T. L., Kurokawa, T., Kuroda, S., Ihsan, A. B., Akasaki, T., Sato, K., Haque, M. A., Nakajima, T. and Gong, J. P., 2013, Physical Hydrogels Composed of Polyampholytes Demonstrate High Toughness and Viscoelasticity, *Nature Materials*, **12** (10): 932

Suneetha, M., Sun Moo, O., Mo Choi, S., Zo, S., Madhusudana Rao, K. and Soo Han, S., 2021, Tissue-Adhesive, Stretchable, and Self-Healable Hydrogels Based on Carboxymethyl Cellulose-Dopamine/PEDOT:PSS via Mussel-Inspired Chemistry for Bioelectronic Applications, *Chemical Engineering Journal*, **426**: 130847

Tamai, Y., Tanaka, H. and Nakanishi, K., 1996, Molecular Dynamics Study of Polymer Water Interaction inHydrogels. 1. Hydrogen Bond Structure, *Macromolecules*, **29** (21): 6750

Tobing, S. D. and Klein, A., 2001, Molecular Parameters and Their Relation to The Adhesive Performance of Acrylic Pressure-Sensitive Adhesives, *Journal of Applied Polymer Science*, **79** (12): 2230

Tsai, W. B. and Wang, M. C., 2005, Effects of An Avidin-Biotin Binding System on Chondrocyte Adhesion And Growth on Biodegradable Polymers, *Macromolecular Bioscience*, **5** (3): 214

Vahedi, M., Barzin, J., Shokrolahi, F. and Shokrollahi, P., 2018, Self-Healing, Injectable Gelatin Hydrogels Cross-Linked by Dynamic Schiff Base Linkages Support Cell Adhesion and Sustained Release of Antibacterial Drugs, *Macromolecular Materials and Engineering*, **303** (9): 1800200

Varshney, N., Sahi, A. K., Poddar, S., Vishwakarma, N. K., Kavimandan, G., Prakash, A. and Mahto, S. K., 2022, Freeze-Thaw-Induced Physically Cross-linked Superabsorbent Polyvinyl Alcohol/Soy Protein Isolate Hydrogels for Skin Wound Dressing: In Vitro and In Vivo Characterization, *ACS Applied Materials & Interfaces*, **14** (12): 14033

Wang, B., Liu, J., Niu, D., Wu, N., Yun, W., Wang, W., Zhang, K., Li, G., Yan, S., Xu, G. and Yin, J., 2021, Mussel-Inspired Bisphosphonated Injectable Nanocomposite Hydrogels with Adhesive, Self-Healing, and Osteogenic Properties for Bone Regeneration, *ACS Applied Materials & Interfaces*, **13** (28): 32673

Wang, H., Yi, X., Liu, T., Liu, J., Wu, Q., Ding, Y., Liu, Z. and Wang, Q., 2023, An Integrally Formed Janus Hydrogel for Robust Wet-Tissue Adhesive and Anti-Postoperative Adhesion, *Advanced Materials*, **35** (23): e2300394

Wang, J., Wang, L., Wu, C., Pei, X., Cong, Y., Zhang, R. and Fu, J., 2020, Antibacterial Zwitterionic Polyelectrolyte Hydrogel Adhesives with Adhesion Strength Mediated by Electrostatic Mismatch, *ACS Applied Materials & Interfaces*, **12** (41): 46816

Wang, L., Hao, F., Tian, S., Dong, H., Nie, J. and Ma, G., 2022, Targeting Polysaccharides Such as Chitosan, Cellulose, Alginate and Starch for Designing Hemostatic Dressings, *Carbohydrate Polymers*, **291**: 119574

Wang, X., Guo, Y., Li, J., You, M., Yu, Y., Yang, J., Qin, G. and Chen, Q., 2022, Tough Wet Adhesion of Hydrogen-Bond-Based Hydrogel with On-Demand Debonding and Efficient Hemostasis, *ACS Appl Mater Interfaces*, **14** (31): 36166

Wang, Y., Xiao, D., Yu, H., Ke, R., Shi, S., Tang, Y., Zhong, Y., Zhang, L., Sui, X., Wang, B., Feng, X., Xu, H. and Mao, Z., 2022, Asymmetric Composite Wound Dressing with Hydrophobic Flexible Bandage and Tissue-Adhesive Hydrogel for Joints Skin Wound Healing, *Composites Part B: Engineering*, **235**: 109762

Wang, Z., Ren, Y., Zhu, Y., Hao, L., Chen, Y., An, G., Wu, H., Shi, X. and Mao, C., 2018, A Rapidly Self-Healing Host-Guest Supramolecular Hydrogel with High Mechanical Strength and Excellent Biocompatibility, *Angewandte Chemie International Edition*, **130** (29): 9146

Wang, Z., Cui, H., Liu, M., Grage, S. L., Hoffmann, M., Sedghamiz, E., Wenzel, W. and Levkin, P. A., 2022, Tough, Transparent, 3D-Printable, and Self-Healing Poly(ethylene glycol)-Gel (PEGgel), *Advanced Materials*, **34** (11): e2107791

Wei, W., Tan, Y., Martinez Rodriguez, N. R., Yu, J., Israelachvili, J. N. and Waite, J. H., 2014, A mussel-derived one component adhesive coacervate, *Acta Biomater*, **10** (4): 1663

Wu, S. J., Yuk, H., Wu, J., Nabzdyk, C. S. and Zhao, X., 2021, A Multifunctional Origami Patch for Minimally Invasive Tissue Sealing, *Advanced Materials*, **33** (11): e2007667

Xie, C., Wang, X., He, H., Ding, Y. and Lu, X., 2020, Mussel-Inspired Hydrogels for Self-Adhesive Bioelectronics, *Advanced Functional Materials*, **30** (25): 1909954

Xie, H., Shi, G., Wang, R., Jiang, X., Chen, Q., Yu, A. and Lu, A., 2024, Bioinspired Wet Adhesive Carboxymethyl Cellulose-Based Hydrogel With Rapid Shape Adaptability And Antioxidant

Activity For Diabetic Wound Repair, *Carbohydrate Polymers*, **334**: 122014

Xu, M., Miao, Y., Yu, J. and Zhang, L., 2021, Physiologically-Regulated Adhesion of Hydrogels for Wound Dressing, *Advanced Materials Interfaces*, **8** (20): 2101131

Xue, B., Gu, J., Li, L., Yu, W., Yin, S., Qin, M., Jiang, Q., Wang, W. and Cao, Y., 2021, Hydrogel Tapes for Fault-Tolerant Strong Wet Adhesion, *Nature Communications*, **12** (1): 7156

Yahia, L., 2015, History and Applications of Hydrogels, *Journal of Biomedical Sciencies*, **4** (2): 1

Yan, L., Zhou, T., Ni, R., Jia, Z., Jiang, Y., Guo, T., Wang, K., Chen, X., Han, L. and Lu, X., 2022, Adhesive Gelatin-Catechol Complex Reinforced Poly(Acrylic Acid) Hydrogel with Enhanced Toughness and Cell Affinity for Cartilage Regeneration, *ACS Applied Bio Materials*, **5** (9): 4366

Yang, J., Cohen Stuart, M. A. and Kamperman, M., 2014, Jack of All Trades: Versatile Catechol Crosslinking Mechanisms, *Chemical Society Reviews*, **43** (24): 8271

Yang, J., Keijsers, J., van Heek, M., Stuiver, A., Cohen Stuart, M. A. and Kamperman, M., 2015, The Effect Of Molecular Composition and Crosslinking on Adhesion of A Bio-Inspired Adhesive, *Polymer Chemistry*, **6** (16): 3121

Yang, S. Y., O'Cearbhaill, E. D., Sisk, G. C., Park, K. M., Cho, W. K., Villiger, M., Bouma, B. E., Pomahac, B. and Karp, J. M., 2013, A Bio-Inspired Swellable Microneedle Adhesive for

Mechanical Interlocking with Tissue, *Nature Communications*, **4** (1): 1702

Yang, Z., Huang, R., Zheng, B., Guo, W., Li, C., He, W., Wei, Y., Du, Y., Wang, H., Wu, D. and Wang, H., 2021, Highly Stretchable, Adhesive, Biocompatible, and Antibacterial Hydrogel Dressings for Wound Healing, *Advanced Science*, **8** (8): 2003627

Ye, Q., Zhou, F. and Liu, W., 2011, Bioinspired Catecholic Chemistry for Surface Modification, *Chemical Society Reviews*, **40** (7): 4244

Ye, T., Wang, J., Jiao, Y., Li, L., He, E., Wang, L., Li, Y., Yun, Y., Li, D., Lu, J., Chen, H., Li, Q., Li, F., Gao, R., Peng, H. and Zhang, Y., 2022, A Tissue-Like Soft All-Hydrogel Battery, *Advanced Materials*, **34** (4): 2105120

Yi, Y., Xie, C., Liu, J., Zheng, Y., Wang, J. and Lu, X., 2021, Self-Adhesive Hydrogels for Tissue Engineering, *Journal of Materials Chemistry B*, **9** (42): 8739

Yilmaz, K. B., Dogan, L., Nalbant, H., Akinci, M., Karaman, N., Ozaslan, C. and Kulacoglu, H., 2011, Comparing Scalpel, Electrocautery and Ultrasonic Dissector Effects: The Impact on Wound Complications and Pro-Inflammatory Cytokine Levels in Wound Fluid From Mastectomy Patients, *Journal of Breast Cancer*, **14** (1): 58

Ying, B., Wu, Q., Li, J. and Liu, X., 2020, An Ambient-Stable and Stretchable Ionic Skin with Multimodal Sensation, *Materials Horizons*, **7** (2): 477

Ying, B., Chen, R. Z., Zuo, R., Li, J. and Liu, X., 2021, An Anti-Freezing, Ambient-Stable and Highly Stretchable Ionic Skin with Strong Surface Adhesion for Wearable Sensing and Soft Robotics, *Advanced Functional Materials*, **31** (42): 2104665

Yu, H., Rouelle, N., Qiu, A., Oh, J. A., Kempaiah, D. M., Whittle, J. D., Aakyiir, M., Xing, W. and Ma, J., 2020, Hydrogen Bonding-Reinforced Hydrogel Electrolyte for Flexible, Robust, and All-in-One Supercapacitor with Excellent Low-Temperature Tolerance, *ACS Applied Materials & Interfaces*, **12** (34): 37977

Yu, J., Qin, Y., Yang, Y., Zhao, X., Zhang, Z., Zhang, Q., Su, Y., Zhang, Y. and Cheng, Y., 2023, Robust Hydrogel Adhesives for Emergency Rescue and Gastric Perforation Repair, *Bioactive Materials*, **19**: 703

Yuk, H., Varela, C. E., Nabzdyk, C. S., Mao, X., Padera, R. F., Roche, E. T. and Zhao, X., 2019, Dry Double-Sided Tape for Adhesion of Wet Tissues and Devices, *Nature*, **575** (7781): 169

Yuk, H., Wu, J., Sarrafian, T. L., Mao, X., Varela, C. E., Roche, E. T., Griffiths, L. G., Nabzdyk, C. S. and Zhao, X., 2021, Rapid and Coagulation-Independent Haemostatic Sealing by A Paste Inspired by Barnacle Glue, *Nature Biomedical Engineering*, **5** (10): 1131

Yuk, H., Wu, J. and Zhao, X., 2022, Hydrogel Interfaces for Merging Humans and Machines, *Nature Reviews Materials*, **7** (12): 935

Zhang, H., Bre, L. P., Zhao, T., Zheng, Y., Newland, B. and Wang, W., 2014, Mussel-Inspired Hyperbranched Poly(amino

ester) Polymer as Strong Wet Tissue Adhesive, *Biomaterials*, **35** (2): 711

Zhang, J., Wan, L., Gao, Y., Fang, X., Lu, T., Pan, L. and Xuan, F., 2019, Highly Stretchable and Self-Healable MXene/Polyvinyl Alcohol Hydrogel Electrode for Wearable Capacitive Electronic Skin, *Advanced Electronic Materials*, **5** (7): 1900285

Zhang, J., Wang, Y., Zhang, J., Lei, I. M., Chen, G., Xue, Y., Liang, X., Wang, D., Wang, G., He, S. and Liu, J., 2022, Robust Hydrogel Adhesion by Harnessing Bioinspired Interfacial Mineralization, *Small*, **18** (31): e2201796

Zhang, L., Zhang, Y., Ma, F., Liu, X., Liu, Y., Cao, Y. and Pei, R., 2022, A Low-Swelling and Toughened Adhesive Hydrogel with Anti-Microbial and Hemostatic Capacities for Wound Healing, *Journal of Materials Chemistry B*, **10** (6): 915

Zhang, M., Yu, J., Shen, K., Wang, R., Du, J., Zhao, X., Yang, Y., Xu, K., Zhang, Q., Zhang, Y. and Cheng, Y., 2021, Highly Stretchable Nanocomposite Hydrogels with Outstanding Antifatigue Fracture Based on Robust Noncovalent Interactions for Wound Healing, *Chemistry of Materials*, **33** (16): 6453

Zhang, W., Wang, R., Sun, Z., Zhu, X., Zhao, Q., Zhang, T., Cholewinski, A., Yang, F. K., Zhao, B., Pinnaratip, R., Forooshani, P. K. and Lee, B. P., 2020, Catechol-Functionalized Hydrogels: Biomimetic Design, Adhesion Mechanism, and Biomedical Applications, *Chemical Society Reviews*, **49** (2): 433

Zhang, W., Wu, B., Sun, S. and Wu, P., 2021, Skin-Like Mechanoresponsive Self-Healing Ionic Elastomer from

Supramolecular Zwitterionic Network, *Nature Communications*, **12** (1): 4082

Zhao, K., Li, B., Sun, Y., Jia, B., Chen, J., Cheng, W., Zhao, L., Li, J., Wang, F., Su, J., Sun, J., Han, B., Liu, Y., Zhang, H. and Liu, K., 2023, Engineered Bicomponent Adhesives with Instantaneous and Superior Adhesion Performance for Wound Sealing and Healing Applications, *Advanced Functional Materials*, **33** (38): 2303509

Zhao, N. and Yuan, W., 2022, Highly Adhesive and Dual-Crosslinking Hydrogel via One-Pot Self-Initiated Polymerization for Efficient Antibacterial, Antifouling and Full-Thickness Wound Healing, *Composites Part B: Engineering*, **230**: 109525

Zhao, X., Chen, X., Yuk, H., Lin, S., Liu, X. and Parada, G., 2021, Soft Materials by Design: Unconventional Polymer Networks Give Extreme Properties, *Chemical Reviews*, **121** (8): 4309

Zhou, D., Li, S., Pei, M., Yang, H., Gu, S., Tao, Y., Ye, D., Zhou, Y., Xu, W. and Xiao, P., 2020, Dopamine-Modified Hyaluronic Acid Hydrogel Adhesives with Fast-Forming and High Tissue Adhesion, *ACS Applied Materials & Interfaces*, **12** (16): 18225

Zhou, L., Dai, C., Fan, L., Jiang, Y., Liu, C., Zhou, Z., Guan, P., Tian, Y., Xing, J., Li, X., Luo, Y., Yu, P., Ning, C. and Tan, G., 2021, Injectable Self-Healing Natural Biopolymer-Based Hydrogel Adhesive with Thermoresponsive Reversible Adhesion for Minimally Invasive Surgery, *Advanced Functional Materials*, **31** (14): 2007457

Zhou, Y., Layani, M., Wang, S., Hu, P., Ke, Y., Magdassi, S. and Long, Y., 2018, Fully Printed Flexible Smart Hybrid Hydrogels, *Advanced Functional Materials*, **28** (9): 1705365

List of publications

This Ph.D. dissertation is based on the following publications.

I. Han G.Y., Park J.Y., Lee T.H., Yi M.B., Kim H.J., 2022

Highly Resilient Dual–Crosslinked Hydrogel Adhesives Based on a Dopamine–Modified Crosslinker

ACS Applied Materials & Interfaces, 14 (32), 36304–36314

II. Han G.Y., Park J.Y., Back J.H., Yi M.B., Kim H.J., 2024

Highly Resilient Noncovalently Associated Hydrogel Adhesives for Wound Sealing Patch

Advanced Healthcare Materials, 13 (12), 2303342

III. Han G.Y., Hwang S.K., Cho K.H., Kim H.J., Cho C.S., 2023

Progress of Tissue Adhesives Based on Proteins and Synthetic Polymers

Biomaterials Research, 27 (57), 1–21

IV. Han G. Y., Kwack H.W., Kim Y.H., Je Y.H., Kim H.J., Cho C.S., 2024

Progress of Polysaccharide–Based Tissue Adhesives

Carbohydrate Polymers, 327 (1), 121634

국문초록

매년 전 세계적으로 100 만 명이 넘는 사람들이 외상성 사고, 수술 절개, 당뇨병성 궤양 등의 다양한 상처를 입는다. 일반적으로 상처 봉합 및 조직 기능 복원을 위해 봉합사, 스테이플, 클립, 피부 봉합 스트립과 같은 침습적 방법이 사용되고 있다. 그중 봉합사는 재료의 유연성으로 깊은 상처에도 사용할 수 있으며 체내에서 자연적으로 분해되는 등 사용의 편리성이 높다는 장점이 있다. 하지만 이러한 침습적 방법은 숙련된 인력과 긴 시술 시간이 요구되며 이차적인 조직손상 및 감염의 위험이 존재한다. 따라서 최근 수술 시간 단축, 통증 감소, 혈액 누출 및 감염 완화 등의 다양한 장점이 있는 생체 접착제를 이용하여 침습적 방법을 대체하려는 연구가 지속적으로 이루어지고 있다.

하이드로겔 기반 생체 접착제는 생물학적 조직과의 유사성과 사용 용이성으로 상처나 절개 부위를 봉합하는 봉합사의 대안으로 과학계의 주목을 받고 있다. 하이드로겔 접착제는 지혈, 세포 접착, 항균 및 항염증 특성과 같은 다양한 기능성을 가져 조직 공학 분야에서 유망한 재료로 여겨지고 있다. 하지만, 기존 하이드로겔 접착제의 약한 피부 접착력과 낮은 기계적 탄성력으로 상용화에 한계가 있었다. 낮은 조직 접착력으로 인한 불완전한 계면 접착은 상처 감염 위험을 증가시키고 조직 재생을 지연시켰다. 또한, 낮은

기계적 탄력성으로 인해 움직임이 자주 발생하는 장기나 가동 범위가 큰 관절과 같은 부위에 적용할 수 없었다.

본 연구에서는 도파민으로 개질된 올리고머를 디자인하고 이를 하이드로겔 접착제를 제조하기 위한 가교제로 적용했다. 도파민 개질 올리고머는 길이가 짧은 다이아크릴레이트와 도파민의 아민그룹 간 Aza-Michael 반응으로 합성하였다. 도파민 개질 올리고머가 다음과 같은 구조적 특징을 가지도록 설계하여 이를 통해 제작한 하이드로겔이 높은 기계적 탄성력, 높은 조직 접착력 및 생체적합성을 보일 수 있게 하였다: 1) 올리고머의 양 말단이 아크릴레이트 그룹으로 기능화, 2) 다량의 도파민 분자가 짧은 간격으로 배치, 3) 가수분해 가능한 에스터결합을 포함. 우선, 도파민 개질 올리고머의 양 말단을 아크릴레이트 그룹으로 기능화하여 가교제로 활용할 수 있게 하였다. 그리고 짧은 다이아크릴레이트 분자를 사용함으로써 도파민 분자가 짧은 간격으로 배치되게 하여 도파민 분자 간의 가역적인 수소결합 및 소수성 상호작용들로 도파민 개질 올리고머가 하이드로겔 네트워크 안에서 응집된 구조를 형성하게 하였다. 이러한 응집구조를 통해 하이드로겔이 높은 기계적 탄력성을 가지게 하였다. 또한, 올리고머가 다량의 도파민 분자를 포함하게 하여 도파민 분자의 수소결합, Schiff-base 반응, Michael addition 반응과 같은 물리적, 화학적 분자 간 상호작용으로 하이드로겔이 견고한 조직 접착을 형성할 수 있게 하였다. 마지막으로, 도파민 개질 올리고머가 가수분해할 수 있는

에스터결합을 가지게 하여 이를 사용하여 제조한 하이드로겔이 생체조건에서 분해될 수 있게 하였다.

도파민개질 올리고머를 가교제로 활용하여 높은 조직 접착력, 기계적 탄성력 및 생체적합성을 보이는 하이드로겔을 제조하였으며, 관절과 같이 크고 잦은 움직임이 발생하는 부위의 드레싱 재료로 사용할 수 있음을 보여주었다. 이후, 도파민으로 개질된 가교제의 구조와 하이드로겔 네트워크 구조 변형을 통해 하이드로겔의 인성을 향상하였다. 도파민 개질 가교제의 주 사슬을 부피가 큰 사슬로 변형함으로써 하이드로겔 접착제의 신축성을 향상하고, 양이온성 선형 고분자를 첨가하여 하이드로겔의 네트워크 구조를 단일 네트워크에서 이중 네트워크로 변형함으로써 하이드로겔 접착제의 모듈러스를 향상했다. 하이드로겔의 네트워크 구조 변형을 통해 인성이 향상된 하이드로겔 접착제를 제조하였으며, 이를 천공을 봉합할 수 있는 상처 봉합 패치로 사용할 수 있음을 보여주었다.

본 연구에서는 높은 접착력을 보이며 신축성 및 탄력성이 뛰어난 하이드로겔 접착제를 성공적으로 개발하였다. 도파민으로 개질된 가교제와 이중 네트워크구조를 도입함으로써, 일반적으로 음의 상관관계를 갖는 조직접착력, 인성, 기계적 회복력 세 물성이 잘 균형 잡힌 하이드로겔 접착제를 제조하였다. 또한, 도파민 개질 가교제가 가수분해 가능한 결합을 포함하여 이를 사용하여 제작한 하이드로겔이 생체조건에서 분해될 수 있게 하였다. 이러한 특성들을

기반으로 본 연구에서 제작한 하이드로겔이 잦은 움직임이 발생하는 신체 부위에의 적용 가능함을 보여주었으며, 최종적으로는 상처 밀봉 패치로서의 사용 가능성을 보여주었다. 본 연구는 가교제만을 사용하여 기능성 하이드로겔을 제작하는 손쉬운 방법을 보여주었으며, 이 가교제는 상처 드레싱 재료를 넘어 전자 피부, 센서 및 조직 지지체 등의 기능성 소재 제조에 활용될 수 있을 것으로 기대된다.

키워드: 하이드로겔 접착제, 가교제, 도파민, 기계적 탄성력, 상처봉합 패치

학 번: 2019-24629